

ISTANBUL TECHNICAL UNIVERSITY ★ GRADUATE SCHOOL OF SCIENCE
ENGINEERING AND TECHNOLOGY

FUNDAMENTAL LATTICE SOLITONS IN DAVEY STEWARTSON SYSTEMS

Ph.D. THESIS

Mahmut BAĞCI

Mathematical Engineering Department

Mathematical Engineering Doctorate Program

FEBRUARY 2016

FUNDAMENTAL LATTICE SOLITONS IN DAVEY STEWARTSON SYSTEMS

Ph.D. THESIS

Mahmut BAĞCI
(509102005)

Mathematical Engineering Department

Mathematical Engineering Doctorate Program

Thesis Advisor: Prof. Dr. Nalan ANTAR
Co-advisor: Assoc. Prof. Dr. İlkey BAKIRTAŞ

FEBRUARY 2016

İSTANBUL TEKNİK ÜNİVERSİTESİ ★ FEN BİLİMLERİ ENSTİTÜSÜ

DAVEY STEWARTSON SİSTEMİNDE TEMEL KAFES SOLİTONLARI

DOKTORA TEZİ

Mahmut BAĞCI
(509102005)

Matematik Mühendisliği Anabilim Dalı

Matematik Mühendisliği Doktora Programı

Tez Danışmanı: Prof. Dr. Nalan ANTAR

Eş Danışman: Doç. Dr. İlkey BAKIRTAŞ

ŞUBAT 2016

Mahmut BAĞCI, a Ph.D. student of ITU Graduate School of Science Engineering and Technology 509102005 successfully defended the thesis entitled “FUNDAMENTAL LATTICE SOLITONS IN DAVEY STEWARTSON SYSTEMS”, which he prepared after fulfilling the requirements specified in the associated legislations, before the jury whose signatures are below.

Thesis Advisor : **Prof. Dr. Nalan ANTAR**
Istanbul Technical University

Co-advisor : **Assoc. Prof. Dr. İlkey BAKIRTAŞ**
Istanbul Technical University

Jury Members : **Prof. Dr. Mevlüt TEYMÜR**
Istanbul Technical University

Prof. Dr. Hilmi DEMİRAY
Işık University

Prof. Dr. Ayşe Hümevra BİLGE
Kadir Has University

Assoc. Prof. Dr. Ahmet KIRIŞ
Istanbul Technical University

Assist. Prof. Dr. Cihan BAYINDIR
Işık University

Date of Submission : **29 December 2015**

Date of Defense : **4 February 2016**

FOREWORD

I have spent five years working towards my PhD under the supervision of two wonderful advisors: Prof. Dr. Nalan Antar and Assoc. Prof. Dr. İlkey Bakırtaş. I would like to thank them for their excellent supervision of this dissertation and for all of their help during my PhD. My great teachers believed in me, and encouraged me to stay focused on the study, even though I had difficult times. Not only they advised me in preparing the thesis, but also taught me other aspects of being in a scientific community. It was great to be in their group, and I am honored to be one of their pupils.

Besides my advisors, I would like to thank my steering committee members, Professors Mevlüt Teymür, Hilmi Demiray and Ayşe Hümeysra Bilge, for their helpful comments and feedback.

I would also like to thank my colleague, İzzet Göksel, for his assistance and fruitful discussions about numerical methods and solitons.

Last but not least, I would like to thank my family, especially my parents, Gül and Mustafa, for their unconditional support and encouragement.

February 2016

Mahmut BAĞCI

TABLE OF CONTENTS

| | <u>Page</u> |
|--|-------------|
| FOREWORD | vii |
| TABLE OF CONTENTS | ix |
| ABBREVIATIONS | xi |
| LIST OF FIGURES | xiii |
| SUMMARY | xxi |
| ÖZET | xxiii |
| 1. INTRODUCTION | 1 |
| 1.1 Purpose of Thesis | 3 |
| 1.2 Literature Review | 5 |
| 1.3 Hypothesis | 6 |
| 2. DERIVATION OF THE NLSM EQUATIONS | 7 |
| 2.1 Maxwell Equations | 7 |
| 2.2 Polarization | 8 |
| 2.3 Derivation of the NLSE | 12 |
| 2.4 Derivation of the NLSE with Mean Terms (NLSM) | 16 |
| 3. NUMERICAL METHODS | 19 |
| 3.1 Spectral Renormalization Method | 19 |
| 3.2 Stability Analysis..... | 22 |
| 3.2.1 Linear stability analysis..... | 22 |
| 3.2.2 Nonlinear stability analysis | 23 |
| 4. NONLINEAR LATTICE SOLITONS OF THE NLSM SYSTEMS | 25 |
| 4.1 Numerical Existence of Fundamental Solitons and Stability Analysis | 25 |
| 4.1.1 Numerical existence of fundamental solitons..... | 26 |
| 4.1.2 Stability analysis of fundamental solitons..... | 27 |
| 4.2 Numerical Existence of Dipole Solitons and Stability Analysis | 35 |
| 4.2.1 Numerical existence of dipole solitons..... | 36 |
| 4.2.2 Stability analysis of dipole solitons | 37 |
| 4.3 Conclusion | 38 |
| 5. VORTEX AND DIPOLE SOLITONS OF THE NLSE IN DEFECTIVE LATTICES | 41 |
| 5.1 Defect Lattices..... | 43 |
| 5.2 Nonlinear Stability of Lattice Solitons | 45 |
| 5.3 Existence of Dipole Solitons and Nonlinear Stability Analysis | 45 |
| 5.3.1 Dipole solitons on a lattice with an edge dislocation | 46 |
| 5.3.2 Dipole solitons on a lattice with a vacancy defect..... | 49 |
| 5.4 Existence of Vortex Solitons and Stability Analysis | 52 |
| 5.4.1 Three-hump vortex on a lattice with an edge dislocation..... | 53 |

| | |
|--|------------|
| 5.4.2 Four-hump vortex on a lattice with a vacancy defect | 55 |
| 5.5 Conclusion | 60 |
| 6. NLSM SOLITONS IN A LATTICE WITH A VACANCY DEFECT | 63 |
| 6.1 Numerical Existence of Fundamental Solitons and Stability Analysis | 64 |
| 6.1.1 Numerical existence of fundamental solitons..... | 64 |
| 6.1.2 Stability analysis of fundamental solitons | 65 |
| 6.2 Numerical Existence of Dipole Solitons and Stability Analysis | 67 |
| 6.3 Numerical Existence of Vortex Solitons and Stability Analysis | 69 |
| 6.4 Comparison of the NLS and NLSM Models | 70 |
| 6.5 Conclusion | 73 |
| 7. FUNDAMENTAL SOLITONS OF THE NLSE IN PARITY-TIME SYMMETRIC LATTICE WITH A VACANCY DEFECT..... | 75 |
| 7.1 $\mathcal{P}\mathcal{T}$ -symmetric Vacancy Defect | 77 |
| 7.1.1 The $\mathcal{P}\mathcal{T}$ -Symmetric lattice with a vacancy defect | 77 |
| 7.2 Linear Stability Analysis | 80 |
| 7.3 Nonlinear Stability Analysis..... | 80 |
| 7.4 Numerical Existence of Fundamental Solitons and Stability Analysis | 81 |
| 7.4.1 Numerical existence of fundamental solitons..... | 81 |
| 7.4.2 Stability analysis of fundamental solitons | 83 |
| 7.5 Conclusion | 90 |
| 8. CONCLUSIONS AND RECOMMENDATIONS | 91 |
| REFERENCES..... | 93 |
| CURRICULUM VITAE | 102 |

ABBREVIATIONS

| | |
|----------------------------------|--|
| BR | : Benney and Roskes |
| DS | : Davey and Stewartson |
| KdV | : Korteweg-de Vries |
| NLSE | : Nonlinear Schrödinger Equation |
| NLSM | : Nonlinear Schrödinger Equation with Mean Terms |
| <i>\mathcal{PT}</i> | : Parity - Time |
| SR | : Spectral Renormalization |

LIST OF FIGURES

| | <u>Page</u> |
|---|-------------|
| Figure 4.1 : Contour image of the periodic lattice ($N=4$). | 25 |
| Figure 4.2 : (Color online) Fundamental soliton in the lattice-free medium at $x_0 = 0$ and $y_0 = 0$. (a) 3D view of the soliton; (b) Contour image of the soliton. | 26 |
| Figure 4.3 : (Color online) Fundamental soliton located at minimum of the periodic lattice at $x_0 = \pi$, $y_0 = 0$ for $V_0 = 12.5$. (a) 3D view of the soliton; (b) Contour image of the soliton..... | 27 |
| Figure 4.4 : (Color online) Domain of existence on the plane (ρ, ν) for the fundamental solitons in the lattice-free medium ($V_0 = 0$) and on the periodic lattice ($V_0 = 12.5$)for $\mu = -1$ | 28 |
| Figure 4.5 : (Color online) Soliton power vs. eigenvalue graph for fixed $\nu = 1$ within the semi-infinite gap in (a) lattice-free medium; (b) case with a periodic lattice. | 28 |
| Figure 4.6 : (Color online) Soliton power vs. eigenvalue graph for fixed $\rho = 1$ within the semi-infinite gap in (a) lattice-free medium; (b) case with a periodic lattice..... | 28 |
| Figure 4.7 : (Color online) Linear instability of the fundamental soliton (a) in the lattice-free medium; (b) on the periodic lattice minimum. | 29 |
| Figure 4.8 : (Color online) Collapse of the fundamental soliton in the lattice-free medium. (a) Snapshots of contour image of the soliton for various z values; (b) Peak amplitude as a function of the propagation distance. | 30 |
| Figure 4.9 : (Color online) Nonlinear evolution of the fundamental soliton located at minimum of the periodic lattice for $V_0 = 12.5$. (a) Snapshots of contour image of the soliton for various z values; (b) Peak amplitude as a function of the propagation distance. | 30 |
| Figure 4.10 : (Color online) Contour image of the fundamental soliton for lattice-free medium with (a) $\rho = 0.5$; (b) $\rho = 1.0$; (c) $\rho = 1.5$. Contour image of the fundamental lattice soliton for (d) $\rho = 0.5$; (e) $\rho = 1.0$; (f) $\rho = 1.5$. All solitons are obtained for $\nu = 1$ | 31 |
| Figure 4.11 : (Color online) Nonlinear evolution of the fundamental solitons for various values of ρ for fixed $\nu = 1$. Peak amplitude as a function of the propagation distance (a) in the lattice-free medium ($V_0 = 0$); (b) in the periodic lattice ($V_0 = 12.5$). | 31 |
| Figure 4.12 : (Color online) Contour image of the fundamental soliton for lattice-free medium with (a) $\nu = 0.5$; (b) $\nu = 1.0$; (c) $\nu = 1.5$. Contour image of the fundamental lattice soliton for (d) $\nu = 0.5$; (e) $\nu = 1.0$; (f) $\nu = 1.5$. All solitons are obtained for $\rho = 1$ | 32 |

| | |
|---|----|
| Figure 4.13: (Color online) Nonlinear evolution of the fundamental solitons for various values of ν for fixed $\rho = 1$. Peak amplitude as a function of the propagation distance (a) in the lattice-free medium ($V_0 = 0$); (b) in the periodic lattice ($V_0 = 12.5$). | 33 |
| Figure 4.14: (Color online) Nonlinear evolution of the fundamental soliton for larger anisotropy coefficients when $\rho = 1.5$ and $V_0 = 12.5$. (a) Mode profile of the fundamental soliton with $\nu = 1.0$ at $z = 5$, $z = 10$, $z = 20$ and $z = 30$. Peak amplitude as a function of the propagation distance (b) for $\nu = 1.0$; (c) for $\nu = 1.5$; (d) for $\nu = 2.0$ | 34 |
| Figure 4.15: (Color online) Nonlinear evolution of the fundamental soliton in the deeper lattice for $\rho = 2$ and $\nu = 3$. (a) Mode profile of the fundamental soliton for $V_0 = 50$ at $z = 5$, $z = 10$, $z = 20$ and $z = 30$. Peak amplitude as a function of the propagation distance (b) for $V_0 = 50$; (c) for $V_0 = 250$; (d) for $V_0 = 500$ | 35 |
| Figure 4.16: (Color online) Nonlinear evolutions of Gaussian, mode obtained by SR method (both for lattice-free medium) and periodic lattice soliton in Potassium Niobate ($KNbO_3$). | 36 |
| Figure 4.17: (a) A dipole profile in the lattice-free medium; (b) Contour image of the dipole; (c) Phase structure of the dipole. | 36 |
| Figure 4.18: (a) A dipole profile located at periodic lattice minima for $V_0 = 12.5$; (b) Contour image of the dipole; (c) Phase structure of the dipole..... | 37 |
| Figure 4.19: Linear evolution of the dipole solitons in (a) the lattice-free medium ($V_0 = 0$); (b) the periodic lattice ($V_0 = 12.5$). | 37 |
| Figure 4.20: Collapse of a dipole in the lattice-free medium; (a) Contour image of the dipole; (b) Peak amplitude as a function of the propagation distance. | 38 |
| Figure 4.21: Nonlinear evolution of the dipole solitons located at minima of the periodic lattice for $V_0 = 12.5$. (a) Contour image of the dipole; (b) Peak amplitude as a function of the propagation distance. | 38 |
| Figure 5.1 : Contour images of lattices: (a) lattice with an edge dislocation; (b) lattice with a vacancy defect; (c) periodic ($N=4$). | 44 |
| Figure 5.2 : (a) A dipole profile centered at the minima of the lattice with an edge dislocation for $x_0 = -x_1 = \pi$; $y_0 = y_1 = \pi$; (b) The phase structure of dipole solitons; (c) The contour plot of dipole solitons superimposed on the underlying lattice. | 46 |
| Figure 5.3 : (a) A dipole profile centered at maxima of the lattice with an edge dislocation for $r = 5\pi/2$; (b) The phase structure of dipole solitons; (c) The contour plot of dipole solitons superimposed on the underlying lattice..... | 47 |
| Figure 5.4 : The power versus μ (eigenvalue) of dipole solitons for the lattice with an edge dislocation..... | 47 |
| Figure 5.5 : Nonlinear instability of a dipole on the minima of the lattice with an edge dislocation. (a) Maximum amplitude as a function of propagation distance; (b) Center of mass; (c) Contour plot of the complex-phase at $z = 100$; (d) Contour plot of the amplitude at $z = 100$ | 48 |

| | |
|---|----|
| Figure 5.6 : Collapse of dipoles on the maxima of the lattice with an edge dislocation. (a) Maximum amplitude as a function of propagation distance; (b) Center of mass; (c) Contour plot of the complex-phase at $z = 0.3$; (d) Contour plot of the amplitude at $z = 0.3$ | 48 |
| Figure 5.7 : (a) A dipole profile centered at minima of the lattice with a vacancy defect for $r = \pi$; (b) The phase structure of dipole solitons; (c) The contour plot of the dipole solitons superimposed on the underlying lattice..... | 49 |
| Figure 5.8 : (a) A dipole profile centered at maxima of the lattice with a vacancy defect for $r = 2\pi$; (b) The phase structure of dipole solitons; (c) The contour plot of the dipole solitons superimposed on the underlying lattice..... | 49 |
| Figure 5.9 : The power versus μ (eigenvalue) of dipole solitons for the lattice with a vacancy defect..... | 50 |
| Figure 5.10 : Nonlinear stability of dipole solitons on the minima of the lattice with a vacancy defect. (a) Maximum amplitude as a function of propagation distance; (b) Center of mass; (c) Contour plot of the complex-phase at $z = 100$; (d) Contour plot of the amplitude at $z = 100$ | 50 |
| Figure 5.11 : Collapse of dipoles on the maxima of the lattice with a vacancy defect. (a) Maximum amplitude as a function of propagation distance; (b) Center of mass; (c) Contour plot of the complex-phase at $z = 0.53$; (d) Contour plot of the amplitude at $z = 0.53$ | 51 |
| Figure 5.12 : Nonlinear stability of dipole solitons on periodic lattice minima. (a) Maximum amplitude as a function of propagation distance; (b) Center of mass; (c) Contour plot of the complex-phase at $z = 100$; (d) Contour plot of the amplitude at $z = 100$ | 52 |
| Figure 5.13 : Collapse of dipoles on periodic lattice maxima. (a) Maximum amplitude as a function of propagation distance; (b) Center of mass; (c) Contour plot of the complex-phase at $z = 0.48$; (d) Contour plot of the amplitude at $z = 0.48$ | 53 |
| Figure 5.14 : (a) A three-hump vortex profile centered at the minima of the lattice for $x_0 = 3\pi/2, x_1 = 0, x_2 = -3\pi/2; y_0 = 0, y_1 = 2\pi, y_2 = 0$; (b) The phase structure of the vortex; (c) The contour plot of the vortex humps superimposed on the underlying lattice..... | 53 |
| Figure 5.15 : (a) A three-hump vortex profile centered at the maxima of the lattice for $x_0 = -x_2 = 4, x_1 = 0; y_0 = -y_1 = y_2 = \pi$; (b) The phase structure of the vortex solitons; (c) The contour plot of the vortex humps superimposed on the underlying lattice..... | 54 |
| Figure 5.16 : The power versus μ (eigenvalue) of three-hump vortex for the lattice with an edge dislocation..... | 54 |
| Figure 5.17 : Nonlinear instability of three vortex solitons on the minima of the lattice with an edge dislocation. (a) Maximum amplitude as a function of propagation distance; (b) Center of mass; (c) Contour plot of the complex-phase at $z = 100$; (d) Contour plot of the amplitude at $z = 100$ | 55 |

| | |
|--|----|
| Figure 5.18: Collapse of three vortex solitons on the maxima of the lattice with an edge dislocation. (a) Maximum amplitude as a function of propagation distance; (b) Center of mass; (c) Contour plot of the complex-phase at $z = 0.4$; (d) Contour plot of the amplitude at $z = 0.4$ | 56 |
| Figure 5.19: (a) A four-hump vortex profile centered at the minima of the lattice with a vacancy defect (close to defect); (b) The phase structure of the vortex; (c) The contour plot of the vortex humps superimposed on the underlying lattice. | 56 |
| Figure 5.20: (a) A four-hump vortex profile centered at the minima of the lattice with a vacancy defect; (b) The phase structure of the vortex; (c) The contour plot of the vortex humps superimposed on the underlying lattice. | 56 |
| Figure 5.21: (a) A four-hump vortex profile centered at the maxima of the lattice with a vacancy defect; (b) The phase structure of the vortex; (c) The contour plot of the vortex humps superimposed on the underlying lattice. | 57 |
| Figure 5.22: The power versus μ (eigenvalue) of four-hump vortex for the lattice with a vacancy defect. | 57 |
| Figure 5.23: Nonlinear instability of four vortex solitons on the minima of the lattice with a vacancy defect (close to defect). (a) Maximum amplitude as a function of propagation distance; (b) Center of mass; (c) Contour plot of the complex phase at $z = 5$; (d) Contour plot of the amplitude at $z = 5$ | 58 |
| Figure 5.24: Nonlinear instability of four vortex solitons on the minima of the lattice with a vacancy defect (away from defect). (a) Maximum amplitude as a function of propagation distance; (b) Center of mass; (c) Contour plot of the complex phase at $z = 100$; (d) Contour plot of the amplitude at $z = 100$ | 59 |
| Figure 5.25: Collapse of four vortex solitons on the maxima of the lattice with a vacancy defect. (a) Maximum amplitude as a function of propagation distance; (b) Center of mass; (c) Contour plot of the complex phase at $z = 0.84$; (d) Contour plot of the amplitude at $z = 0.84$ | 59 |
| Figure 5.26: Nonlinear stability of four vortex solitons on the minima of the periodic lattice. (a) Maximum amplitude as a function of propagation distance; (b) Center of mass; (c) Contour plot of the complex phase at $z = 100$; (d) Contour plot of the amplitude at $z = 100$ | 60 |
| Figure 5.27: Collapse of four vortex solitons on the maxima of the periodic lattice. (a) Maximum amplitude as a function of propagation distance; (b) Center of mass; (c) Contour plot of the complex-phase at $z = 0.48$; (d) Contour plot of the amplitude at $z = 0.48$ | 61 |
| Figure 6.1 : Contour image of (a) The lattice without defect (periodic); (b) Lattice with a vacancy defect; and diagonal cross-section of (c) The lattice without defect; (d) The lattice with a vacancy defect. | 64 |

| | |
|--|----|
| Figure 6.2 : Fundamental soliton situated at center of the lattice with a vacancy defect. (a) 3D view of the soliton; (b) Contour image of the soliton. | 65 |
| Figure 6.3 : Band-gap formation of NLSM system with periodic potential and the lattice with a vacancy defect. | 65 |
| Figure 6.4 : Soliton power as a function of the eigenvalue μ within the semi-infinite band gap for the lattice with a vacancy defect. | 66 |
| Figure 6.5 : Linear evolution of the fundamental soliton located in the lattice with a vacancy defect. | 66 |
| Figure 6.6 : Evolution of the fundamental soliton located at center of the lattice with a vacancy defect; (a) Contour image of the soliton; (b) Peak amplitude as a function of the propagation distance. | 67 |
| Figure 6.7 : (a) A dipole profile located near empty (vacancy) cell of the lattice with a vacancy defect; (b) Contour image of the dipole; (c) Phase structure of the dipole. | 68 |
| Figure 6.8 : Linear evolution of the dipole solitons in the lattice with a vacancy defect. | 68 |
| Figure 6.9 : Evolution of the dipole solitons located near vacancy defect of the lattice; (a) Contour image of the dipole; (b) Peak amplitude as a function of the propagation distance. | 69 |
| Figure 6.10 : (a) A vortex profile located near empty (vacancy) cell of the lattice; (b) Contour image of the vortex; (c) Phase structure of the vortex. | 70 |
| Figure 6.11 : Linear evolution of the vortex solitons in the lattice with a vacancy defect. | 70 |
| Figure 6.12 : Evolution of the vortex solitons on the lattice with a vacancy defect; (a) Contour image of the vortex; (b) Peak amplitude as a function of the propagation distance. | 71 |
| Figure 6.13 : The first nonlinear band-gap formation for the NLSE and NLSM system with the lattice that possesses a vacancy defect. | 71 |
| Figure 6.14 : Soliton power as a function of the eigenvalue μ within the semi-infinite band gap for the NLSE and NLSM systems with the lattice that possesses a vacancy defect. In all cases, we set peak depth $V_0 = 12.5$ | 72 |
| Figure 7.1 : Contour image of real part for the \mathcal{PT} -symmetric (a) lattice without defect; (b) lattice with a vacancy defect. Diagonal cross-section of (c) lattice without defect; (d) lattice with a vacancy defect. | 79 |
| Figure 7.2 : (a) Contour image of imaginary part for the \mathcal{PT} -symmetric lattices; (b) Diagonal cross-section of imaginary part for the \mathcal{PT} -symmetric lattices. | 79 |
| Figure 7.3 : Diagonal cross-section of (a) real parts; (b) imaginary parts in $V(x,y)$ and $V(-x,-y)$ for $V_0 = 12.5$, $W_0 = 0.1$ and $\varepsilon = 1$ | 79 |
| Figure 7.4 : Fundamental soliton located at the center of the \mathcal{PT} -symmetric periodic lattice for $\varepsilon = 0$ and $W_0 = 0.1$. Contour image of (a) Real part; (b) Imaginary part; (c) Diagonal cross-section of the soliton; (d) Phase portrait of the soliton. | 82 |

| | |
|--|----|
| Figure 7.5 : Fundamental soliton located at the center of the \mathcal{PT} -symmetric periodic lattice for $\varepsilon = 0$ and $W_0 = 0.3$. Contour image of (a) Real part; (b) Imaginary part; (c) Diagonal cross-section of the soliton; (d) Phase portrait of the soliton..... | 82 |
| Figure 7.6 : Fundamental soliton located at the center of the \mathcal{PT} -symmetric lattice with a vacancy defect for $\varepsilon = 1$ and $W_0 = 0.1$. Contour image of (a) Real part; (b) Imaginary part; (c) Diagonal cross-section of the soliton; (d) Phase portrait of the soliton..... | 83 |
| Figure 7.7 : Fundamental soliton located at the center of the \mathcal{PT} -symmetric lattice with a vacancy defect for $\varepsilon = 1$ and $W_0 = 0.3$. Contour image of (a) Real part; (b) Imaginary part; (c) Diagonal cross-section of the soliton; (d) Phase portrait of the soliton..... | 83 |
| Figure 7.8 : Soliton power as a function of the eigenvalue μ within the semi-infinite band gap for lattices (a) without defect ($\varepsilon = 0$); (b) with a vacancy defect ($\varepsilon = 1$). All lattices share a common peak depth $V_0 = 12.5$ | 84 |
| Figure 7.9 : Eigenvalues in the stability spectrum of the fundamental soliton located at the center of the \mathcal{PT} -symmetric lattice without defect (a) for $W_0 = 0.1$; (b) for $W_0 = 0.3$ | 84 |
| Figure 7.10 : Eigenvalues in the stability spectrum of the fundamental soliton located at the center of the \mathcal{PT} -symmetric lattice with a vacancy defect (a) for $W_0 = 0.1$; (b) for $W_0 = 0.3$ | 85 |
| Figure 7.11 : Evolution of fundamental soliton located at the center of the \mathcal{PT} -symmetric lattice without defect for $\varepsilon = 0$ and $W_0 = 0.1$; (a) Contour image of the soliton; (b) Peak amplitude as a function of the propagation distance..... | 85 |
| Figure 7.12 : Evolution of fundamental soliton located at the center of the \mathcal{PT} -symmetric lattice without defect for $\varepsilon = 0$ and $W_0 = 0.3$; (a) Contour image of the soliton; (b) Peak amplitude as a function of the propagation distance..... | 86 |
| Figure 7.13 : Evolution of fundamental soliton located at the center of the \mathcal{PT} -symmetric lattice with a vacancy defect for $\varepsilon = 1$ and $W_0 = 0.1$; (a) Contour image of the soliton; (b) Peak amplitude as a function of the propagation distance..... | 87 |
| Figure 7.14 : Evolution of fundamental soliton located at the center of the \mathcal{PT} -symmetric lattice with a vacancy defect for $\varepsilon = 1$ and $W_0 = 0.3$; (a) Contour image of the soliton; (b) Peak amplitude as a function of the propagation distance..... | 87 |
| Figure 7.15 : Nonlinear evolution of an unstable fundamental soliton in the \mathcal{PT} -symmetric lattice with a vacancy defect for $\varepsilon = 1$ and $W_0 = 0.1$; (a) Solution profile at $z = 4.5$; (b) Solution profile at $z = 5.6$; (c) Power evolution versus distance z | 88 |
| Figure 7.16 : Diagonal cross-section of the lattice with a vacancy defect while $\varepsilon = 0.0$, $\varepsilon = 0.2$, $\varepsilon = 0.6$ and $\varepsilon = 1.0$ in Eq. (7.7)..... | 88 |
| Figure 7.17 : Soliton power versus defect's strength (ε) for the \mathcal{PT} -symmetric lattice with a vacancy defect for $V_0 = 12.5$ and $\mu = -1$ | 89 |

| | |
|--|----|
| Figure 7.18: Nonlinear evolution of the fundamental solitons in the \mathcal{PT} -symmetric lattice with a vacancy defect for four values of ε . Peak amplitude as a function of the propagation distance (a) when $W_0 = 0.1$; (b) when $W_0 = 0.3$ | 89 |
| Figure 7.19: Diagonal cross-section of the lattice with a vacancy defect while $\varepsilon = 0$, $\varepsilon = 1$, $\varepsilon = 2$ and $\varepsilon = 3$ in Eq. (7.7). | 90 |

FUNDAMENTAL LATTICE SOLITONS IN DAVEY STEWARTSON SYSTEMS

SUMMARY

Nonlinear wave problems are of wide physical and mathematical interest and arise in a variety of scientific fields such as nonlinear optics, fluid dynamics, plasma physics, etc. The solutions of the governing nonlinear wave equations often exhibit important phenomena, such as stable localized waves (e.g., solitons) or self-similar structures and wave collapse (i.e., blow-up) where the solution tends to infinity in finite time or at finite propagation distance.

Recently, wave collapse and the role of ground-state on global-existence theory are investigated for the Nonlinear Schrödinger equation (NLSE) with Mean Terms (NLSM or Davey Stewartson Systems). It is found that NLSM collapse can be arrested by small nonlinear saturation.

Another way of arresting wave collapse is adding an external potential (lattice) to the governing equation (model). In recent years, there has been considerable interest in the study of solitons that are generated by the NLSE with various type external lattices, in particular those that can be generated in nonlinear optical materials. On the other hand, NLSM systems with additional external potentials have not been studied in current literature yet. NLSM system with an external potential is given by

$$\begin{aligned} iu_z + \frac{1}{2}\Delta u + |u|^2 u - \rho\phi u - V(x,y)u &= 0, \\ \phi_{xx} + \nu\phi_{yy} &= (|u|^2)_{xx}. \end{aligned} \quad (1)$$

where u corresponds to the field associated with the first-harmonic, $\phi(x,y,t)$ corresponds to the mean field, ρ and ν are real constants that depend on the physical parameters, and $V(x,y)$ is an external optical potential. The NLSE can be obtained from the NLSM system by simply setting $\rho = 0$.

The external optical potential $V(x,y)$ can be written as the intensity of a sum of phase-modulated plane waves

$$V(x,y) = \frac{V_0}{N^2} \left| \sum_{n=0}^{N-1} e^{i(k_x^n x + k_y^n y)} \right|^2 \quad (2)$$

where $V_0 > 0$ is constant and corresponds to the peak depth of the potential, i.e., $V_0 = \max_{x,y} V(x,y)$, $(k_x^n, k_y^n) = [K\cos(2\pi n/N), K\sin(2\pi n/N)]$ is a wave vector. The potentials for $N = 2, 3, 4, 6$ yield periodic lattices that correspond to standard 2D crystal structures, whereas $N = 5, 7$ correspond to quasicrystals. The lattice-free medium can be obtained by setting $V_0 = 0$.

In this dissertation, we aim to investigate the existence and stability properties of solitons in the (2+1)-dimensional NLSE and NLSM system with various types of external lattices.

Chapter 2 describes the derivation of the NLSE and NLSM system by asymptotic methods.

In Chapter 3, a numerical algorithm which is a modification of Spectral Renormalization (SR) method is given at the beginning. This algorithm will be used on each stage of the study to compute solutions of the models (NLSE and NLSM systems). Then, numerical methods for investigating the stability properties of solitons are explained.

Chapter 4 is dedicated to the fundamental and dipole solitons in the NLSM systems. First we demonstrate the existence of solitons and, examine the stability properties of these solitons in the lattice-free medium. Then, we explain the effect of a periodic external potential as a collapse arrest mechanism in the NLSM system. The results of this part are considered as the main contribution to the thesis.

Chapter 5 includes the multi-humped structures (dipoles and vortices) obtained in the NLSE with defective lattices. The NLSE is a special form of NLSM system. Therefore, understanding the dynamics of dipoles and vortices in the NLSE can be considered as a fundamental step for the NLSM systems.

In Chapter 6, we present the fundamental and dipole solitons in the NLSM systems with a vacancy defect in the light of Chapter 5. Solitons in defective lattices have a significant importance in nonlinear science, this part of the study helps us to understand the effects of defects on the soliton properties in the NLSM systems.

Chapter 7 deals with the existence and stability properties of fundamental solitons in the (2+1)-dimensional NLSE with a defective \mathcal{PT} -Symmetric external potential.

Results of this dissertation are summarized in Chapter 8 where also a few ideas are outlined to further extend the research in this area.

DAVEY STEWARTSON SİSTEMİNDE TEMEL KAFES SOLİTONLARI

ÖZET

Eğrisel (nonlinear) dalga denklemlerinin çözümleri, optik, akışkanlar dinamiği veya plazma fiziği gibi alanlarda geniş olarak yer tutan önemli bir konudur. Fizik ve matematikte çeşitli yönetici denklemler (modeller) kullanılarak dalga çözümleri elde edilebilir. Elde edilen çözümlerin yapısı ve kararlılığı kullanılan fiziksel modele ve bu model için kullanılan parametrelere göre değişir. Bu çözümler kararlı lokalize dalgalar (soliton) veya sönümlü dalgalar olabilir.

Sayısal yöntemlerden faydalanarak birçok dalga denkleminin soliton çözümlerinin varlığı gösterilmiştir. Bu dalga denklemlerine örnek olarak Korteweg-de Vries (KdV) denklemi, eğrisel Schrödinger (NLS) denklemi veya bu çalışmada da model olarak kullanılan NLS denkleminin kuadratik katkıları içeren (NLS with mean term) NLSM sistemi gösterilebilir. NLSM sistemi, Davey-Stewartson ve Benney-Roskes tipi sistem olarak da bilinmektedir.

Çözüm elde edilmek istenen ortam (malzeme) simetri merkezli (centro-symmetric) ise üçüncü dereceden (kübik) NLS denklemi yönetici denklem olarak kullanılabilir. Simetri merkezli olmayan ortamda çözüm elde edebilmek için NLS denkleminin ikinci dereceden (kuadratik) katkıları eklenmelidir. Kübik NLS denkleminin kuadratik katkıları eklendiğinde aşağıda verilen NLSM sistemi elde edilmektedir.

$$\begin{aligned}iu_z + \sigma \Delta u + |u|^2 u - \rho \phi u &= 0, \\ \phi_{xx} + v \phi_{yy} &= (|u|^2)_{xx}.\end{aligned}\tag{3}$$

Burada u birinci harmoniğin genliğe katkısını, ϕ kuadratik etkileri göstermektedir. ρ bağlantı katsayısını, v kullanılan malzemenin (ortamın) yönlere bağımlılığını (anizotropisini) yansıtan sabiti göstermektedir. $\rho < 0$ durumunda su dalgaları, $\rho > 0$ durumunda elektromanyetik dalgalar elde edilir. $\rho = 0$ durumunda sistem NLS denkleminin indirgenir.

Yönetici denklemlere doyurulabilir doğrusal olmayan terim veya dış potansiyel (latis veya kafes) ekleyerek kararlı çözümler elde etmek, literatürde bilinen bir yöntemdir. Son yıllarda, düzenli (kristal veya yarı kristal) potansiyeller kullanılarak elde edilen temel dipol ve çoklu (vorteks) solitonlarla ilgili çok sayıda çalışma yayınlanmıştır. Ayrıca karmaşık (kompleks) değerli (Parity Time Symmetric) potansiyellerin varlığında dalga çözümlerine önem verilmektedir. Kompleks değerli potansiyeller parite zaman (\mathcal{PT}) simetrik olarak tanımlanmaktadır.

NLSM sistemi için bir dış potansiyelin (kafesin) varlığında çözümlerin incelendiği herhangi bir çalışma bulunmamaktadır. Bu çalışmada, NLS denklemi ve NLSM sisteminin sayısal çözümleri çeşitli dış potansiyeller kullanılarak hesaplanmaktadır.

Kullanılan fiziksel sistemin yönetici modeli, bir dış potansiyel içeren NLSM Sistemi,

$$iu_z + \frac{1}{2}\Delta u + |u|^2 u - \rho\phi u - V(x,y)u = 0, \quad (4)$$

$$\phi_{xx} + \nu\phi_{yy} = (|u|^2)_{xx}.$$

ile verilir. Burada $V(x,y)$ potansiyeli göstermektedir. Potansiyelleri elde etmek için kullanılan genel form

$$V(x,y) = \frac{V_0}{N^2} \left| \sum_{n=0}^{N-1} e^{i(k_x^n x + k_y^n y)} \right|^2 \quad (5)$$

şekindedir. Potansiyel derinliği V_0 sabiti ile belirlenmektedir. Dalga vektörü $(k_x^n, k_y^n) = [K\cos(2\pi n/N), K\sin(2\pi n/N)]$ ile tanımlanır. $N = 2, 3, 4, 6$ durumları periyodik potansiyelleri, $N = 5, 7$ durumları yarı kristal potansiyelleri elde etmek için kullanılır.

Çalışmanın ilk bölümünde NLS denklemleri ve NLSM sistemleri asimptotik yöntemler kullanılarak elde edilmiştir. Bu kısım, tezin sonraki bölümlerinde sayısal olarak elde edilen çözümlerin fiziksel karşılıklarını anlamamıza yardımcı olmuştur.

Denklemler elde edildikten sonra soliton çözüm elde etmek için Ablowitz ve Musslimani'nin ortaya koyduğu Spektral Renormalizasyon (SR) yöntemi NLSM sistemine uyarlanmıştır. SR yönteminde, NLSM sistemi Fourier uzayında ele alınıp, $u(x,y,z) = f(x,y)e^{-i\mu z}$ çözüm önerisi ile doğrusal olmayan terime göre bir yakınsama faktörü belirlenir. Bu çalışmada yakınsama koşulu 10^{-8} olarak alınmıştır. SR yöntemiyle soliton çözüm elde etmek için kullanılan Gaussian başlangıç koşulu aşağıdaki şekildedir.

$$w_0(x,y) = \sum_{n=0}^{M-1} e^{-A[(x+x_n)^2 + (y+y_n)^2] + i\theta_n} \quad (6)$$

Burada x_n, y_n solitonların yerini, θ_n faz farkını, M soliton sayısını (temel, dipol, çoklu) belirlemek için kullanılır. A değeri, solitonu belirlenen yere odaklamak ve yakınsaklığı sağlamak için kullanılır.

SR algoritması çalışmanın her aşamasında soliton çözüm elde ederken kullanılmaktadır.

Elde edilen soliton çözümlerin doğrusal ve eğrisel kararlılık analizleri için kullanılan sayısal yöntemler ayrıca açıklanmıştır. Kararlılık analizi yapılmadan önce soliton gücü (P) ile kararlılığı arasındaki ilişkiyi ortaya koyan Vakhitov-Kolokolov (VK) kararlılık kriterleri açıklanmıştır.

Güç (P) – özdeğer (μ) analizi yapıldıktan sonra NLSM sisteminin ana denklemindeki mekansal türevler (u_{xx} ve u_{yy}) sonlu farklar yöntemiyle doğrudan çözülüp solitonlar z eksenini boyunca dördüncü dereceden Runge-Kutta yöntemiyle ilerletilerek solitonların eğrisel kararlılığının sayısal analizi yapılmıştır. Eğrisel kararlılık analizi yapılırken SR yöntemi ile elde edilen temel solitonun genliğine ve fazına %1 gürültü (noise) eklenmiştir.

Doğrusal kararlılık analizi için SR yöntemiyle elde edilen temel soliton pertürbe edilip çözüm etrafında doğrusallaştırılmıştır.

Kullanılacak sayısal yöntemler açıklandıktan sonra ilk olarak NLSM sistemi için periyodik potansiyelin olduğu veya olmadığı durumlarda soliton çözüm elde edilebileceği gösterilmiştir. NLSM sisteminde yer alan parametrelerin (ρ , ν) çeşitli değerleri için bant yapısı ve güç analizleri karşılaştırmalı olarak ortaya konmuştur.

SR yöntemi kullanılarak elde edilen bu temel solitonların doğrusal ve eğrisel kararlılık analizleri yapılmıştır. Potansiyelin olduğu ve olmadığı durumlarda temel solitonların doğrusal olarak kararsız oldukları belirlenmiştir. Sonrasında, potansiyelin olmadığı durumda elde edilen kararsız solitonların periyodik potansiyelin varlığında eğrisel kararlılığa sahip olabilecekleri ortaya konmuştur.

Ayrıca NLSM sisteminde elde edilen solitonların şekli (mod profili) ile kararlılığı arasındaki bağlantı gözlenmiştir. Potansiyelin var olduğu durumda kararsız olan solitonların daha derin potansiyel içindeki davranışları incelenmiş ve derin potansiyelin kararsız solitonları kararlı hale getirebileceği (veya çökmeyi geciktirebileceği) saptanmıştır. Bu bölümün sonunda NLSM sisteminde ikili (dipol) solitonlar elde edilmiş ve kararlılıkları incelenmiştir.

Sonraki bölümde, periyodik ve periyodik olmayan (düzensizlik içeren) potansiyellerin varlığında NLS denkleminin ikili (dipol) ve çoklu (vorteks) soliton çözümleri incelenmiştir. Boşluk düzensizliği (vacancy defect) içeren potansiyel ile sınır düzensizliği (edge dislocation) içeren potansiyel ayrı ayrı ele alınmıştır. Bu potansiyellerin maksimumlarına ve minimumlarına odaklanan ikili ve çoklu solitonlar elde edilmiştir. Maksimuma odaklanan tüm solitonların kararsız oldukları görülürken, minimuma odaklanan solitonların belirli koşullar altında eğrisel kararlılığa sahip olabilecekleri ortaya konmuştur.

Elde edilen solitonların güç analizlerinden yola çıkarak kararlılık analizi sonuçlarının VK kararlılık kriterleri ile uyum içinde olduğu tespit edilmiştir. Sınır düzensizliği içeren potansiyelin daha güçlü bir düzensizlik yarattığı ve bu potansiyel için kararlı soliton elde etmenin boşluk düzensizliğine göre daha zor olduğu gözlenmiştir.

NLS denklemi için düzensiz potansiyellerin varlığında eğrisel olarak kararlı çözümler elde edildikten sonra NLSM sistemi için boşluk düzensizliği içeren potansiyelin varlığında temel, ikili ve çoklu solitonların elde edilebileceği ve bu soliton yapılarının belirli koşullar altında eğrisel kararlılığa sahip olabilecekleri gösterilmiştir.

Bu analizlerden yola çıkılarak, boşluk düzensizliği içeren potansiyelin varlığında, NLS denklemi ve NLSM sisteminin bant yapıları ve soliton güçleri karşılaştırılmıştır. Karşılaştırma sonucunda, ele alınan modellerin bant yapıları benzer olsa da soliton güçleri arasında önemli farklar olduğu görülmüştür.

Çalışmanın son bölümünde karmaşık (kompleks) değerli (\mathcal{PT} -simetrik) potansiyellerin varlığında NLS denkleminin soliton çözümleri incelenmiştir. Burada periyodik \mathcal{PT} -simetrik potansiyel ile boşluk düzensizliği içeren \mathcal{PT} -simetrik potansiyelin varlığında temel solitonlar elde edilmiştir. Bu solitonların doğrusal kararlılıklarını test etmek için doğrusal tayfları (spektrumları) incelenmiştir. Eğrisel kararlılık analizleri iki durum için karşılaştırmalı olarak yapılmış ve her bir durum için solitonların kararsız oldukları görülmüştür. Karşılaştırma sonucunda boşluk düzensizliğinin olduğu durumda elde edilen solitonların ilerleme mesafelerinin periyodik potansiyel solitonlarına göre daha uzun olduğu (daha geç çöktükleri) tespit edilmiştir. Ayrıca potansiyel içindeki sanal kısmın derinliği arttıkça elde edilen solitonların ilerleme mesafelerinin kısaldığı (daha hızlı çöktükleri veya patladıkları) saptanmıştır.

Tezin sonuç bölümünde, NLS denklemleri ve NLSM sistemi için elde edilen sonuçlar özetlenmiş ve sonraki çalışmalar için öneriler ortaya konmuştur.

1. INTRODUCTION

The theoretical and experimental studies on nonlinear waves have a significant importance and arise in many branches of science, from applied mathematics and physics to chemistry and biology. The solutions of the governing nonlinear wave equations often exhibit important phenomena, such as stable localized waves (e.g., solitons) or self-similar structures and wave collapse (i.e., blow-up) [1–11].

The soliton theory is an interdisciplinary topic, where many ideas from mathematical physics, nonlinear optics, solid state physics and quantum theory are mutually benefited from each other. Solitons are localized nonlinear waves and their properties have provided a deep and fundamental understanding of complex nonlinear systems.

It is known that a large number of the nonlinear evolution equations (models) admit soliton solutions as numerical methods (calculations) and theoretical analysis confirm. Solitary waves have the striking property that the shape of wave is kept stable after interaction. This is similar to the elastic collision of particles. In 1965, Kruskal and Zabusky discovered that the pulse-like solitary wave solution to the Korteweg-de Vries (KdV) equation had a property which was previously unknown: namely, that this solution interacted elastically with another such solution [12]. They termed these solutions as solitons.

In 1976, a different method was introduced by Petviashvili to construct localized solutions in the two dimensional Korteweg-de Vries equation [13]. Petviashvili's method can be successfully applied to nonlinear systems only if the degree of the nonlinearity is fixed in the associated evolution equation. In fact, in nonlinear optics, many equations involve nonlinearities with different homogeneities, such as cubic-quintic, or even lack of homogeneity, as in saturable nonlinearity [14–16].

The next significant improvement in this direction was made by Zakharov and Shabat [17], they showed that by method similar to the KdV equation, the nonlinear Schrödinger equation (NLSE) can be integrated (see also [18–20]). The NLSE is given

as

$$iu_z(x, y, z) + \Delta u + |u|^2 u = 0, \quad u(x, y, 0) = u_0(x, y), \quad (1.1)$$

where u is the slowly-varying envelope of the wave, z is the direction of propagation, (x, y) are the transverse directions, and u_0 is the initial condition.

In 1965, Kelley [21] carried out direct numerical calculations for the NLSE and these calculations indicated the possibility of wave collapse. Vlasov *et al.* [22], by using the Virial Theorem, demonstrated that the solution of the NLSE can become singular in finite distance (or time). On the contrary, Weinstein [23] showed that when the power (which is also conserved) is sufficiently small, then the solution exists globally, i.e., for all $z > 0$.

In recent years there has been considerable interest in the study of solitons in systems with various types of lattices, in particular those that can be generated in nonlinear optical materials [24, 25]. Ablowitz *et al.* investigated fundamental, dipole and vortex soliton solutions of the focusing cubic $(2 + 1)$ -dimensional NLSE with periodic and quasicrystal (e.g., Penrose) potentials [14, 15].

On the other hand, in many applications, the leading nonlinear polarization effect in an optical material is quadratic; they are referred to as $\chi^{(2)}$ materials (e.g., uniaxial tetragonal 4mm material like BaTiO₃, SBN and KTN) [26]. It is shown that the pulse dynamics in multidimensional nonresonant $\chi^{(2)}$ materials cannot be generally described by the NLSE (1.1) [27–29]. These dynamics are governed by generalized NLSE with coupling to a mean term (hereafter denoted as NLSM systems). NLSM systems are sometimes referred to as Benney and Roskes (BR) or Davey and Stewartson (DS) type [30–32].

NLSM system is physically derived from an expansion of the slowly-varying wave amplitude in the first and second harmonics of the fundamental frequency and a mean term. This system describes the nonlocal-nonlinear coupling between a dynamic field that is related with the first harmonic and a static field that is related with the mean term [33]. The general NLSM system is given by

$$iu_z + \sigma \Delta u + |u|^2 u - \rho \phi u = 0, \quad \phi_{xx} + \nu \phi_{yy} = (|u|^2)_{xx} \quad (1.2)$$

where $u(x, y, z)$ is the normalized amplitude of the envelope of the electric field (which is associated with the first-harmonic), $\phi(x, y, z)$ is the normalized static field, ρ is a

coupling constant that comes from the combined optical rectification and electro-optic effects, and ν is the coefficient that comes from the anisotropy of the material (see [27, 28, 34]).

It is well known that the (1+1)-dimensional NLSM equation is integrable whereas (2+1)-dimensional model is integrable only in a certain parameter regime, namely for $\rho = 2$ and $\nu = -1$. In our case, ν corresponds to asymmetry parameter which comes from the anisotropy of the material and is positive. Therefore, the system we deal with is not integrable even without an external lattice which will be the case in this study. It is also known that higher dimensional NLSM systems suffer from collapse.

The NLSM system (1.2) reduces to the NLSE when $\rho = 0$, because in that case the mean field ϕ does not couple to the first harmonic u . Furthermore, when $\nu = 0$ the system reduces to a classical NLSE with the cubic term $(1 - \rho) |u|^2 u$. In optics $\rho > 0$, whereas in water waves $\rho < 0$.

1.1 Purpose of Thesis

An important challenge in nonlinear science is to find out mechanisms arresting wave collapse. Recently, wave collapse and the role of ground-state on global-existence theory have been investigated for the NLSM systems [33], the results of this study have shown that there is a striking mathematical similarity between collapse dynamics in the NLSE and NLSM cases. Furthermore, in [35–38], it was pointed out that NLSM collapse can be arrested by small nonlinear saturation.

Another way of arresting wave collapse is adding an external potential (lattice) to the governing equation (model). In recent years, there has been considerable interest in the study of solitons in various type external lattices for the NLSE [14, 15, 24, 25]. On the other hand, NLSM systems with additional external potentials have not been studied in current literature yet. The NLSM system with an external potential is given by

$$iu_z + \frac{1}{2}\Delta u + |u|^2 u - \rho\phi u - V(x, y)u = 0, \quad \phi_{xx} + \nu\phi_{yy} = (|u|^2)_{xx}. \quad (1.3)$$

Here, by setting $\rho = 0$, the NLSE with an external potential can be obtained. $V(x, y)$ is an external optical potential that can be written as the intensity of a sum of

phase-modulated plane waves [25]

$$V(x, y) = \frac{V_0}{N^2} \left| \sum_{n=0}^{N-1} e^{i(k_x^n x + k_y^n y)} \right|^2 \quad (1.4)$$

where $V_0 > 0$ is constant and corresponds to the peak depth of the potential, i.e., $V_0 = \max_{x,y} V(x, y)$, $(k_x^n, k_y^n) = [K \cos(2\pi n/N), K \sin(2\pi n/N)]$ is a wave vector. The potentials for $N = 2, 3, 4, 6$ yield periodic lattices that correspond to standard 2D crystal structures, whereas $N = 5, 7$ correspond to quasicrystals. The lattice-free medium can be obtained by setting $V_0 = 0$.

In this study, we aim to investigate the existence and stability properties of solitons in the (2+1)-dimensional NLSE and NLSM system with various types of external lattices. This dissertation is organized as follows.

Chapter 2 describes the derivation of the NLSE and NLSM system. Derivation of the governing equations (models) helps us to understand the physical aspects of our study.

In Chapter 3, a numerical algorithm which is a modification of Spectral Renormalization (SR) method [39] is explained at the beginning. This algorithm will be used on each stage of the study to compute solutions of the models (NLSE and NLSM systems). Then, numerical methods for investigating the stability properties of solitons are given.

Chapter 4 is dedicated to the fundamental and dipole solitons in the NLSM system. First we demonstrate the existence of solitons and examine the stability properties of these solitons in the lattice-free medium. Then we explain the effect of a periodic external potential as a collapse arrest mechanism in the NLSM system. The results of this part are considered as the main contribution to the thesis.

Chapter 5 includes the multi-humped structures (dipoles and vortices) that are obtained in the NLSE with defective lattices. This part of the study has been published in journal of "Optics Communications" under the title of "Vortex and Dipole Solitons in Lattices Possessing Defects and Dislocations" [40]. The NLSE is a special form of the NLSM system. Therefore, understanding the dynamics of dipoles and vortices in the NLSE can be considered as a fundamental step for the NLSM system.

In Chapter 6, we investigate the fundamental and dipole solitons in the NLSM system with a vacancy defect in the light of Chapter 5. Solitons in defective lattices have a

significant importance in nonlinear science, this part of the study helps us to understand the effects of defects on the soliton properties in the NLSM system.

In Chapter 7, the existence and stability properties of fundamental solitons in the (2+1)-dimensional NLSE with a defective \mathcal{PT} -Symmetric external potential are demonstrated. This part of the study has also been published in journal of "Optics Communications" under the title of "Fundamental Solitons in Parity-Time Symmetric Lattice with a Vacancy Defect" [41].

In the final part, results of this dissertation are summarized.

1.2 Literature Review

Nonlinear wave problems are of wide physical and mathematical interest and arise in a variety of scientific fields such as nonlinear optics, fluid dynamics, plasma physics, etc. [1–11].

NLSM equations were originally derived by Benney and Roskes [30] for a finite water depth of h ignoring surface tension effect. In 1974, Davey and Stewartson [31] studied the evolution of a 3D wave packet for a finite water depth and obtained an equivalent form of these equations. The integrability of the NLSM system was studied in 1975 by Ablowitz and Haberman [42] for the shallow water limit. In 1977, the results of Benney and Roskes extended to account for surface tension by Djordevic and Reddekopp [43]. Ablowitz *et al.* [27,28] found, from first principles, that NLSM type equations describe the evolution of the electromagnetic field in a quadratically polarized media.

The results of Papanicolaou *et al.* [44] reveal that, similar to the NLSE collapse, the NLSM collapse occurs with a modulated profile. Physical mechanisms that arrest the collapse have been studied extensively in nonlinear optics, e.g., nonlinear saturation [35–38]. Merle and Raphael [45] investigated the collapse behaviour of the NLSE and other related equations in detail. Furthermore, Gaeta and coworkers [46] carried out detailed optical experiments that reveal the nature of the singularity formation in cubic media and showed experimentally that collapse occurs with a self-similar profile.

Recently, the regions of collapse were investigated by Crasovan *et al.* [34] for various ρ and ν values. In the aforementioned work, for simplicity, only the nonlinear evolution of an initial Gaussian beam with various input powers and/or beam ellipticity has

been considered instead of the solution of the NLSM equation, and it is shown that by increasing the parameter ρ or by considering an initially highly elliptic beam, the sudden increment of the soliton amplitude can be suppressed. However, during the evolution, just after few diffraction units (around $z = 5$), the localization of the mode is lost as the mode starts to spread out.

1.3 Hypothesis

The effect of external potentials on the existence and stability of fundamental solitons is important in many applications. NLSM (or DS type) systems with additional external potentials has not been investigated in current literature yet. In this dissertation, we will first numerically show the existence of fundamental solitons in various external potentials for the NLSM systems and then explore the properties of those solitons in detail. We expect that, wave collapse can be arrested in the NLSM systems by adding an external lattice.

2. DERIVATION OF THE NLSM EQUATIONS

An important and rich area of application of nonlinear wave propagation is the field of nonlinear optics. Asymptotic methods play an important role in this field. For example, since the scales are so disparate in Maxwell's equations, long-distance transmission in fiber optic communications depends critically on asymptotic models. Hence the NLSE is central for understanding phenomena and detailed descriptions of the dynamics [29]. Herein, we will outline the derivation of the NLSE and NLSM system.

2.1 Maxwell Equations

We begin by considering Maxwell's equations for electromagnetic waves with no source charges or currents [47, 48],

$$\nabla \times \mathbf{H} = \frac{\partial \mathbf{D}}{\partial t} \quad (2.1)$$

$$\nabla \times \mathbf{E} = -\frac{\partial \mathbf{B}}{\partial t} \quad (2.2)$$

$$\nabla \cdot \mathbf{D} = 0 \quad (2.3)$$

$$\nabla \cdot \mathbf{B} = 0 \quad (2.4)$$

where \mathbf{H} is the magnetic field, \mathbf{E} is the electromagnetic field, \mathbf{D} is the electromagnetic displacement and \mathbf{B} is the magnetic induction. We first consider non-magnetic media so there is no magnetization term in \mathbf{B} . The magnetic induction \mathbf{B} and magnetic field \mathbf{H} are then related by

$$\mathbf{B} = \mu_0 \mathbf{H}. \quad (2.5)$$

The constant μ_0 is the magnetic permeability of free space. We allow for induced polarization of the media giving rise to the following relation

$$\mathbf{D} = \epsilon_0 (\mathbf{E} + \mathbf{P}), \quad (2.6)$$

where ϵ_0 is the electric permittivity of free space, a constant. When we apply an electric field \mathbf{E} to an ideal dielectric material a response of the material can occur and

the material is said to become polarized. Typically in these materials the electrons are tightly bound to the nucleus and a displacement of these electrons occurs. The macroscopic effect (summing over all displacements) yields the induced polarization \mathbf{P} .

Since we are working with non-magnetic media, we can reduce Maxwell's equations to those involving only the electromagnetic field \mathbf{E} and the polarization \mathbf{P} . To that end, we take the curl of Eq. (2.2) and use Eq. (2.5) and Eq. (2.1) to find

$$\begin{aligned}\nabla \times (\nabla \times \mathbf{E}) &= -\frac{\partial}{\partial t} (\nabla \times \mathbf{B}) \\ &= -\mu_0 \frac{\partial}{\partial t} (\nabla \times \mathbf{H}) \\ &= -\mu_0 \frac{\partial^2}{\partial t^2} \mathbf{D}.\end{aligned}$$

The vector identity

$$\nabla \times (\nabla \times \mathbf{E}) = \nabla (\nabla \cdot \mathbf{E}) - \nabla^2 \mathbf{E}, \quad (2.7)$$

is useful here. With this, along with relation (2.6), we find the following equations for the electromagnetic field

$$\begin{aligned}\nabla^2 \mathbf{E} - \nabla (\nabla \cdot \mathbf{E}) &= \frac{1}{c^2} \frac{\partial^2}{\partial t^2} (\mathbf{E} + \mathbf{P}(\mathbf{E})) \\ \nabla \cdot (\mathbf{E} + \mathbf{P}(\mathbf{E})) &= 0,\end{aligned} \quad (2.8)$$

where the constant c^2 is the square of the speed of light in a vacuum;

$$c^2 = \frac{1}{\mu_0 \epsilon_0}. \quad (2.9)$$

Notice that we have made explicit the connection between the polarization \mathbf{P} and the electromagnetic field \mathbf{E} .

2.2 Polarization

In homogeneous, non-magnetic media, matter responds to intense electromagnetic fields in a nonlinear manner. In order to model this, we use a well-known relationship between the polarization vector \mathbf{P} and the electromagnetic field \mathbf{E} that is a good approximation to a wide class of physically relevant media [29]:

$$\mathbf{P}(\mathbf{E}) = \int \chi^{(1)} * (\mathbf{E}) + \int \chi^{(2)} * (\mathbf{E}\mathbf{E}) + \int \chi^{(3)} * (\mathbf{E}\mathbf{E}\mathbf{E}) \quad (2.10)$$

where $\chi^{(1)}$ is the linear susceptibility, $\chi^{(2)}$ is the second order susceptibility (which describes second harmonic generation or quadratic nonlinearity) and $\chi^{(3)}$ is the third order susceptibility (which describes third harmonic generation or cubic nonlinearity). $\chi^{(1)}$, $\chi^{(2)}$ and $\chi^{(3)}$ tensors are (3x3), (3x9) and (3x27) matrices, respectively.

Notice that we can break up Eq. (2.10) into a linear and nonlinear part ($\mathbf{P} = \mathbf{P}_L + \mathbf{P}_{NL}$). Also, it involves tensors, so the operation $*$ is a special type of convolution that is defined as follows [27–29, 49, 50]

$$P_{L,i} = \left(\chi^{(1)} * (\mathbf{E}) \right)_i = \sum_{j=1}^3 \int_{-\infty}^{\infty} \chi_{ij}^{(1)}(t - \tau) E_j(\tau) d\tau \quad (2.11)$$

$$P_{NL,i}^{(2)} = \left(\chi^{(2)} * (\mathbf{E}\mathbf{E}) \right)_i = \sum_{j,k} \int_{-\infty}^{\infty} \chi_{ijk}(t - \tau_1, t - \tau_2) E_j(\tau_1) E_k(\tau_2) d\tau_1 d\tau_2. \quad (2.12)$$

$$P_{NL,i}^{(3)} = \left(\chi^{(3)} * (\mathbf{E}\mathbf{E}\mathbf{E}) \right)_i = \sum_{j,k,l} \int_{-\infty}^{\infty} \chi_{ijkl}^{(3)}(t - \tau_1, t - \tau_2, t - \tau_3) E_j(\tau_1) E_k(\tau_2) E_l(\tau_3) d\tau_1 d\tau_2 d\tau_3. \quad (2.13)$$

For notational purposes, the polarization vector is written as follows:

$$\mathbf{P} = \begin{pmatrix} P_x \\ P_y \\ P_z \end{pmatrix} \equiv \begin{pmatrix} P_1 \\ P_2 \\ P_3 \end{pmatrix}.$$

In glass, and hence fiber optics, the quadratic term $\chi^{(2)}$ is zero. This is cubically nonlinear and is a so-called “centro-symmetric material” [27, 28, 49, 50].

In Eq. (2.13), the sums are over the indices $\{1, 2, 3\}$ and the integration is over all of \mathbb{R}^3 . If the material is “isotropic”, $\chi_{ij}^{(1)} = 0, i \neq j$ (exhibiting properties with the same values when measured along axes in all directions), then the matrix $\chi^{(1)}$ is diagonal. We will also usually identify subscripts $i = 1, 2, 3$ as $i = x, y, z$. In cubically nonlinear or “Kerr” materials (such as glass), it turns out that the only important terms in the $\chi^{(3)}$ tensor correspond to $\chi_{xxxx}^{(3)}$, which is equal to $\chi_{yyyy}^{(3)}$ and $\chi_{zzzz}^{(3)}$. From now on, we will suppress the superscript in χ when context makes the choice clear. For example $\chi_{xx}^{(1)} = \chi_{xx}$ and $\chi_{xxxx}^{(3)} = \chi_{xxxx}$ follow due to the number of entries in the subscript.

We can now pose the problem of determining the electromagnetic field \mathbf{E} in Kerr media as solving Eq. (2.8) subject to Eq. (2.11) and Eq. (2.13). Consider the asymptotic expansion

$$\mathbf{E} = \varepsilon \mathbf{E}^{(1)} + \varepsilon^2 \mathbf{E}^{(2)} + \varepsilon^3 \mathbf{E}^{(3)} + \dots, |\varepsilon| \ll 1. \quad (2.14)$$

The electric field \mathbf{E} can be expanded in each cartesian component of j as

$$E_j = \varepsilon E_j^{(1)} + \varepsilon^2 E_j^{(2)} + \varepsilon^3 E_j^{(3)} + \dots,$$

and the electric field is given in harmonics as

$$E_j^{(n)}(x, y, z, t) = \sum_{m=-n}^n e^{im\theta} E_{j,m}^{(n)}(X, Y, Z, T)$$

where $\theta = kz - \omega t$ is rapidly varying phase, ω is the central frequency of the pulse, k is the wavenumber and the slowly varying space coordinates are $X = \varepsilon x, Y = \varepsilon y, Z = \varepsilon z, T = \varepsilon t$ [26]. Then, to leading order, we assume that the electromagnetic field is initially polarized along the x -axis; it propagates along the z -axis (no transverse y variations), and for simplicity we define $A(X, Y, Z, T) = E_{x,1}^{(1)}(X, Y, Z, T)$. Hence

$$\mathbf{E}^{(1)} = \begin{pmatrix} E_{x,1}^{(1)} \\ 0 \\ 0 \end{pmatrix}, \quad E_{x,1}^{(1)} = A(X, Z, T) e^{i\theta} + c.c., \quad (2.15)$$

where $c.c.$ denotes the complex conjugate of the preceding term. In order to simplify the calculations, we assume that \mathbf{E} and hence A are independent of y (i.e., $Y = \varepsilon y$).

Derivatives are replaced as follows

$$\begin{aligned} \partial_x &= \varepsilon \partial_X \\ \partial_t &= -\omega \partial_\theta + \varepsilon \partial_T \\ \partial_z &= k \partial_\theta + \varepsilon \partial_Z. \end{aligned} \quad (2.16)$$

Substituting in the asymptotic expansion for \mathbf{E} we note the important simplification that the assumption of slow variation has on the polarization \mathbf{P} :

$$\begin{aligned} P_{L,x} &= \sum_{j=1}^3 \int_{-\infty}^{\infty} \chi_{xj}^{(1)}(t - \tau) E_j(\tau) d\tau \\ &= \varepsilon \int_{-\infty}^{\infty} \chi_{xx}(t - \tau) \left(A(X, Z, T) e^{i(kz - \omega\tau)} + c.c. \right) d\tau + O(\varepsilon^2) \\ &= \varepsilon \int_{-\infty}^{\infty} \chi_{xx}(t - \tau) e^{i\omega(t - \tau)} \left(A(X, Z, T) e^{i(kz - \omega t)} + c.c. \right) d\tau + O(\varepsilon^2). \end{aligned}$$

Now make the substitution $t - \tau = u$ to get

$$P_{L,x} = \varepsilon \int_{-\infty}^{\infty} \chi_{xx}(u) e^{i\omega u} \left(A(X, Z, \varepsilon t - \varepsilon u) e^{i(kz - \omega t)} + c.c. \right) du + O(\varepsilon^2).$$

We expand the slowly varying amplitude A around the point εt

$$P_{L,x} = \varepsilon \int_{-\infty}^{\infty} du \chi_{xx}(u) e^{i\omega u} \\ \times \left[\left(1 - \varepsilon u \frac{\partial}{\partial T} + \frac{(\varepsilon u)^2}{2} \frac{\partial^2}{\partial T^2} + \dots \right) A(X, Z, T) e^{i(kz - \omega t)} + c.c. \right] + O(\varepsilon^2).$$

The Fourier transform of χ_{xx} written as $\hat{\chi}_{xx}$ and its derivatives are

$$\hat{\chi}_{xx}(\omega) = \int_{-\infty}^{\infty} \chi_{xx}(u) e^{i\omega u} du \\ \hat{\chi}'_{xx}(\omega) = \int_{-\infty}^{\infty} iu \chi_{xx}(u) e^{i\omega u} du \\ \hat{\chi}''_{xx}(\omega) = \int_{-\infty}^{\infty} -u^2 \chi_{xx}(u) e^{i\omega u} du.$$

Then we can write the linear part of the polarization as

$$P_{L,x} = \varepsilon \left(\hat{\chi}_{xx}(\omega) + \hat{\chi}'_{xx}(\omega) i\varepsilon \partial_T - \hat{\chi}''_{xx}(\omega) \frac{(\varepsilon \partial_T)^2}{2} + \dots \right) (Ae^{i\theta} + c.c.) + O(\varepsilon^2) \\ = \varepsilon \hat{\chi}_{xx}(\omega + i\varepsilon \partial_T) (Ae^{i\theta} + c.c.) + O(\varepsilon^2).$$

The last line is in a convenient notation where the term $\hat{\chi}_{xx}(\omega + i\varepsilon \partial_T)$ is an operator that we can expand around ω to get the previous line. In the nonlinear polarization equation (2.13), there will be interactions due to the leading-order mode $Ae^{i\theta}$ for example, the nonlinear term includes E_x^3 which leads to terms such as $A^3 e^{3i\theta}$. Then we denote the corresponding linear polarization term (containing interaction terms) as

$$P_{L,x}^{\text{interactions}} = \hat{\chi}_{xx}(\omega_m + i\varepsilon \partial_T) (B_m e^{im\theta} + c.c.),$$

where $\omega_m = m\omega$ and B_m contains the nonlinear terms generated by the interaction (e.g. $B_3 = A^3$). Similarly there are nonlinear polarization terms. For example, a typical term in the nonlinear polarization is

$$P_{NL,x} = \varepsilon^3 \hat{\chi}_{xxxx}(\omega_m + i\varepsilon \partial_{T_1}, \omega_n + i\varepsilon \partial_{T_2}, \omega_l + i\varepsilon \partial_{T_3}) \\ \times B_m(T_1) B_n(T_2) B_l(T_3) |_{T_1=T_2=T_3=T} e^{i(m+n+l)\theta + c.c.} \quad (2.17)$$

All other terms are of smaller order $O(\varepsilon^4)$.

2.3 Derivation of the NLSE

So far, we have derived expressions for the polarization with a cubic nonlinearity (third-order susceptibility). Now we will use Eq. (2.8) to derive the NLSE. This will give the leading-order equation for the slowly varying amplitude of the x -component of the electromagnetic field E_x [29].

We begin the derivation of the NLSE by showing that $E_z \ll E_x$. Recall Eq. (2.3) with Eq. (2.6),

$$\nabla \cdot (\mathbf{E} + \mathbf{P}) = 0.$$

Since there is no y dependence, we get

$$\partial_x(E_x + P_x) + \partial_z(E_z + P_z) = 0. \quad (2.18)$$

We assume

$$\begin{aligned} E_x &= \varepsilon A(X, Z, T) e^{i\theta} + c.c. + O(\varepsilon^2) \\ E_z &= \varepsilon A_z(X, Z, T) e^{i\theta} + c.c. + O(\varepsilon^2), \end{aligned} \quad (2.19)$$

Because the x -component of the electromagnetic field E_x appears so often, we label its slowly varying amplitude with A , whereas for the z -component of the E -field, E_z , we label the slowly varying amplitude with A_z (note: A_z does not mean derivative with respect to z). Substituting the derivatives Eq. (2.16) into Eq. (2.18) we find

$$(k\partial_\theta + \varepsilon\partial_z)(E_z + P_z) = -\varepsilon\partial_x(E_x + P_x), \quad (2.20)$$

which, when we use the ansatz (2.19), yields

$$\begin{aligned} &\varepsilon(k\partial_\theta + \varepsilon\partial_z) \left(A_z e^{i\theta} + c.c. + \hat{\chi}_{zz}(\omega + i\varepsilon\partial_T) \left(A_z e^{i\theta} + c.c. \right) \right) \\ &= -\varepsilon\partial_x \left(\varepsilon A e^{i\theta} + c.c. + \hat{\chi}_{xx}(\omega + i\varepsilon\partial_T) \left(\varepsilon A e^{i\theta} + c.c. \right) \right) + \dots \end{aligned}$$

The leading-order equation is

$$\begin{aligned} \varepsilon i k A_z (1 + \hat{\chi}_{zz}(\omega)) &= -\varepsilon^2 \frac{\partial A}{\partial X} (1 + \hat{\chi}_{xx}(\omega)) \\ \rightarrow A_z &= -\varepsilon \frac{1 + \hat{\chi}_{xx}(\omega)}{i k (1 + \hat{\chi}_{zz}(\omega))} \frac{\partial A}{\partial X} \\ &= \frac{-\varepsilon}{i k} \frac{\partial A}{\partial X} = A_X, \quad \text{if } \hat{\chi}_{xx} = \hat{\chi}_{zz}. \end{aligned}$$

Assuming $\partial A / \partial X$ is $O(1)$, this implies $A_z = O(\varepsilon)$, which implies $E_z = O(\varepsilon^2)$. While we used the divergence equation in Eq. (2.8) with Eq. (2.6) to calculate this

relationship, we could have proved the same result with the z -component of the dynamic equation in Eq. (2.8). We also claim that if we had studied the y -component, then it would have followed that $E_y = O(\varepsilon^3)$. Also, $P_{NL,z} = O(\varepsilon^4)$ which is obtained from the symmetry of the third-order susceptibility tensor $\chi^{(3)}$ since $\chi_{zxxx} = 0$, etc. (e.g., for glass).

Now we will use the dynamic equation in Eq. (2.8) to investigate the behavior of the x -component of the electromagnetic field via multiple scales. The dynamic equation (2.8) becomes

$$\nabla^2 E_x - \frac{\partial}{\partial x} \left(\frac{\partial E_x}{\partial x} + \frac{\partial E_z}{\partial z} \right) = \frac{1}{c^2} \frac{\partial^2}{\partial t^2} (E_x + P_x). \quad (2.21)$$

The asymptotic expansions for E_x and E_z take the form

$$\begin{aligned} E_x &= \varepsilon \left(A e^{i\theta} + c.c. \right) + \varepsilon^2 E_x^{(2)} + \varepsilon^3 E_x^{(3)} + \dots \\ E_z &= \varepsilon^2 \left(A_z e^{i\theta} + c.c. \right) + \varepsilon^3 E_z^{(2)} + \dots \end{aligned} \quad (2.22)$$

The polarization in the x -direction depends on the linear and nonlinear polarization terms, $P_{L,x}$ and $P_{NL,x}$, but the nonlinear term comes in at $O(\varepsilon^3)$ due to the cubic nonlinearity. Explicitly, we have

$$P_x = \varepsilon \left(\hat{\chi}_{xx}(\omega) + \hat{\chi}'_{xx}(\omega) i \varepsilon \partial_T - \frac{\hat{\chi}''_{xx}(\omega)}{2} \varepsilon^2 \partial_T^2 + \dots \right) \left(A e^{i\theta} + c.c. \right) + P_{NL,x}. \quad (2.23)$$

Expanding the derivatives and using Eq. (2.16) in Eq. (2.21) gives

$$\begin{aligned} &\left((k\partial_\theta + \varepsilon\partial_Z)^2 + \varepsilon^2 \partial_X^2 \right) E_x - \varepsilon \partial_X (\varepsilon \partial_X E_x + (k\partial_\theta + \varepsilon\partial_Z) E_z) \\ &= \frac{1}{c^2} (-\omega\partial_\theta + \varepsilon\partial_T)^2 (E_x + P_{L,x} + P_{NL,x}). \end{aligned} \quad (2.24)$$

The leading-order equation is

$$O(\varepsilon): \quad \left(-k^2 + \left(\frac{\omega}{c} \right)^2 \right) A = - \left(\frac{\omega}{c} \right)^2 \hat{\chi}_{xx}(\omega) A.$$

Since we assume $A \neq 0$ the above equation determines the dispersion relation; namely solving for $k(\omega)$ we find the dispersion relation

$$\begin{aligned} k^2 &= \left(\frac{\omega}{c} \right)^2 (1 + \hat{\chi}_{xx}(\omega)) \\ k(\omega) &= \frac{\omega}{c} (1 + \hat{\chi}_{xx}(\omega))^{1/2} \\ &\equiv \frac{\omega}{c} n_0(\omega). \end{aligned} \quad (2.25)$$

The term $n_0(\omega)$ is called the linear index of refraction; if it were constant then c/n_0 would be the "effective speed of light". The slowly varying amplitude $A(X, Z, T)$ is

still free and will be determined by going to higher order terms and removing secular terms.

From Eq. (2.24) and the asymptotic expansions for E_x and $P_{L,x}$ in Eq. (2.22) and (2.23) (the nonlinear polarization term, $P_{NL,x}$, does not come in until the next order), we find [29]

$$\begin{aligned} O(\varepsilon^2) : & \left(k^2 - \left(\frac{\omega}{c} \right)^2 \right) \partial_\theta^2 E_x^{(2)} \\ & = \left[-2ik \partial_Z A - \frac{2i\omega}{c^2} (1 + \hat{\chi}_{xx}(\omega)) \partial_T A - \left(\frac{\omega}{c} \right)^2 i \hat{\chi}'_{xx}(\omega) \partial_T A \right] e^{i\theta}. \end{aligned}$$

To remove secularities, we must equate the terms in brackets to zero. This can be written as

$$2k \frac{\partial A}{\partial Z} + \left(\frac{2\omega}{c^2} (1 + \hat{\chi}_{xx}(\omega)) + \left(\frac{\omega}{c} \right)^2 \hat{\chi}'_{xx}(\omega) \right) \frac{\partial A}{\partial T} = 0. \quad (2.26)$$

Notice that if we differentiate the dispersion relation (2.25) with respect to ω we find

$$2kk' = \frac{2\omega}{c^2} (1 + \hat{\chi}_{xx}(\omega)) + \left(\frac{\omega}{c} \right)^2 \hat{\chi}'_{xx}(\omega).$$

This means that we can rewrite Eq. (2.26) in terms of the group velocity $v_g = 1/k'(\omega)$

$$\frac{\partial A}{\partial Z} + \frac{1}{v_g} \frac{\partial A}{\partial T} = 0. \quad (2.27)$$

To obtain a more accurate equation for the slowly varying amplitude A , we will now remove secular terms at the next order and obtain the NLSE.

As before, we perturb Eq. (2.27)

$$2ik \left(\frac{\partial A}{\partial Z} + \frac{1}{v_g} \frac{\partial A}{\partial T} \right) = \varepsilon f_1 + \varepsilon^2 f_2 + \dots.$$

Using this and Eq. (2.24) to $O(\varepsilon^3)$ and then choosing f_1 to remove secular terms, we find after some calculation

$$\begin{aligned} O(\varepsilon^3) : & 2ik \left(\frac{\partial A}{\partial Z} + k'(\omega) \frac{\partial A}{\partial T} \right) \\ & + \varepsilon \left[\partial_X^2 + \partial_Z^2 - \frac{1}{c^2} \left(1 + \hat{\chi}_{xx}(\omega) + 2\omega \hat{\chi}'_{xx}(\omega) + \frac{1}{2} \omega^2 \hat{\chi}''_{xx}(\omega) \right) \partial_T^2 \right] A \\ & + 3\varepsilon \left(\frac{\omega}{c} \right)^2 \hat{\chi}_{xxx}(\omega, \omega, -\omega) |A|^2 A = 0. \end{aligned} \quad (2.28)$$

We now see in Eq. (2.28) a term due to the nonlinear polarization $P_{NL,x}$ i.e., the term with $\hat{\chi}_{xxx}(\omega, \omega, -\omega)$. In fact, there are three choices for m, n, p in the leading-order term for the nonlinear polarization [recall Eq. (2.17)] that give rise to the exponential

$e^{i\theta}$ (the coefficient of $e^{i\theta}$ is the only term that induces secularity). Namely, two of these integers are +1 and the other one is -1. In the bulk media we are working in, the third-order susceptibility tensor is the same in all cases. This means

$$\begin{aligned}\hat{\chi}_{xxxx}(\omega, \omega, -\omega) + \hat{\chi}_{xxxx}(\omega, -\omega, \omega) + \hat{\chi}_{xxxx}(-\omega, \omega, \omega) \\ = 3\hat{\chi}_{xxxx}(\omega, \omega, -\omega) \\ \equiv 3\hat{\chi}_{xxxx}(\omega).\end{aligned}$$

Let us investigate the coefficient of A_{TT} that arises from the linear polarization. If we differentiate the dispersion relation (2.25) two times with respect to ω we get the following result

$$k^2 + kk'' = \frac{1}{c^2} \left(1 + \hat{\chi}_{xx}(\omega) + 2\omega\hat{\chi}'_{xx}(\omega) + \frac{1}{2}\omega^2\hat{\chi}''_{xx}(\omega) \right).$$

Then we can conveniently rewrite the linear polarization term as

$$\varepsilon \left[\partial_X^2 + \partial_Z^2 - (k'^2 + kk'') \partial_T^2 \right] A.$$

Now, make the following change of variable

$$\xi = T - k'(\omega)Z, \quad Z' = \varepsilon Z$$

$$\partial_Z = -k'\partial_\xi + \varepsilon\partial_{Z'}, \quad \partial_T = \partial_\xi.$$

Substituting this into the third-order equation (2.28), we find

$$2ik\frac{\partial A}{\partial Z'} + \frac{\partial^2 A}{\partial X^2} - kk''\frac{\partial^2 A}{\partial \xi^2} + 2k\nu|A|^2A = 0. \quad (2.29)$$

Here we took

$$\nu = \frac{3(\omega/c)^2\hat{\chi}_{xxxx}(\omega)}{2k}. \quad (2.30)$$

It is useful to note that had we included variation in the y-direction, then the term $\partial^2 A/\partial Y^2$ would be added to Eq. (2.29) and we would have found

$$2ik\frac{\partial A}{\partial Z'} + \nabla^2 A - kk''\frac{\partial^2 A}{\partial \xi^2} + 2k\nu|A|^2A = 0, \quad (2.31)$$

Where

$$\nabla^2 A = \frac{\partial^2 A}{\partial X^2} + \frac{\partial^2 A}{\partial Y^2}.$$

If there is no variation in the X-direction then we get the (1+1)-dimensional (one space dimension and one time dimension) NLSE describing the slowly varying wave amplitude A of an electromagnetic wave in cubically nonlinear bulk media

$$i\frac{\partial A}{\partial Z} + \left(\frac{-k''(\omega)}{2} \right) \frac{\partial^2 A}{\partial \xi^2} + \nu|A|^2A = 0, \quad (2.32)$$

where we have removed the prime from Z' for convenience [29].

2.4 Derivation of the NLSE with Mean Terms (NLSM)

We will discuss the effects of including a nonzero quadratic nonlinear polarization. This implies that the second-order susceptibility tensor $\chi^{(2)}$ in the nonlinear polarization is non-zero.

Recall the definition of the nonlinear polarization for quadratic and cubic media is written schematically as,

$$\mathbf{P}_{NL}(\mathbf{E}) = \int \chi^{(2)} * (\mathbf{E}\mathbf{E}) + \int \chi^{(3)} * (\mathbf{E}\mathbf{E}\mathbf{E})$$

and the i th component of the quadratic term in the nonlinear polarization is

$$P_{NL,i}^{(2)} = \left(\chi^{(2)} * (\mathbf{E}\mathbf{E}) \right)_i = \sum_{j,k} \int_{-\infty}^{\infty} \chi_{ijk}(t - \tau_1, t - \tau_2) E_j(\tau_1) E_k(\tau_2) d\tau_1 d\tau_2. \quad (2.33)$$

In the derivation of the nonlinear Schrödinger equation with cubic nonlinearity, the nonlinear terms entered the calculation at third order. The multi-scale procedure for $\chi^{(2)} \neq 0$ follows the same lines as before:

$$\mathbf{E} = \varepsilon \mathbf{E}^{(1)} + \varepsilon^2 \mathbf{E}^{(2)} + \varepsilon^3 \mathbf{E}^{(3)} + \dots$$

$$\mathbf{E}^{(1)} = \begin{pmatrix} E_x^{(1)} \\ 0 \\ 0 \end{pmatrix}$$

$$E_x^{(1)} = A(X, Y, Z, T) e^{i\theta} + c.c.,$$

see Eq. (2.14) and Eq. (2.15); to be general, we allow the amplitude A to depend on $X = \varepsilon x$, $Y = \varepsilon y$, $Z = \varepsilon z$ and $T = \varepsilon t$. The new terms of interest due to the quadratic nonlinearity are [27, 28]:

$$E_x^{(2)} = 4 \left(\frac{\omega}{c} \right)^2 \frac{\hat{\chi}_{xxx}}{\Delta(\omega)} \left(A^2 e^{2i\theta} + c.c. \right) + \phi_x$$

$$E_y^{(2)} = \phi_y$$

$$E_z^{(2)} = i \frac{n_x^2}{kn_z^2} \frac{\partial A}{\partial X} e^{i\theta} + c.c. + \phi_z$$

$$n_x^2 = 1 + \hat{\chi}_{xx}(\omega), \quad n_z^2 = 1 + \hat{\chi}_{zz}(\omega), \quad k = \frac{\omega}{c} n_x(\omega)$$

$$\Delta(\omega) = \left[(2k(\omega))^2 - (k(2\omega))^2 \right] \neq 0.$$

We assume that $\chi_{yy} = \chi_{xx}$. Notice the inclusion of "mean" terms ϕ_x, ϕ_y, ϕ_z . If $|\Delta(\omega)| \ll 1$ then second harmonic resonance generation occurs [51]. We will assume that $\Delta(\omega) \neq 0$ and $\Delta(\omega)$ is not small.

In the derivation of NLSE for cubic media, the only term at third order that gave rise to secularity was $e^{i\theta}$. Now, at third order, we have two sources for secularity, $e^{i\theta}$ and the mean term e^{i0} . Removing these secular terms in the usual way as before leads to the following equations:

$$O(\varepsilon^3) : \quad e^{i\theta} \rightarrow 2ik\partial_Z A + \left(\partial_X^2 + \partial_Y^2 - kk''\partial_\xi^2\right) A + \left(M_1|A|^2 + M_0\phi_x\right) A = 0 \quad (2.34)$$

$$e^{i0} \rightarrow \left(\alpha_x\partial_X^2 + \partial_Y^2 + s_x\partial_\xi^2\right) \phi_x - \left(N_1\partial_\xi^2 - N_2\partial_X^2\right) |A|^2 = 0. \quad (2.35)$$

In this, the change of variable, $\xi = T - k'(\omega)Z$, was made and the following definitions used:

$$\begin{aligned} M_0 &= 2\left(\frac{\omega}{c}\right)^2 \hat{\chi}_{xxx}(\omega, 0), \\ M_1 &= 3\left(\frac{\omega}{c}\right)^2 \hat{\chi}_{xxx}(\omega, \omega, -\omega) + \frac{8(\omega/c)^4 \hat{\chi}_{xxx}(2\omega, -\omega) \hat{\chi}_{xxx}(\omega, \omega)}{\Delta(\omega)}, \\ N_1 &= \frac{2}{c^2} \hat{\chi}_{xxx}(\omega, -\omega), \quad N_2 = \frac{c^2 N_1}{1 + \hat{\chi}_{xx}(\omega)}, \\ \alpha_x &= \frac{1 + \hat{\chi}_{xx}(\omega)}{1 + \hat{\chi}_{zz}(\omega)}, \quad s_x = k'(\omega)^2 - \frac{1 + \hat{\chi}_{xx}(\omega)}{c^2}. \end{aligned}$$

There are several things to notice. First, if $\hat{\chi}_{xxx} = 0$ then $N_1 = N_2 = M_0 = 0$, $M_1 = 2(\omega/c)^2 \hat{\chi}_{xxx}(\omega, -\omega)$. Thus Eq. (2.34) reduces to the NLSE obtained earlier for cubic media. Since Eq. (2.34) of NLSE-type but includes a mean term ϕ_x we call it the NLSE with mean (NLSM). We must solve these coupled equations (2.34) and (2.35) for ϕ_x and A . It turns out, when $\chi_{xx} = \chi_{yy}$ that the mean terms ϕ_y, ϕ_z decouple from the ϕ_x equation and they can be solved in terms of ϕ_x and A [27, 28]. These equations, (2.34) and (2.35), are a three-dimensional generalization of the BR type equations [30]. Moreover, when A is independent of time, t , i.e., independent of ξ , then equations (2.34) and (2.35) are (2+1)-dimensional and reduce to the BR form and wave collapse is possible [33].

3. NUMERICAL METHODS

3.1 Spectral Renormalization Method

In order to compute localized solutions (i.e., soliton solutions) to nonlinear evolution equations, various techniques have been used. Ablowitz and Musslimani [39] proposed a generalized numerical scheme for computing solitons in nonlinear wave guides called Spectral Renormalization (SR). The essence of the method is to transform the governing equation into Fourier space and find a nonlinear nonlocal integral equation coupled to an algebraic equation. The coupling prevents the numerical scheme from diverging. The optical mode is then obtained from an iteration scheme, which converges rapidly. This method can efficiently be applied to a large class of problems including higher order nonlinear terms with different homogeneities.

In this work, we use a modification of the spectral renormalization method with which we can compute localized solutions in the NLSM system. The NLSM system with an external potential is given by

$$\begin{aligned} iu_z + \sigma \Delta u + |u|^2 u - \rho u \phi - V(x, y)u &= 0 \\ \phi_{xx} + \nu \phi_{yy} &= \left(|u|^2 \right)_{xx}. \end{aligned} \quad (3.1)$$

We seek a soliton solution of system (3.1) in the form $u(x, y, z) = f(x, y)e^{-i\mu z}$ where $f(x, y)$ is a complex-valued function and μ is the propagation constant (or eigenvalue). Substituting this form of solution into system (3.1), the following nonlinear eigenequation for f is obtained

$$\begin{aligned} \mu f e^{-i\mu z} + \sigma \Delta f e^{-i\mu z} + |f|^2 f e^{-i\mu z} - \rho f e^{-i\mu z} \phi - V(x, y) f e^{-i\mu z} &= 0 \\ \phi_{xx} + \nu \phi_{yy} &= \left(|f|^2 \right)_{xx} \end{aligned} \quad (3.2)$$

simplifying these equations we obtain

$$\begin{aligned} \mu f + \sigma \Delta f + |f|^2 f - \rho f \phi - V(x, y) f &= 0 \\ \phi_{xx} + \nu \phi_{yy} &= \left(|f|^2 \right)_{xx}. \end{aligned} \quad (3.3)$$

Applying Fourier Transform to system (3.3), we get

$$\begin{aligned}\mu \hat{f} - \sigma (k_x^2 + k_y^2) \hat{f} + \mathcal{F} \left[|f|^2 f - \rho f \phi - V(x, y) f \right] &= 0 \\ (k_x^2 + \nu k_y^2) \hat{\phi} &= k_x^2 \mathcal{F} \left[|f|^2 \right]\end{aligned}\quad (3.4)$$

where \mathcal{F} denotes Fourier transformation ($\mathcal{F}(f) = \hat{f}$) and $\vec{k} = (k_x, k_y)$ are Fourier variables.

Let us to define $|\vec{k}|^2 = \sigma (k_x^2 + k_y^2)$ for simplicity. Add and subtract a term $r \hat{f}$ to the system (3.4), where $r > 0$ and used to avoid a possible singularity in the denominator.

This procedure leads us to the following equations

$$\begin{aligned}[\mu - |\vec{k}|^2] \hat{f} + r \hat{f} - r \hat{f} &= -\mathcal{F} \left[|f|^2 f - \rho f \phi - V(x, y) f \right] \\ \hat{\phi} &= \frac{k_x^2}{k_x^2 + \nu k_y^2} \mathcal{F} \left[|f|^2 \right].\end{aligned}\quad (3.5)$$

This system can be written as

$$\begin{aligned}\hat{f} &= \frac{\mathcal{F} \left[|f|^2 f - \rho f \phi - V(x, y) f + (\mu + r) f \right]}{r + |\vec{k}|^2} \\ \hat{\phi} &= \frac{k_x^2}{k_x^2 + \nu k_y^2} \mathcal{F} \left[|f|^2 \right].\end{aligned}\quad (3.6)$$

In order to apply Fourier iteration method, we introduce a new field variable $f(x, y) = \lambda w(x, y)$, where $\lambda \neq 0$ is a real valued constant to be determined. The system with the new variable and indices given by

$$\begin{aligned}\hat{w}_{n+1} &= \frac{\mathcal{F} \left[|\lambda|^2 |w_n|^2 w_n - \rho w_n \phi - V(x, y) w_n + (\mu + r) w_n \right]}{r + |\vec{k}|^2} \\ \hat{\phi}_n &= \frac{k_x^2}{k_x^2 + \nu k_y^2} |\lambda|^2 \mathcal{F} \left[|w_n|^2 \right].\end{aligned}\quad (3.7)$$

After obtaining \hat{w}_{n+1} , the system is normalized to calculate λ parameter

$$\begin{aligned}\int_{-\infty}^{\infty} \int_{-\infty}^{\infty} \hat{w} \hat{w}^* dk &= \int_{-\infty}^{\infty} \int_{-\infty}^{\infty} \frac{|\lambda|^2 F \left[|w|^2 w \right] \hat{w}^*}{r + |\vec{k}|^2} dk - \rho \int_{-\infty}^{\infty} \int_{-\infty}^{\infty} \frac{\mathcal{F} [w \phi] \hat{w}^*}{r + |\vec{k}|^2} dk \\ &\quad - \int_{-\infty}^{\infty} \int_{-\infty}^{\infty} \frac{\mathcal{F} [V w] \hat{w}^*}{r + |\vec{k}|^2} dk + \int_{-\infty}^{\infty} \int_{-\infty}^{\infty} \frac{(\mu + r) \hat{w} \hat{w}^*}{r + |\vec{k}|^2} dk \\ \hat{\phi} &= \frac{k_x^2}{k_x^2 + \nu k_y^2} |\lambda|^2 \mathcal{F} \left[|w|^2 \right].\end{aligned}\quad (3.8)$$

Let $\phi = |\lambda|^2 \Phi$, then

$$\begin{aligned}
& \int_{-\infty}^{\infty} \int_{-\infty}^{\infty} |\hat{w}|^2 dk + \int_{-\infty}^{\infty} \int_{-\infty}^{\infty} \frac{\mathcal{F}[Vw] \hat{w}^*}{r + |\vec{k}|^2} dk - \int_{-\infty}^{\infty} \int_{-\infty}^{\infty} \frac{(\mu + r) |\hat{w}|^2}{r + |\vec{k}|^2} dk \\
&= |\lambda|^2 \int_{-\infty}^{\infty} \int_{-\infty}^{\infty} \frac{\mathcal{F}[|w|^2 w] \hat{w}^*}{r + |\vec{k}|^2} dk - \rho |\lambda|^2 \int_{-\infty}^{\infty} \int_{-\infty}^{\infty} \frac{\mathcal{F}[w \Phi] \hat{w}^*}{r + |\vec{k}|^2} dk \\
& \qquad \qquad \qquad \hat{\Phi} = \frac{k_x^2}{k_x^2 + \nu k_y^2} \mathcal{F}[|w|^2].
\end{aligned} \tag{3.9}$$

Solving $|\lambda|^2$, the system takes the form

$$\begin{aligned}
|\lambda|^2 &= \frac{\int_{-\infty}^{\infty} \int_{-\infty}^{\infty} \left[\left(|\vec{k}|^2 - \mu \right) |\hat{w}|^2 + \mathcal{F}[Vw] \hat{w}^* \right] \frac{dk}{r + |\vec{k}|^2}}{\int_{-\infty}^{\infty} \int_{-\infty}^{\infty} \mathcal{F}[|w|^2 w - \rho w \Phi] \hat{w}^* \frac{dk}{r + |\vec{k}|^2}} \\
& \qquad \qquad \qquad \Phi = \mathcal{F}^{-1} \left[\frac{k_x^2}{k_x^2 + \nu k_y^2} \mathcal{F}[|w|^2] \right].
\end{aligned} \tag{3.10}$$

We define two scalar quantities SL and SR as follows

$$\begin{aligned}
SL &= \int_{-\infty}^{\infty} \int_{-\infty}^{\infty} \left[\left(|\vec{k}|^2 - \mu \right) |\hat{w}|^2 + \mathcal{F}[Vw] \hat{w}^* \right] dk \\
SR &= \int_{-\infty}^{\infty} \int_{-\infty}^{\infty} \mathcal{F}[|w|^2 w - \rho w \Phi] \hat{w}^* dk.
\end{aligned} \tag{3.11}$$

It has been found that this method often prevents the numerical scheme from diverging. Thus, the soliton is obtained from a convergent iterative scheme. These quantities can be efficiently calculated by using Fast-Fourier Transforms in MATLAB, when external potential V and initial condition w are given. Since $SL = SR$ when w is solution of the system, the iteration continues until the relative error $\delta = |\lambda_{m+1}/\lambda_m - 1|$ reaches 10^{-8} . Convergence is usually obtained in 20 – 40 steps (number of iteration). In this study, to obtain fundamental, dipole or vortex solitons, we use multi-humped Gaussian as initial condition which given by

$$w_0(x, y, 0) = \sum_{n=0}^{M-1} e^{-A[(x+x_n)^2 + (y+y_n)^2] + i\theta_n} \tag{3.12}$$

where x_n, y_n represent the location of the solitons, θ_n is the phase difference, M corresponds to the number of humps and A is a positive integer.

This numerical method is applicable to the NLSE by using a value of $\rho = 0$ in the algorithm.

3.2 Stability Analysis

The question of solitons' evolutions under perturbations is very important for applications. In this study, we consider the (linear and nonlinear) stability properties of the (2+1)D NLSM system with an external potential which given in Eq. (3.1).

3.2.1 Linear stability analysis

To examine the linear evolution of the solitons, we linearized the system (3.1) around the fundamental soliton (which computed by SR method). By denoting $u = e^{-i\mu z}[u_0(x, y) + \tilde{u}(x, y, z)]$ and $\phi = \phi_0(x, y) + \tilde{\phi}(x, y)$, where $u_0(x, y)$ is the fundamental soliton and $\tilde{u}, \tilde{\phi} \ll 1$ is the infinitesimal perturbation, the linearized system for \tilde{u} is

$$\begin{aligned} i\tilde{u}_z + \sigma\Delta\tilde{u} + (\mu - V(x, y) + 2|u_0|^2)\tilde{u} - \rho(\phi_0\tilde{u} + \tilde{\phi}u_0) + u_0^2\tilde{u}^* &= 0, \\ \tilde{\phi}_{xx} + \nu\tilde{\phi}_{yy} &= (u_0\tilde{u}^* + \tilde{u}u_0^*)_{xx} \end{aligned} \quad (3.13)$$

where $|u|^2 = uu^*$.

Starting from a white-noise initial condition, we simulated this linearized equation over a long distance (using finite differences on \tilde{u}_{xx} and \tilde{u}_{yy} and the fourth-order Runge-Kutta method to advance in z).

If the peak amplitude of the perturbed soliton grows significantly in a finite distance (or time) then the fundamental soliton is considered to be linearly unstable. Otherwise, it is linearly stable.

The soliton power ($P \equiv P[u] := \iint_{-\infty}^{\infty} |u|^2 dx dy$) plays an important role in determining the stability properties of the solitons.

An important analytic result on soliton stability was obtained by Vakhitov and Kolokolov ([52]). They proved, by use of the linearized perturbation equation, that a necessary condition for stability of the soliton $u(x; \mu)$ is

$$\frac{dP}{d\mu} < 0, \quad (3.14)$$

i.e., the soliton is stable only if its power decreases with increasing propagation constant μ . This condition is called the slope condition.

3.2.2 Nonlinear stability analysis

In order to investigate the nonlinear stability of solitons, we directly compute Eq. (3.1) over a long distance, (finite difference method was used for calculation of derivatives u_{xx} and u_{yy} , and fourth-order Runge-Kutta method to advance in z). The initial conditions were taken to be a fundamental soliton, dipole or vortex with 1% random noise in amplitude and phase.

Key analytic results on soliton stability were obtained in Refs. [53, 54]. They proved that the necessary condition for orbital (nonlinear) stability is the slope condition (3.14).

A necessary condition for collapse in the 2D cubic NLSE ($\sigma = 1$ and $\rho = 0$ in the NLSM system) is that the power of the beam exceeds the critical power $P_c \approx 11.7$ [23].

Solitons can become unstable in two ways : Focusing instability or drift instability [55].

(a) If the slope condition is not satisfied, this leads to a focusing instability.

(b) The spectral condition is associated with the eigenvalue problem. If the spectral condition is violated it leads to a drift instability, i.e., the fundamental soliton moves from the potential maximum towards a nearby lattice minimum.

4. NONLINEAR LATTICE SOLITONS OF THE NLSM SYSTEMS

In this chapter, we investigate the fundamental and dipole solitons in the lattice-free medium and in a periodic external lattice for the (2+1)-dimensional NLSM system. We use the NLSM system with a periodic external potential as model;

$$\begin{aligned} iu_z + \frac{1}{2}\Delta u + |u|^2 u - \rho\phi u - V(x,y)u &= 0, \\ \phi_{xx} + \nu\phi_{yy} &= (|u|^2)_{xx}. \end{aligned} \quad (4.1)$$

Here, $V(x,y)$ is an external optical potential that can be written as the intensity of a sum of phase-modulated plane waves [25]

$$V(x,y) = \frac{V_0}{N^2} \left| \sum_{n=0}^{N-1} e^{i(k_x^n x + k_y^n y)} \right|^2. \quad (4.2)$$

We will consider the periodic optical potential that corresponds to $N = 4$. Contour image of this periodic lattice ($N=4$) is displayed in Fig. 4.1 for a bounded region. Here, $k_x^n = k_y^n = 1$ and $V_0 = 12.5$. The lattice-free medium can be obtained by setting $V_0 = 0$.

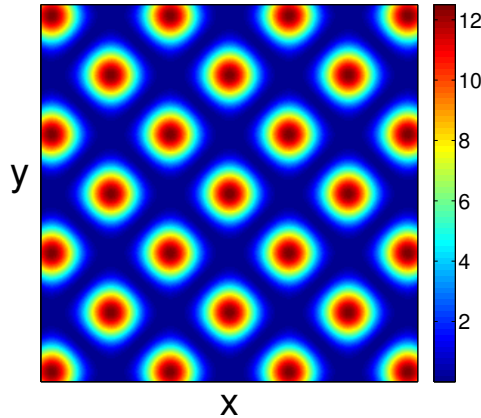


Figure 4.1 : Contour image of the periodic lattice ($N=4$).

4.1 Numerical Existence of Fundamental Solitons and Stability Analysis

The fundamental solitons are obtained in the lattice-free medium and in the periodic lattice for the (2+1)-dimensional NLSM system. We use the spectral renormalization

method (which explained in Chapter 3) to calculate solutions of the NLSM system. Linear and nonlinear stability properties of these solitons are also analyzed. For nonlinear stability analysis, we perform direct numerical simulations of the NLSM system where the initial condition is the soliton solution (1% random noise added to the amplitude and phase) that is obtained by the use of SR method.

Hereafter, unless different values are specified, we set $\rho = 1$, $\nu = 1$ and $\mu = -1$.

4.1.1 Numerical existence of fundamental solitons

Here, we show the existence of fundamental solitons in the periodic lattice with depth $V_0 = 12.5$ for the NLSM system. Fundamental solitons are found numerically (by SR method) with the initial condition

$$w_0(x, y) = e^{-A[(x+x_0)^2+(y+y_0)^2]} \quad (4.3)$$

where x_0 and y_0 represent the location of fundamental soliton on the lattice and, A is a positive integer which is set to 1 for fundamental solitons. The origin is a local maximum of the periodic lattice and, to locate the initial condition on the lattice minima (generally taken to be one of the closest minima to the central maximum), we determine the location of the picked local minimum of the lattice and calculate those values. The point $x_0 = \pi$, $y_0 = 0$ is a local minimum of the lattice close to the origin. Based on the previously obtained results about lattice solitons ([14], [15]), we picked a lattice minima to locate the initial condition since lattice solitons on maxima tend to be unstable due to either collapse or drift instability.

In order to compare the fundamental lattice solitons' properties to lattice-free solitons', we depicted NLSM solitons of lattice-free medium in Fig. 4.2.

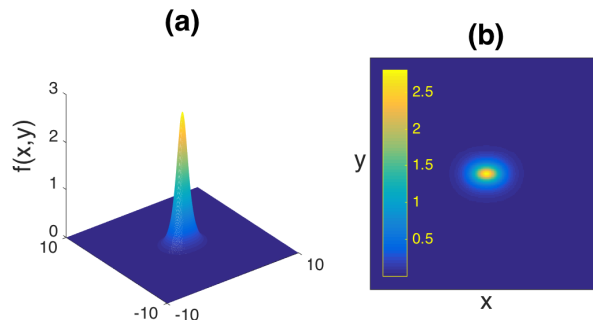


Figure 4.2 : (Color online) Fundamental soliton in the lattice-free medium at $x_0 = 0$ and $y_0 = 0$. (a) 3D view of the soliton; (b) Contour image of the soliton.

Similarly, in Fig. 4.3, we obtain a fundamental soliton located at local minimum of the periodic lattice for the potential depth $V_0 = 12.5$.

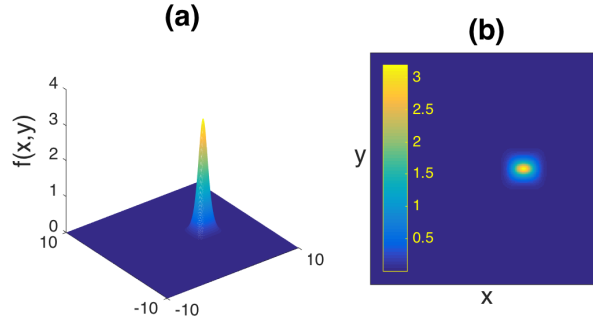


Figure 4.3 : (Color online) Fundamental soliton located at minimum of the periodic lattice at $x_0 = \pi$, $y_0 = 0$ for $V_0 = 12.5$. (a) 3D view of the soliton; (b) Contour image of the soliton.

Solitons can form when their propagation constant, or eigenvalue (μ), is within certain region, often called gaps, a concept that is borrowed from the Floquet-Bloch theory for linear propagation. To determine the first nonlinear band-gap formation, we set the potential depth V_0 to a fixed value. For each value of V_0 , by increasing the μ values, we check both the convergence and the localization of the mode by SR method. When the mode becomes more extended, usually the convergence is slower and after a certain value of μ , typically both the convergence cannot be reached and the localization of the mode is lost.

The fundamental solitons are shown to exist in a semi-infinite gap $\mu \leq 1.6$ for $V_0 = 12.5$ (in the periodic lattice), and $\mu \leq 0$ for $V_0 = 0$ (in the lattice-free medium) when $\rho = 1$ and $\nu = 1$.

Also, the existence (or gap) domain of the fundamental solitons on the plane (ρ, ν) is depicted in Fig. 4.4 for $V_0 = 0$ and $V_0 = 12.5$.

As can be seen from the Fig. 4.4, the gaps boundary of the lattice-free case is wider than that of the case with a periodic lattice and the gap boundaries are getting closer to each other as ρ and ν parameters are getting larger.

4.1.2 Stability analysis of fundamental solitons

Herein, we investigate the linear and nonlinear stability properties of fundamental solitons that were previously obtained by SR method.

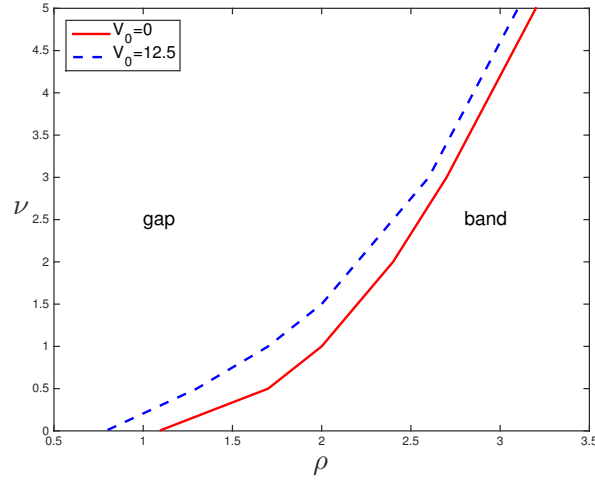


Figure 4.4 : (Color online) Domain of existence on the plane (ρ, ν) for the fundamental solitons in the lattice-free medium ($V_0 = 0$) and on the periodic lattice ($V_0 = 12.5$) for $\mu = -1$.

Before examining the stability of fundamental solitons, we investigate soliton power (P) vs. eigenvalue (μ) graphs for fixed ν , varying ρ and fixed ρ , varying ν values in Fig. 4.5 and Fig. 4.6, respectively.

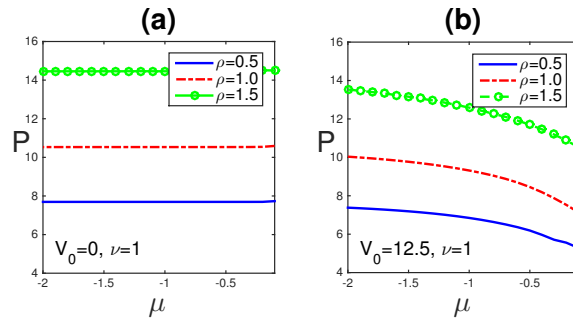


Figure 4.5 : (Color online) Soliton power vs. eigenvalue graph for fixed $\nu = 1$ within the semi-infinite gap in (a) lattice-free medium; (b) case with a periodic lattice.

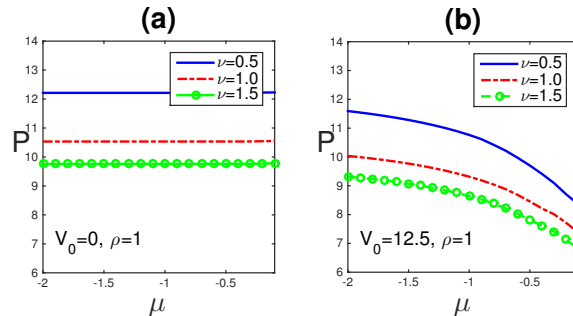


Figure 4.6 : (Color online) Soliton power vs. eigenvalue graph for fixed $\rho = 1$ within the semi-infinite gap in (a) lattice-free medium; (b) case with a periodic lattice.

As can be seen from Fig. 4.5 and Fig. 4.6, for the lattice-free medium, soliton powers are constant for both cases, not changing with the eigenvalue (although changing with ρ and ν). On the other hand, powers are reducing with increasing eigenvalues (all with a negative slope $dP/d\mu < 0$) which may indicate the stability of lattice solitons. It is also observed from the figures that the powers of the fundamental solitons increase as ρ increases whereas powers of the solitons decrease as ν increases. As a result, one may conclude that increasing the parameter ρ may have an adverse affect on soliton stability.

To examine the linear stability of the fundamental solitons (see Fig. 4.2 and Fig. 4.3), we plot linear evolution of the peak amplitude for these solitons from $z = 0$ to $z = 5$ (see Fig. 4.7). It is observed from the figure that the peak amplitude of the fundamental soliton blows up in a finite distance, indicating the linear instability of both cases.

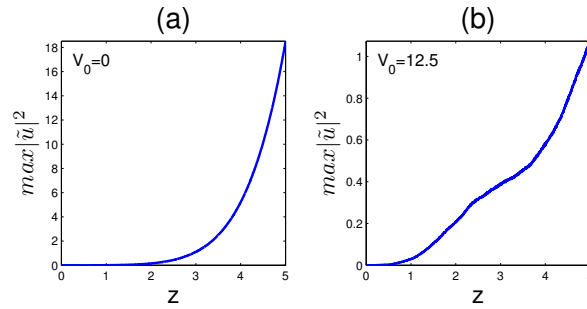


Figure 4.7 : (Color online) Linear instability of the fundamental soliton (a) in the lattice-free medium; (b) on the periodic lattice minimum.

The nonlinear stability of fundamental solitons are studied by means of investigating the nonlinear evolution of the peak amplitude of the soliton.

In Fig. 4.8, the nonlinear evolution of the fundamental soliton (see Fig. 4.2) in the lattice-free medium is plotted. As can be seen from Fig. 4.8, during the evolution, the contour image of the fundamental soliton shrinks due to self-focusing, peak amplitude increases and blows up at around $z = 5.59$. This indicates that the fundamental soliton in the lattice-free medium is nonlinearly unstable for this parameter regime.

In order to capture collapse, we added a periodic lattice to the system. Evolution of the fundamental soliton (see Fig. 4.3) located on periodic lattice minimum is plotted in Fig. 4.9.

As can be seen from the figure, contour image of the lattice soliton is preserved (neither shrinks nor extends) and the peak amplitude of the fundamental soliton oscillates with

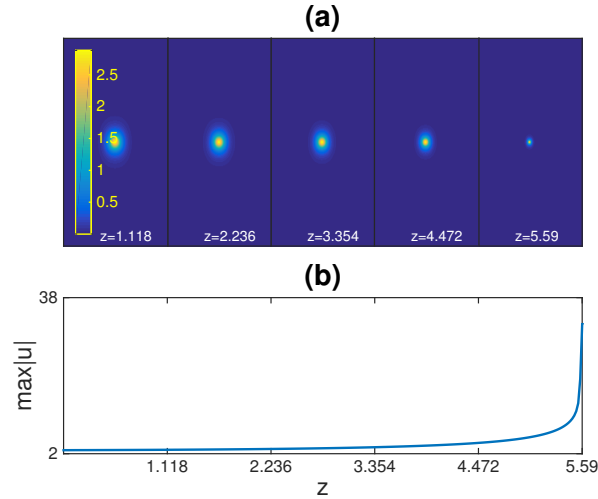


Figure 4.8 : (Color online) Collapse of the fundamental soliton in the lattice-free medium. (a) Snapshots of contour image of the soliton for various z values; (b) Peak amplitude as a function of the propagation distance.

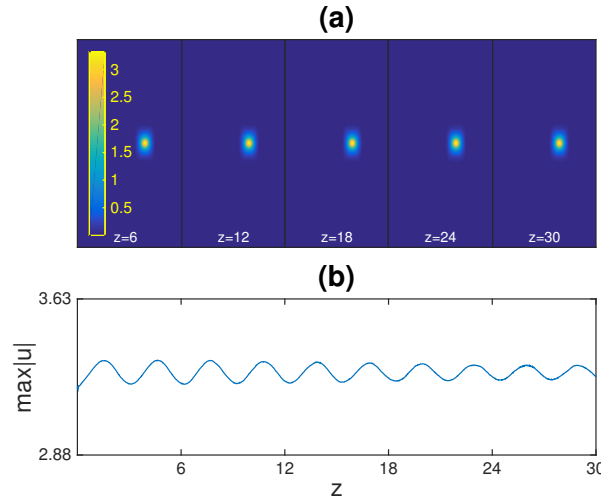


Figure 4.9 : (Color online) Nonlinear evolution of the fundamental soliton located at minimum of the periodic lattice for $V_0 = 12.5$. (a) Snapshots of contour image of the soliton for various z values; (b) Peak amplitude as a function of the propagation distance.

relatively small amplitude during the evolution. Therefore, the fundamental soliton located at minimum of the periodic lattice is found to be nonlinearly stable for these parameters.

Furthermore, mode profiles and nonlinear evolutions of fundamental solitons for various ρ and v values are investigated.

In order to investigate the differences in the shape of the mode for different ρ and v parameters, contour images of the fundamental solitons in the lattice-free medium and on a lattice minimum are depicted in Fig. 4.10 for fixed $v = 1$ and varying ρ values.

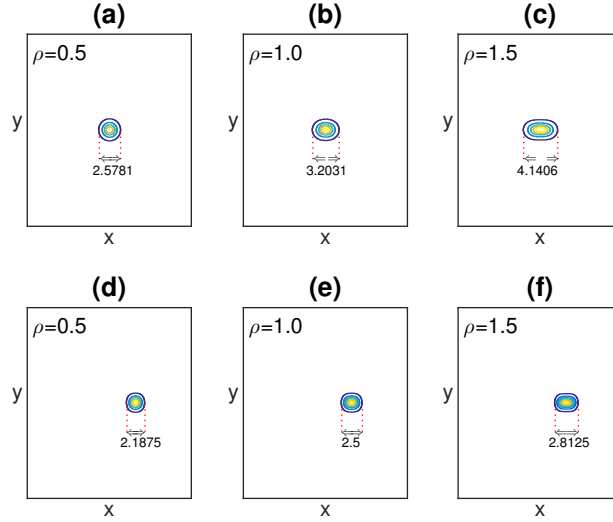


Figure 4.10 : (Color online) Contour image of the fundamental soliton for lattice-free medium with (a) $\rho = 0.5$; (b) $\rho = 1.0$; (c) $\rho = 1.5$. Contour image of the fundamental lattice soliton for (d) $\rho = 0.5$; (e) $\rho = 1.0$; (f) $\rho = 1.5$. All solitons are obtained for $\nu = 1$.

One can see from the Fig. 4.10 that contour images of the fundamental solitons become more astigmatic along the x -axis as ρ increases. Now, the important question arises about the relation of the mode ellipticity to the nonlinear stability properties of the mode. In order to investigate this, in Fig. 4.11 we have plotted the maximum amplitude versus the propagation distance graphs of each soliton that are shown in Fig. 4.10.

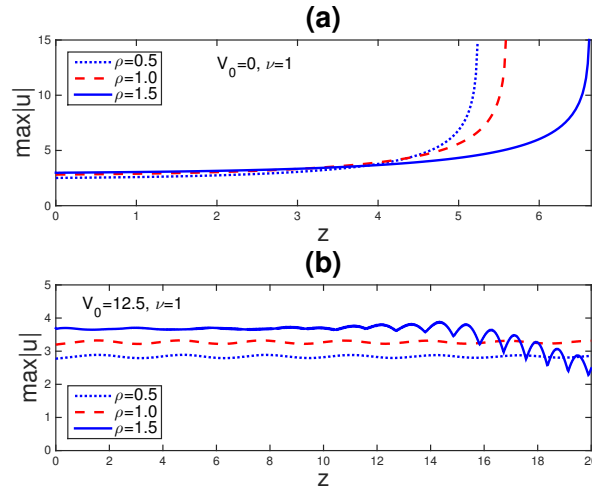


Figure 4.11 : (Color online) Nonlinear evolution of the fundamental solitons for various values of ρ for fixed $\nu = 1$. Peak amplitude as a function of the propagation distance (a) in the lattice-free medium ($V_0 = 0$); (b) in the periodic lattice ($V_0 = 12.5$).

Fig. 4.11 (a) shows that fundamental solitons in the lattice-free medium blow up after a finite distance in each case. Moreover, it is seen that the collapse distance may be extended (collapse may be delayed) by increasing ρ in lattice-free medium, but the

collapse will eventually occur due to the instant growth of the maximum amplitude. Since it has been previously observed that the mode becomes more astigmatic in x direction for larger values of ρ , one can conclude that the delay in the collapse for the lattice-free case can be achieved by increasing the parameter ρ . In Fig. 4.11 (b) it is numerically shown that the blow-up of the fundamental soliton is arrested by adding a periodic external lattice to the system. On the other hand, for the periodic lattice soliton obtained for $\rho = 1.5$, a decay in the soliton amplitude is observed during the evolution (starting at around $z = 15$. See Fig. 4.11 (b)). This is a result of distribution of the soliton to the neighbouring lattice sites. As distribution process continues, the soliton becomes more and more extended and eventually disappears. In other words, this parameter regime, increasing ρ up to the value 1.5 may corrupt the soliton in finite distance.

Similarly, contour images of the fundamental solitons in the lattice-free medium and on a lattice minimum are depicted in Fig. 4.12 for fixed $\rho = 1$ and varying ν values.

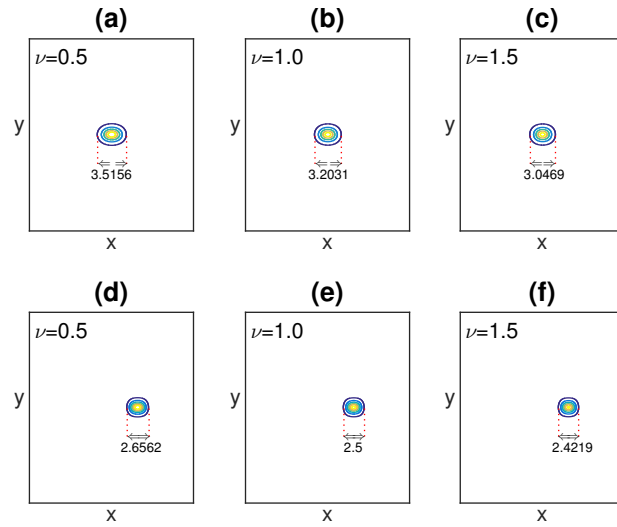


Figure 4.12 : (Color online) Contour image of the fundamental soliton for lattice-free medium with (a) $\nu = 0.5$; (b) $\nu = 1.0$; (c) $\nu = 1.5$. Contour image of the fundamental lattice soliton for (d) $\nu = 0.5$; (e) $\nu = 1.0$; (f) $\nu = 1.5$. All solitons are obtained for $\rho = 1$.

As shown in Fig. 4.12, contour image of the fundamental solitons become less astigmatic along the x -axis as ν increases for both the lattice-free case and the case with a periodic lattice. This figure also reveals that although the parameter ν has an effect on the mode astigmatism, it is not as pronounced as the effect of ρ . Therefore, one may expect that the blow-up distances would be more or less the same for the solitons shown in Fig. 4.12.

The nonlinear evolutions of the fundamental solitons that are shown in Fig. 4.12 are investigated. In Fig. 4.13 (a), it is observed that fundamental solitons in the lattice-free medium blow up after a finite distance (around $z = 5.5$) for the taken values of ν . Moreover, it is seen that although the collapse process is not that sensitive to the changes in parameter ν , one may still predict that the collapse occurs more quickly for larger values of ν for the lattice-free solitons. Again, the collapse cannot be arrested since the maximum amplitude will blow up eventually for the lattice-free case. In Fig. 4.13(b), it is shown that the collapse of the fundamental soliton is arrested by adding a periodic external lattice to the system.

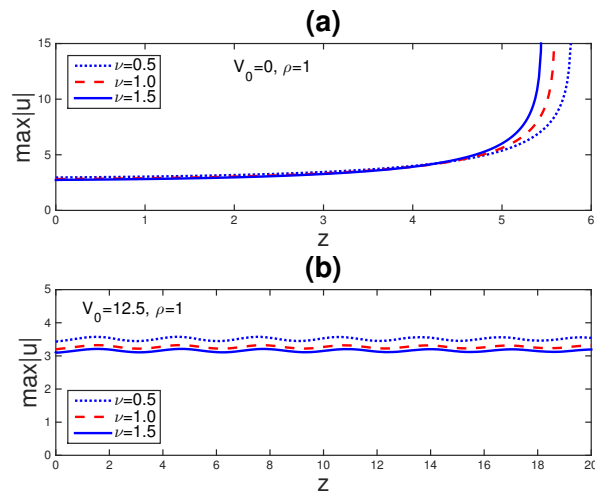


Figure 4.13 : (Color online) Nonlinear evolution of the fundamental solitons for various values of ν for fixed $\rho = 1$. Peak amplitude as a function of the propagation distance (a) in the lattice-free medium ($V_0 = 0$); (b) in the periodic lattice ($V_0 = 12.5$).

Based on our findings, we put forward a mechanism to obtain more robust lattice solitons for larger values of ρ . We consider the exact soliton that becomes more and more extended (due to decaying amplitude) during the evolution that is shown in Fig. 4.11 (b) corresponding to $\rho = 1.5$. In Fig. 4.14 (a), mode profile of this lattice soliton is depicted for various z values up to $z = 30$ to show the decay in the amplitude and the deterioration of the soliton during the evolution. It is clear that although this soliton does not blow up in finite distance, it cannot be considered as a robust one. In Fig. 4.14 (b), the maximum amplitude versus the propagation distance z of this soliton is depicted. Again, the decay in the amplitude is clear after $z \cong 15$. To improve the stability properties of this soliton, we started to increase the value of the parameter ν to $\nu = 1.5$ and $\nu = 2$ and depicted the maximum amplitude versus z graphs for each case

in Fig. 4.14 (c) and (d), respectively. It is clearly seen from these figures that larger values of ν prevents this type of instability to occur.

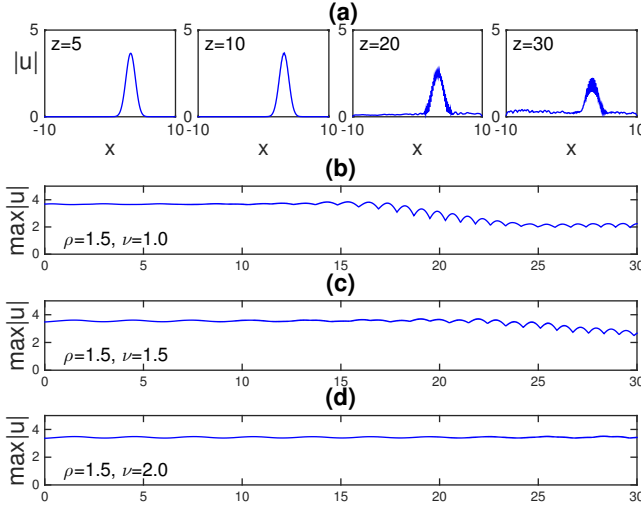


Figure 4.14 : (Color online) Nonlinear evolution of the fundamental soliton for larger anisotropy coefficients when $\rho = 1.5$ and $V_0 = 12.5$. (a) Mode profile of the fundamental soliton with $\nu = 1.0$ at $z = 5$, $z = 10$, $z = 20$ and $z = 30$. Peak amplitude as a function of the propagation distance (b) for $\nu = 1.0$; (c) for $\nu = 1.5$; (d) for $\nu = 2.0$.

Is there another way to suppress collapse and/or improve the stability properties of the lattice solitons? In real physical parameter regime, changing the parameters ρ or ν to improve stability, may not be a realistic approach, since these parameters are fixed values depending on the type of material that is considered. On the other hand, a deeper lattice can easily be formed in most cases. It is known that a deep lattice may suppress collapse in lattice solitons (See [14]). To see the effect of a deeper lattice on soliton stability at large values of ρ and ν , (namely for $\rho = 2$, $\nu = 3$), we investigate the nonlinear evolution of the fundamental solitons for larger values of the lattice depth V_0 (50, 250, 500) in Fig. 4.15.

In Fig. 4.15 (a) and (b), it is shown that the instability due to the decay in the maximum amplitude can not be suppressed by increasing ν up to 3 and considering a deeper lattice ($V_0 = 50$). With a similar nature to the previous case, the amplitude starts to decrease at around $z = 15$ and the deterioration of the soliton during the evolution is observed. In Fig. 4.15 (c) and (d), it is numerically shown that increasing the lattice depth to $V_0 = 250$ and $V_0 = 500$ respectively, stability properties of the lattice soliton improve and stability is achieved since the maximum amplitude of the soliton starts to oscillate with respect to the propagation distance z .

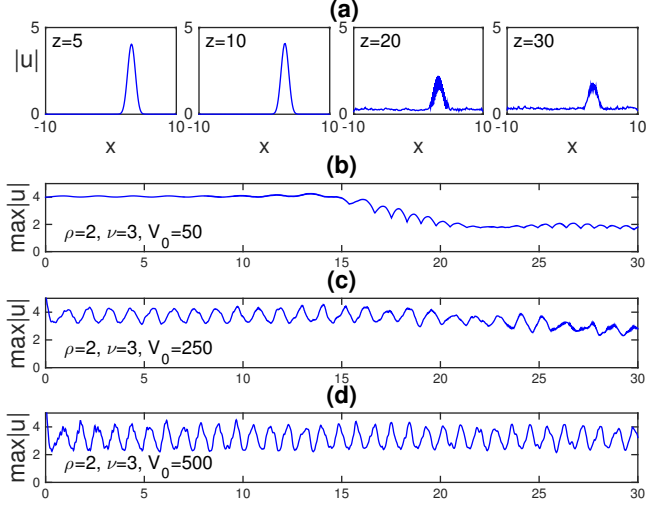


Figure 4.15 : (Color online) Nonlinear evolution of the fundamental soliton in the deeper lattice for $\rho = 2$ and $\nu = 3$. (a) Mode profile of the fundamental soliton for $V_0 = 50$ at $z = 5$, $z = 10$, $z = 20$ and $z = 30$. Peak amplitude as a function of the propagation distance (b) for $V_0 = 50$; (c) for $V_0 = 250$; (d) for $V_0 = 500$.

As the last example of using the periodic lattice as a collapse arrest mechanism for fundamental solitons, we took $\rho = 0.5$ and $\nu = 1.5$, typical values corresponding to the propagation of focused beams in Potassium Niobate (KNbO_3). In Fig. 4.16, nonlinear evolution of a standard Gaussian, the soliton obtained by SR method (both are in lattice-free medium) and the periodic lattice soliton are depicted with respect to the evolution distance z . It is seen from the figure that in this parameter regime, standard Gaussian collapses immediately due to the sudden increment in the amplitude, the amplitude of the soliton obtained by SR method starts to increase which is considered as the sign of collapse in finite time; whereas, the periodic lattice soliton is observed to be nonlinearly stable since the maximum amplitude oscillates with propagation distance.

4.2 Numerical Existence of Dipole Solitons and Stability Analysis

Here, we numerically demonstrate the existence of dipole solitons in the lattice-free medium and in the periodic lattice. The linear and nonlinear (in)stability of these dipoles are also examined.

For the spectral renormalization, the following initial condition is used,

$$\begin{aligned}
 w_0(x, y) = & e^{-A[(x+x_0)^2 + (y+y_0)^2] + i\theta_0} \\
 & + e^{-A[(x+x_1)^2 + (y+y_1)^2] + i\theta_1}
 \end{aligned} \tag{4.4}$$

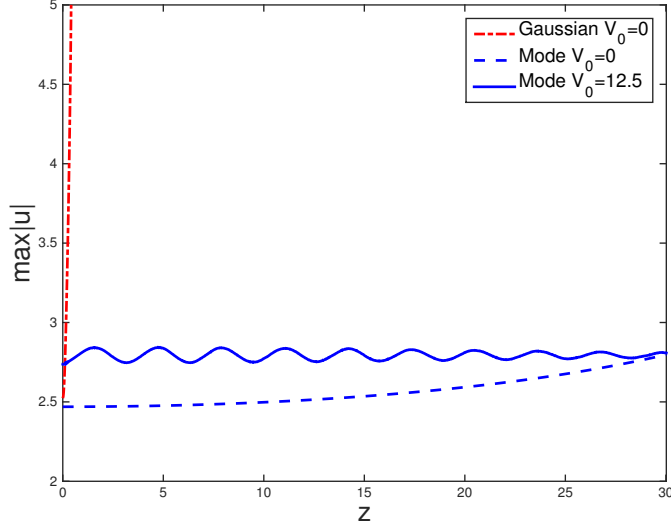


Figure 4.16 : (Color online) Nonlinear evolutions of Gaussian, mode obtained by SR method (both for lattice-free medium) and periodic lattice soliton in Potassium Niobate ($KNbO_3$).

where (x_0, y_0) and (x_1, y_1) represent the locations of dipole solitons; θ_0, θ_1 are the phase differences of dipole solitons and A is a positive integer.

4.2.1 Numerical existence of dipole solitons

A dipole or two-phased localized vortex found numerically by

$$A = 1, \quad x_n = r \cos \theta_n, \quad y_n = r \sin \theta_n \quad (4.5)$$

r is adjusted to locate dipole soliton on the lattice minima and numerical convergence of the mode can be quite sensitive to the value of r . Here, we set $\theta_n = n\pi + \pi/2$ and $r = \pi$.

A dipole profile, its contour image and its phase structure in the lattice-free medium is plotted in Fig. 4.17.

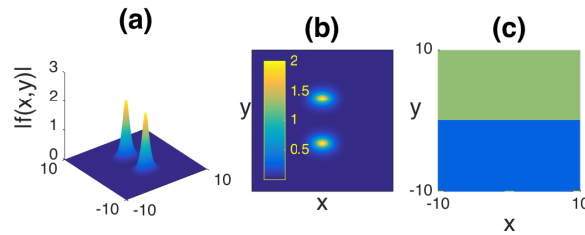


Figure 4.17 : (a) A dipole profile in the lattice-free medium; (b) Contour image of the dipole; (c) Phase structure of the dipole.

Similarly, dipole humps located at the periodic lattice minima is plotted in Fig. 4.18.

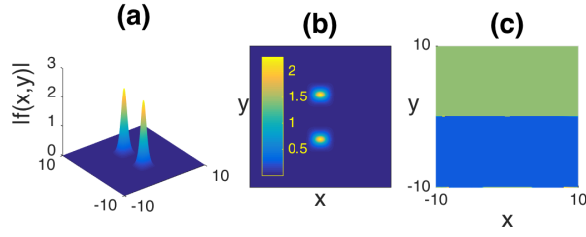


Figure 4.18 : (a) A dipole profile located at periodic lattice minima for $V_0 = 12.5$; (b) Contour image of the dipole; (c) Phase structure of the dipole.

4.2.2 Stability analysis of dipole solitons

The linear and nonlinear stability properties of the dipole solitons (that obtained above) are studied.

Linear evolutions of the dipole solitons in the lattice-free medium (see Fig. 4.17) and in the periodic lattice (see Fig. 4.18) are investigated in Fig. 4.19.

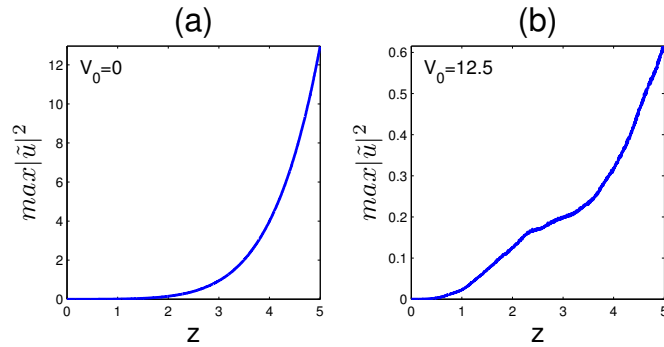


Figure 4.19 : Linear evolution of the dipole solitons in (a) the lattice-free medium ($V_0 = 0$); (b) the periodic lattice ($V_0 = 12.5$).

The peak amplitudes of the dipole solitons blow up in finite distance in both cases and, similar to the fundamental solitons, the dipole in the lattice-free medium blows up faster than the dipole in the periodic lattice minimum.

The nonlinear stability properties of dipole solitons (see Fig. 4.17) in the lattice-free medium are showed in Fig. 4.20.

Contour image of the dipole shrinks and peak amplitude of the dipole increases during the evolution (see Fig. 4.20). Thus, the dipole structure in the lattice-free medium is nonlinearly unstable.

On the other hand, contour image of the dipole (see Fig. 4.18) is preserved in the periodic lattice minima and peak amplitude of the dipole oscillates with relatively small amplitude during the evolution (see Fig. 4.21). This suggests that the dipole

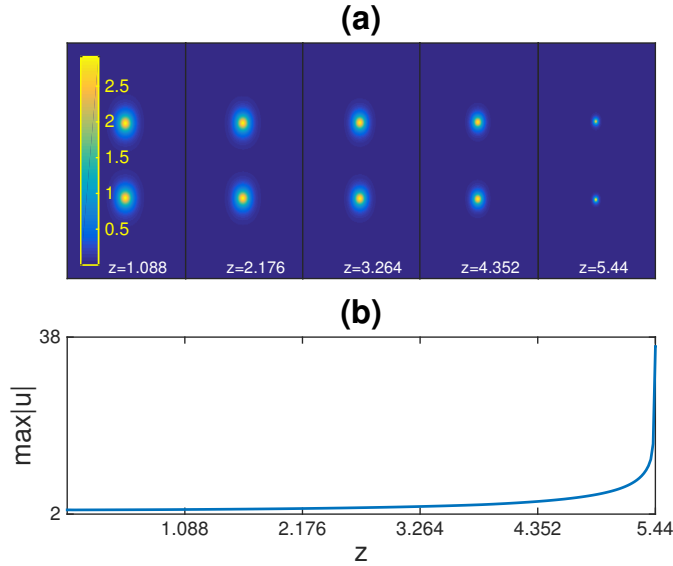


Figure 4.20 : Collapse of a dipole in the lattice-free medium; (a) Contour image of the dipole; (b) Peak amplitude as a function of the propagation distance.

that located at minima of the periodic lattice is nonlinearly stable in this parameter regime.

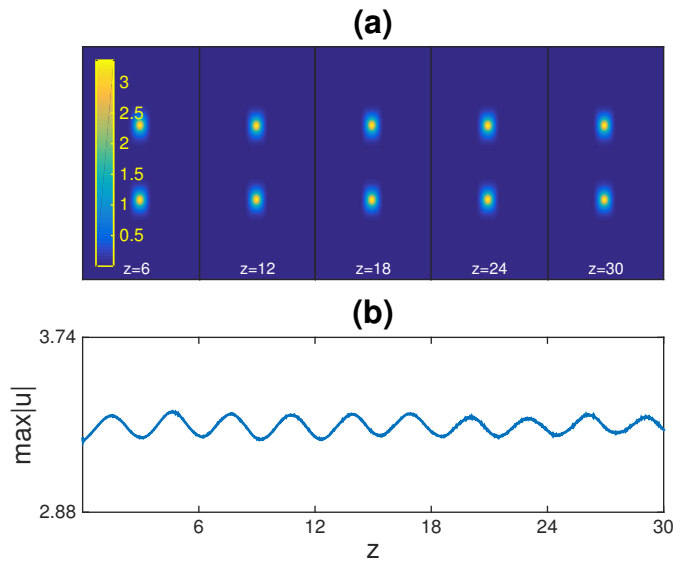


Figure 4.21 : Nonlinear evolution of the dipole solitons located at minima of the periodic lattice for $V_0 = 12.5$. (a) Contour image of the dipole; (b) Peak amplitude as a function of the propagation distance.

4.3 Conclusion

Numerical existence of fundamental and dipole solitons in the lattice-free medium and in the periodic external lattice have been demonstrated for the NLSM system. The linear and nonlinear stability of these solitons are also examined.

By examining the linear evolution of the solitons, it's shown that the solitons in the lattice-free medium and in the periodic lattice are linearly unstable in each case due to blow-up in finite distance.

The nonlinear stability properties of the solitons have been examined by direct simulations and the results showed that

(i) the fundamental and dipole solitons are found to be nonlinearly unstable in the lattice-free medium due to collapse.

(ii) collapse can be suppressed by adding a periodic lattice to the existing system.

Furthermore, it has been noted that there is a relation between the shape and nonlinear stability property of a fundamental soliton. It is numerically observed that in lattice-free medium, if the mode is more astigmatic in x direction, the collapse distance increases (delay in collapse process). This can be achieved by increasing the parameter ρ in lattice-free medium but collapse will eventually occur.

In conclusion, we have demonstrated the possibility of arresting collapse of the NLSM solitons by adding an external periodic lattice to the governing equation. Instead of changing the parameters ρ and ν that are strictly dependent to the optical material in which the mode is focused, changing the lattice depth provides great controllability on soliton stability and more robust solitons can be obtained.

5. VORTEX AND DIPOLE SOLITONS OF THE NLSE IN DEFECTIVE LATTICES

This chapter is devoted to study of the numerical existence of dipole and vortex solitons for the two-dimensional NLSE with external potentials that possess strong irregularities, i.e., edge dislocations and vacancy defects. This part of the study has been published in journal of "Optics Communications" under the title of "Vortex and Dipole Solitons in Lattices Possessing Defects and Dislocations" [40].

In recent years, there has been considerable interest in studying solitons in systems with periodic potentials or lattices, in particular, those that can be generated in the nonlinear optical materials [24, 56–60]. The literature studying the complex-phase solutions in the presence of irregular type potentials is quite limited [61]. In [62], properties of solitons supported by optical lattices featuring topological dislocations are investigated and it has been found that these solitons experience attractive and repulsive forces around the dislocations. A recent review on lattice solitons addresses various type of optical lattices and potential stabilization of these structures [63].

The external potential of complex systems can be much more general and physically richer than a periodic lattice. For example, atomic crystals can have various irregularities, such as defects and edge dislocations, and also quasicrystal structures, which have long-range orientational order but no translational symmetry [64–66]. In general, when the lattice periodicity is slightly perturbed, the band-gap structure and soliton properties also become slightly perturbed, and solitons are expected to exist in much the same as in the perfectly periodic case [67, 68]. But when the perturbation is large as it is discussed in [25], very little is known. In [69] a new method is presented to create a lattice with defects by manipulating individual sites in a 2D optical lattice. The modified optical lattice is created by interference of plane waves and spiral phase waves. We note that, irregular lattice structures can be fabricated physically [70–73].

Vortex-type solitons in the presence of a (optically or magnetically) induced lattice have been investigated analytically and experimentally in Bose-Einstein condensates

(BECs) (cf. [74, 75]) and in optical Kerr media (cf. [1, 76–80]). Such structures appear as special solutions of the focusing two-dimensional cubic NLSE with an external potential. Using a fixed point spectral computational scheme, multiple dipole and vortex solitons are shown to exist in the (2+1)-dimensional NLSE with an external quasicrystal lattice [15]. Stable fundamental solitons for the two-dimensional NLSE with external potentials that possess large variations from periodicity are obtained numerically in [25], but the existence and stability properties of multiple dipole and/or vortex structures have not been studied extensively in the current literature. Our results can find applications to photonic band-gap systems.

In this study, we compute multiple dipole and vortex soliton solutions of the focusing cubic (2+1)-dimensional NLSE with external potentials (lattices) that possess defects and dislocations. This is achieved using the spectral renormalization method which is a fixed point spectral scheme. Nonlinear stability properties of these solitons are also analyzed.

The governing equation used in this study is the focusing (2+1)-dimensional NLSE with an external potential,

$$iu_z + \Delta u + |u|^2 u - V(x, y)u = 0. \quad (5.1)$$

In optics, $u(x, y, z)$ corresponds to the complex-valued, slowly varying amplitude of the electric field in the xy plane propagating in the z direction, $\Delta u \equiv u_{xx} + u_{yy}$ corresponds to diffraction, the cubic term in u originates from the nonlinear (Kerr) change of the refractive index and $V(x, y)$ is an external optical potential that can be written as the intensity of a sum of N phase-modulated plane waves, i.e.(see [25]),

$$V(x, y) = \frac{V_0}{N^2} \left| \sum_{n=0}^{N-1} e^{i\vec{k}_n \cdot \vec{x} + i\theta_n(x, y)} \right|^2. \quad (5.2)$$

where $V_0 > 0$ is constant and corresponds to the peak depth of the potential, i.e., $V_0 = \max_{x, y} V(x, y)$, $\vec{x} = (x, y)$, \vec{k}_n is a wave vector, $\theta_n(x, y)$ is a phase function that characterizes edge irregularities or vacancy defects.

In order to compute localized solutions (i.e., soliton solutions) to nonlinear evolution equations, various techniques have been used. For a detailed information on numerical methods for solving wave equations see [81]. Below we mention some of these methods. Shooting, relaxation techniques and the self consistency method have

been around for decades, but they are not always efficient and / or applicable for multidimensional problems. A different method was introduced by Petviashvili [13] to construct localized solutions in the two-dimensional Korteweg-de Vries equation (usually referred to as the Kadomtsev-Petviashvili equation). The idea behind the Petviashvili's method is to transform the underlying governing equation to Fourier space and determine a convergence factor based upon the degree (homogeneity) of a single nonlinear term. This method has been extensively used to find localized solutions in a wide range of nonlinear systems. This method can be successfully applied to nonlinear systems only if the degree of the nonlinearity is fixed in the associated evolution equation.

In recent years, Lakoba and Yang proposed generalizations of Petviashvili's iteration method to scalar and vector Hamiltonian equations with arbitrary form of nonlinearity and potential functions in [82]. Later they extended this method to eliminate from the iterations a mode that is responsible either for the divergence or the slow convergence of the iterations [83]. The conjugate gradient method is yet another iterative method for solving linear systems. Lately, the conjugate gradient method method was modified for finding solitary waves of nonlinear evolution equations [84, 85].

In this part, soliton solutions are obtained by the spectral renormalization method (which explained in Chapter 3). To do this, we seek a solution of Eq. (5.1) in the form $u(x, y, z) = f(x, y)e^{-i\mu z}$ where $f(x, y)$ is a complex-valued function and μ is real propagation constant (frequency).

As initial condition, we use multi-humped Gaussian (two-humped for dipoles, three-humped and four-humped for vortex modes) centered at either maxima or minima of the lattice structure. Convergence is usually obtained quickly in the semi infinite band gap when the mode is strongly localized. Further it is observed that, the mode becomes more extended as μ gets closer to the nonlinear band gap edge and convergence of such a mode slows down during the iterations.

5.1 Defect Lattices

Defect lattices that are considered in this study are the lattice with an edge dislocation and the lattice with a vacancy defect [25].

The lattice with an edge dislocation is mathematically formulated as

$$V(x,y) = \frac{V_0}{25} [2\cos(k_x x + \theta(x,y)) + 2\cos(k_y y) + 1]^2 \quad (5.3)$$

where the phase function θ defined as

$$\theta(x,y) = \frac{3\pi}{2} - \tan^{-1}\left(\frac{y}{x}\right) \quad (5.4)$$

The second type of potential that we study is an irregular 2D square lattice with a vacancy defect. The formulation of this lattice can be given as

$$V(x,y) = \frac{V_0}{25} \left| 2\cos(k_x x) + 2\cos(k_y y) + e^{i\theta(x,y)} \right|^2 \quad (5.5)$$

where the phase function θ is given by

$$\theta(x,y) = \tan^{-1}\left(\frac{y-y_0}{x}\right) - \tan^{-1}\left(\frac{y+y_0}{x}\right) \quad (5.6)$$

Physically, $\theta(x,y)$ corresponds to two first order phase dislocations displaced in the y direction by a distance of $2y_0$ in the y direction. A vacancy defect can thus be obtained using $y_0 = \pi/K$ where $K = k_x = k_y$.

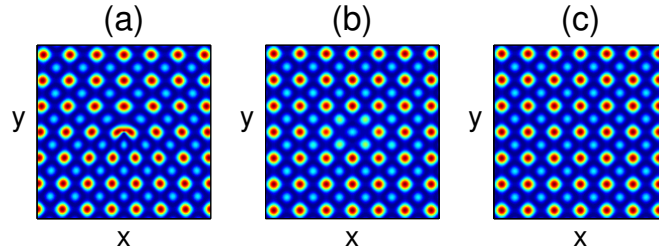


Figure 5.1 : Contour images of lattices: (a) lattice with an edge dislocation; (b) lattice with a vacancy defect; (c) periodic (N=4).

Contour images of a periodic lattice and, the lattices with an edge dislocation and a vacancy defect are displayed in Fig. 5.1. As can be seen from this figure, the density of lattice sites changes vertically across the lattice with an edge dislocation and there is an empty cell at the center of the lattice which is known as vacancy defect. We also note that, by setting $\theta = 0$ in Eq. (5.5), the irregularity in the lattice with a vacancy defect is removed and this lattice becomes a perfectly periodic one which is demonstrated in Fig. 5.1(c).

5.2 Nonlinear Stability of Lattice Solitons

To investigate the nonlinear stability of solitons, we directly compute Eq.(5.1) over a long distance, (finite difference method were used on derivatives u_{xx} and u_{yy} , and fourth-order Runge-Kutta method to advance in z). The initial conditions were taken to be a dipole or a vortex.

Key analytic results on soliton stability were obtained in Refs. [53, 54]. They proved that the necessary condition for orbital (nonlinear) stability is the slope condition:

$$\frac{dP}{d\mu} < 0, \quad (5.7)$$

i.e., the soliton is stable only if its power decreases with increasing propagation constant μ .

A necessary condition for collapse in the 2D cubic NLSE is that the power of the beam exceeds the critical power $P_c \approx 11.7$ ([23]).

While investigating the nonlinear stability, we evaluated the maximum amplitude versus the propagation distance, the change in the location of centers of mass and the phase structure of the vortex / dipole solitons. A stable soliton should nearly preserve:

1. its peak amplitude, as opposed undergoing self-focusing and / or finite-distance collapse.
2. its position on the lattice, i.e., be drift-stable (drift-unstable solitons are typically characterized by “humps” that drift from lattice maxima toward nearby minima).
3. its phase structure.

If all three conditions are met then the soliton will be considered nonlinearly stable.

The center of mass is monitored as

$$\langle x \rangle, \langle y \rangle = \frac{1}{P} \iint_{-\infty}^{\infty} (x, y) |u|^2 dx dy. \quad (5.8)$$

5.3 Existence of Dipole Solitons and Nonlinear Stability Analysis

In this section, we numerically demonstrate the existence of a dipole and investigate its nonlinear stability properties for a lattice with an edge dislocation and and a vacancy

defect respectively. For the spectral renormalization, we used the following initial conditions, centered at the lattice maxima and minima:

$$w_0(x,y) = e^{-A[(x+x_0)^2+(y+y_0)^2]+i\theta_0} + e^{-A[(x+x_1)^2+(y+y_1)^2]+i\theta_1} \quad (5.9)$$

where (x_0, y_0) , (x_1, y_1) represent the locations of dipole solitons, θ_0, θ_1 are the phase differences, A is a positive integer.

For the dipoles demonstrated in this study, we took the eigenvalue $\mu = -1$ and the lattice depth $V_0 = 12.5$.

5.3.1 Dipole solitons on a lattice with an edge dislocation

A dipole or two-phased localized vortex on the lattice with an edge dislocation is specified by the initial conditions defined in Eq.(5.9). Here, we take $K = k_x = k_y = 1$ where x_n, y_n and θ_n are given as

$$A = \pi, x_n = r \cos \theta_n, y_n = r \sin \theta_n, \theta_n = n\pi. \quad (5.10)$$

r is adjusted to locate dipole soliton (on minima or maxima) and numerical convergence of the mode can be quite sensitive to the value of r .

A dipole soliton profile, the phase structure and contour plot of dipole humps superimposed on the lattice with an edge dislocation located on the lattice minima are plotted in Fig. 5.2. Similarly, a dipole soliton which located on the lattice maxima is shown in Fig. 5.3.

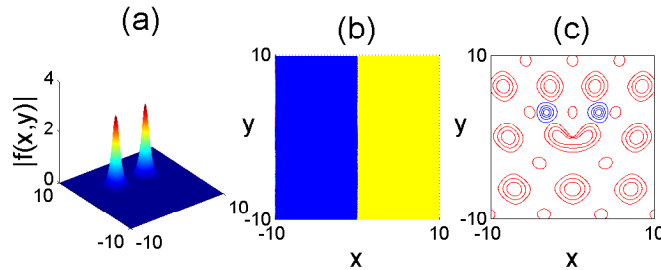


Figure 5.2 : (a) A dipole profile centered at the minima of the lattice with an edge dislocation for $x_0 = -x_1 = \pi$; $y_0 = y_1 = \pi$; (b) The phase structure of dipole solitons; (c) The contour plot of dipole solitons superimposed on the underlying lattice.

In Fig. 5.4, we plotted the dipole soliton power versus the propagation constant μ for dipoles on a lattice with an edge dislocation. As seen from the figure, the slope condition is satisfied for dipoles located on the lattice minima but this condition is

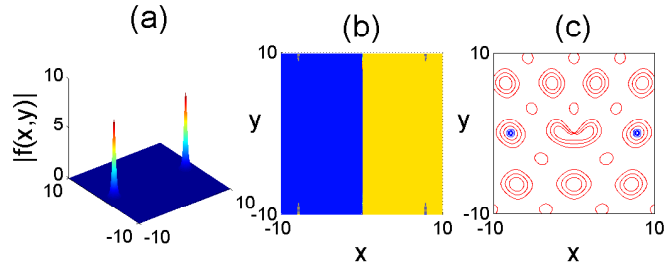


Figure 5.3 : (a) A dipole profile centered at maxima of the lattice with an edge dislocation for $r = 5\pi/2$; (b) The phase structure of dipole solitons; (c) The contour plot of dipole solitons superimposed on the underlying lattice.

violated for dipoles located on the lattice maxima. According to this graph, dipoles on minima are not expected to suffer from collapse.

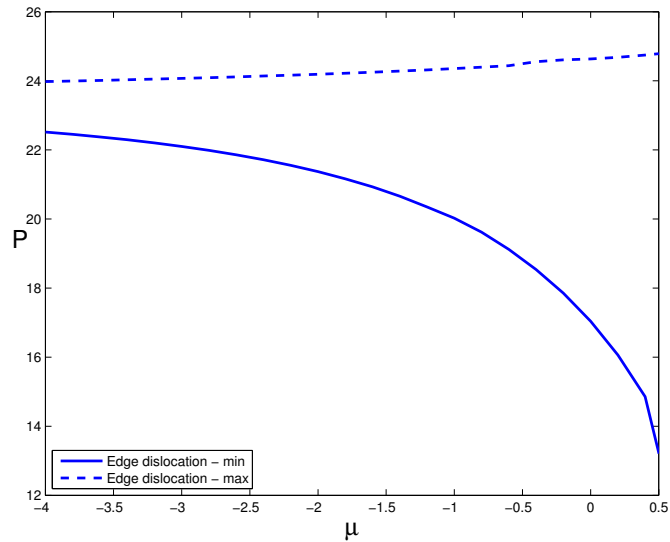


Figure 5.4 : The power versus μ (eigenvalue) of dipole solitons for the lattice with an edge dislocation.

In order to examine the nonlinear stability properties of the dipole solitons found above, we directly compute Eq. (5.1) over a long distance. We plot the maximum amplitude of the dipole soliton centered at the lattice maxima (and minima) versus the propagation distance, the centers of mass, the phase structure and the contour plot of the humps on the underlying lattice during the evolution.

We first present the nonlinear stability properties of dipole solitons on the minima of the lattice with an edge dislocation (see Fig. 5.5).

Although the maximum amplitude of these dipole solitons oscillates mildly, dipole humps move from their initial locations during the direct simulation (drift instability) and the phase structure is entangled as well. These facts indicate the nonlinear

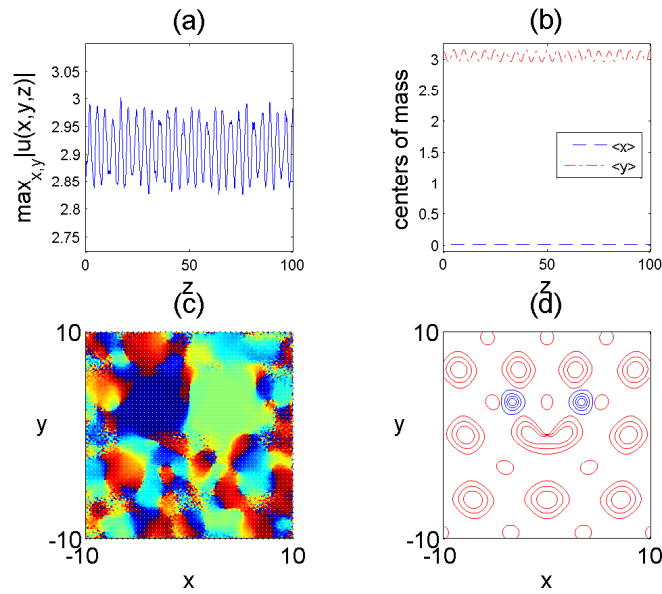


Figure 5.5 : Nonlinear instability of a dipole on the minima of the lattice with an edge dislocation. (a) Maximum amplitude as a function of propagation distance; (b) Center of mass; (c) Contour plot of the complex-phase at $z = 100$; (d) Contour plot of the amplitude at $z = 100$.

instability of a dipole that is centered at the minima of the lattice with an edge dislocation.

The nonlinear stability properties of the dipole solitons on the maxima of the lattice with an edge dislocation are demonstrated in Fig. 5.6.

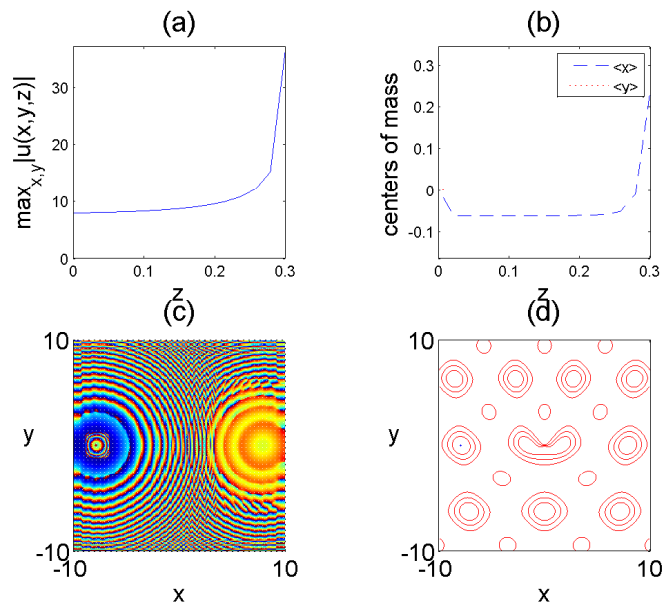


Figure 5.6 : Collapse of dipoles on the maxima of the lattice with an edge dislocation. (a) Maximum amplitude as a function of propagation distance; (b) Center of mass; (c) Contour plot of the complex-phase at $z = 0.3$; (d) Contour plot of the amplitude at $z = 0.3$.

It is seen from the Fig. 5.6 that the maximum amplitude of dipole solitons increase significantly just after few diffraction lengths (approximately $z = 0.25$) due to strong localization. The phase structure also breaks up. This reveals that dipole solitons on the lattice maxima are nonlinearly unstable for these parameters. Actually, this is expected since solitons on lattice maxima are typically drift-unstable ([55]) and also their power is above the collapse threshold (see [15, 25]).

The results obtained by the direct simulation are consistent with the slope condition as expected.

5.3.2 Dipole solitons on a lattice with a vacancy defect

Using the spectral renormalization method, we find dipole solitons on the lattice with a vacancy defect, both located on the lattice minima and the lattice maxima. The dipole profiles are shown in Fig. 5.7 and Fig. 5.8 respectively. Here, we take $r = \pi$ for a dipole on lattice minima and $r = 2\pi$ for a dipole on lattice maxima.

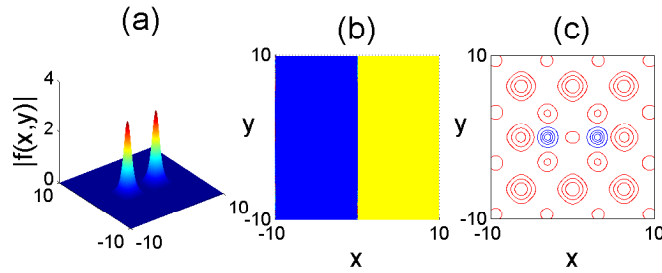


Figure 5.7 : (a) A dipole profile centered at minima of the lattice with a vacancy defect for $r = \pi$; (b) The phase structure of dipole solitons; (c) The contour plot of the dipole solitons superimposed on the underlying lattice.

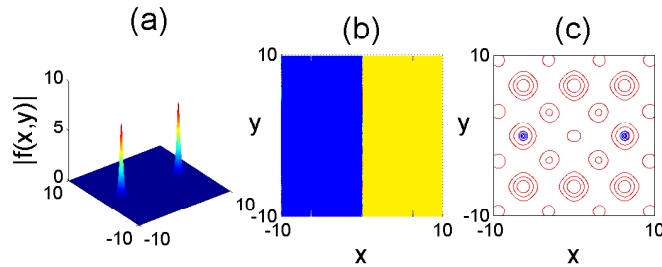


Figure 5.8 : (a) A dipole profile centered at maxima of the lattice with a vacancy defect for $r = 2\pi$; (b) The phase structure of dipole solitons; (c) The contour plot of the dipole solitons superimposed on the underlying lattice.

In Fig. 5.9, the dipole soliton power versus the propagation constant μ for dipoles on a lattice with a vacancy defect. Similar to the edge dislocation case, the slope condition is satisfied for dipoles on the lattice minima but is violated for dipoles on the lattice maxima.

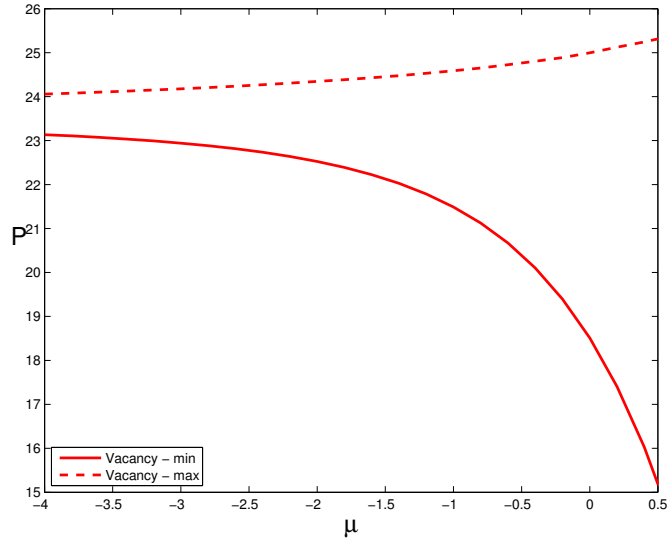


Figure 5.9 : The power versus μ (eigenvalue) of dipole solitons for the lattice with a vacancy defect.

The nonlinear stability properties of the dipole soliton located on minima of the lattice are shown in Fig. 5.10.

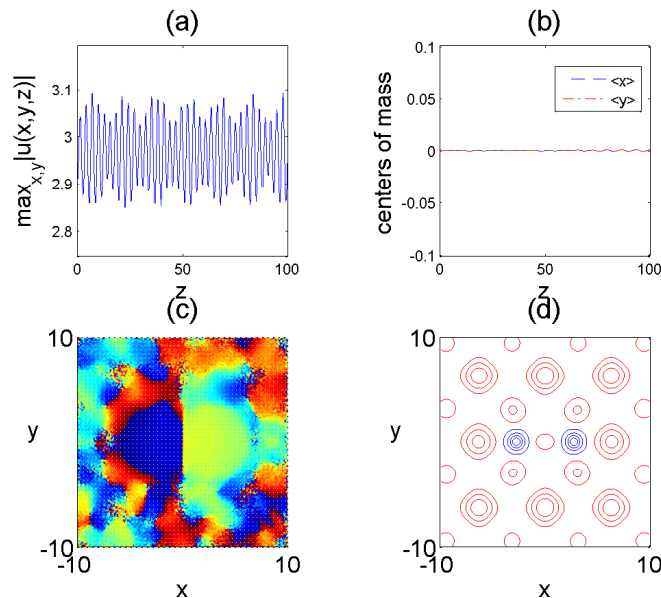


Figure 5.10 : Nonlinear stability of dipole solitons on the minima of the lattice with a vacancy defect. (a) Maximum amplitude as a function of propagation distance; (b) Center of mass; (c) Contour plot of the complex-phase at $z = 100$; (d) Contour plot of the amplitude at $z = 100$.

As can be seen from the Fig. 5.10, the maximum amplitude of the dipole oscillates with relatively small amplitude and dipole humps stay nearly at the same place during the direct simulation (no drift instability). The phase structure is also preserved. Hence, the dipole that centered at minima of the lattice with a vacancy defect is found to be nonlinearly stable.

On the other hand, dipole solitons centered at the lattice maxima are nonlinearly unstable due to sharp increment in the maximum amplitude just after approximately $z = 0.4$. Further, the phase structure breaks up during the simulation. There is no drift instability as the humps stay at their initial locations but the first two features are enough to conclude that the the dipole on the lattice maxima with a vacancy defect is nonlinearly unstable due to collapse (see Fig. 5.11).

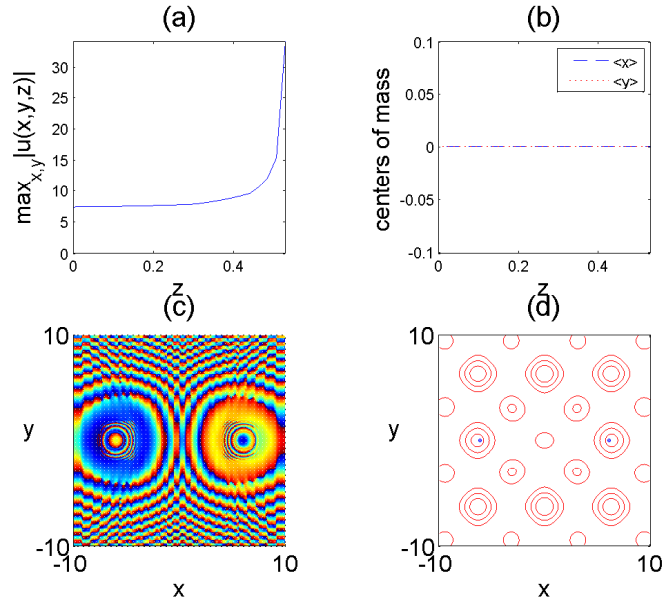


Figure 5.11 : Collapse of dipoles on the maxima of the lattice with a vacancy defect. (a) Maximum amplitude as a function of propagation distance; (b) Center of mass; (c) Contour plot of the complex-phase at $z = 0.53$; (d) Contour plot of the amplitude at $z = 0.53$.

In order to compare the nonlinear stability properties of dipoles located on the periodic lattice (which can be obtained by substituting $N = 4$ into Eq. (5.2)) and dipoles located on a lattice with a vacancy defect, we have also examined the stability of a dipole on periodic lattice minima. The maximum amplitude, the location of the centers of mass of dipole solitons on periodic lattice minima versus the propagation distance $z = 100$ are plotted in Fig. 5.12. The phase structure and the contour plots of the maximum amplitudes at the final point $z = 100$ are also depicted in the same figure. It is clearly

seen that, the dipole solitons on periodic lattice minima is nonlinearly stable since the maximum amplitude oscillates with relatively small amplitude and the dipole solitons preserve their locations during the evolution. This result is in the same essence with that of the stability property of a dipole on the minima of the lattice with a vacancy defect.

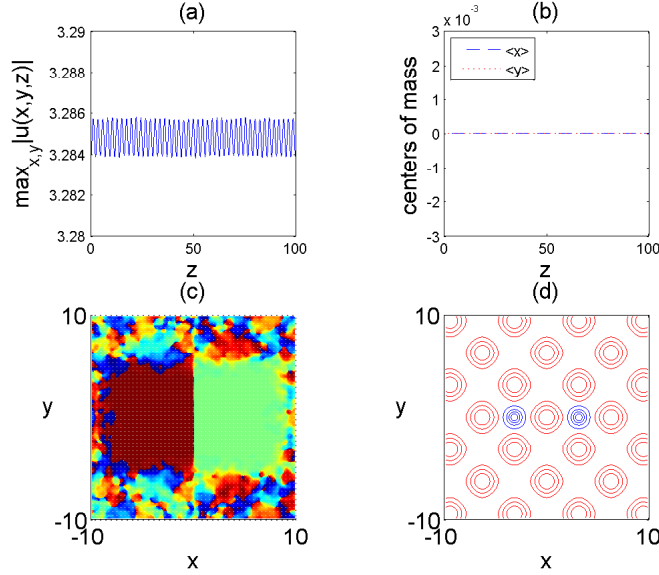


Figure 5.12 : Nonlinear stability of dipole solitons on periodic lattice minima. (a) Maximum amplitude as a function of propagation distance; (b) Center of mass; (c) Contour plot of the complex-phase at $z = 100$; (d) Contour plot of the amplitude at $z = 100$.

The nonlinear stability properties of the dipole solitons on periodic lattice maxima is demonstrated in Fig. 5.13. The dipole on periodic lattice maxima is found to be nonlinearly unstable since it exhibits strong localization after a few diffraction lengths and break up in the phase structure. As the result, the collapse dynamics of both dipoles located on the periodic lattice maxima and the lattice with a vacancy defect are observed to be very similar.

5.4 Existence of Vortex Solitons and Stability Analysis

Vortex solitons on defect lattices, including both three and four-hump vortex solitons are found numerically with the initial condition defined in Eq. (5.11).

$$w_0(x, y) = \sum_{n=0}^{M-1} e^{-A[(x+x_n)^2 + (y+y_n)^2] + i\theta_n} \quad (5.11)$$

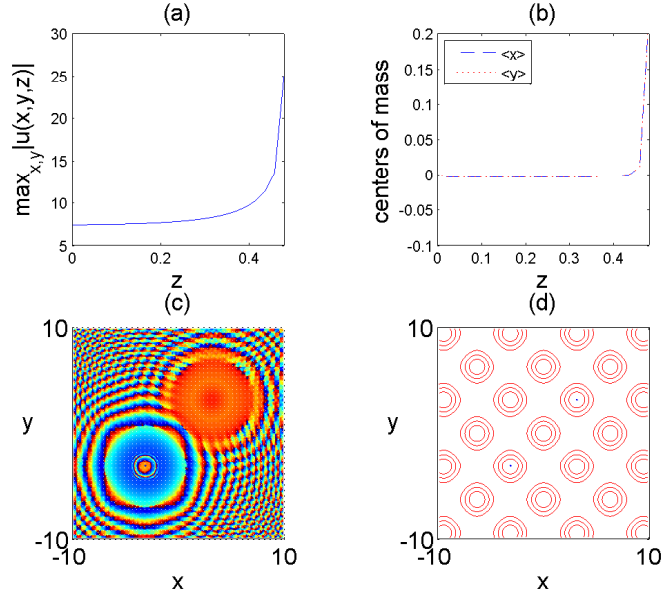


Figure 5.13 : Collapse of dipoles on periodic lattice maxima. (a) Maximum amplitude as a function of propagation distance; (b) Center of mass; (c) Contour plot of the complex-phase at $z = 0.48$; (d) Contour plot of the amplitude at $z = 0.48$.

where x_n, y_n represent the location of the vortex humps, θ_n is the phase difference, M corresponds to the number of humps and A is a positive integer.

5.4.1 Three-hump vortex on a lattice with an edge dislocation

Despite the strong irregularity, 3-hump vortex solitons are found numerically, on the lattice with an edge dislocation. Three-hump vortex solitons both at the lattice maxima and minima are investigated separately.

In order to generate a three-hump vortex structure, we take $k_x = k_y = 1$ and $M = 3$ in Eq. (5.11). A three-hump vortex profile, its phase structure and the contour plot of vortex solitons on the lattice minimum near the edge dislocation, with $A = 1$, is shown in Fig. 5.14.

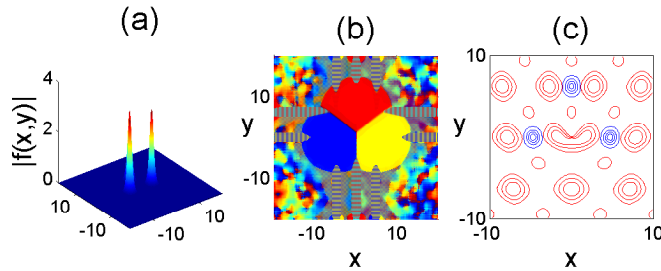


Figure 5.14 : (a) A three-hump vortex profile centered at the minima of the lattice for $x_0 = 3\pi/2, x_1 = 0, x_2 = -3\pi/2$; $y_0 = 0, y_1 = 2\pi, y_2 = 0$; (b) The phase structure of the vortex; (c) The contour plot of the vortex humps superimposed on the underlying lattice.

Similarly, a three-hump vortex at the lattice maxima, with $A = 1$, is shown in Fig.5.15.

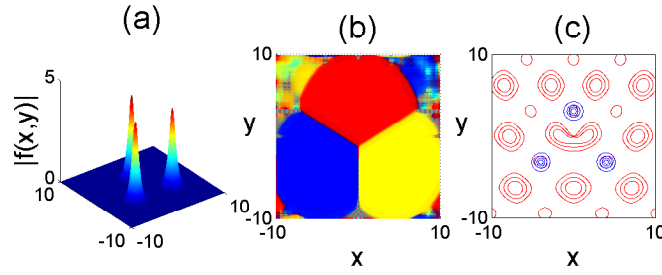


Figure 5.15 : (a) A three-hump vortex profile centered at the maxima of the lattice for $x_0 = -x_2 = 4, x_1 = 0; y_0 = -y_1 = y_2 = \pi$; (b) The phase structure of the vortex solitons; (c) The contour plot of the vortex humps superimposed on the underlying lattice.

In Fig. 5.16, we plotted the three hump soliton power versus the propagation constant μ on a lattice with an edge dislocation. As seen from the figure, the slope condition is satisfied for three hump solitons located on both lattice minima and maxima. But, collapse is expected since the critical for collapse ($P_c \approx 11.7$) is exceeded for the case that the humps are located on the lattice maxima (see Fig.5.18).

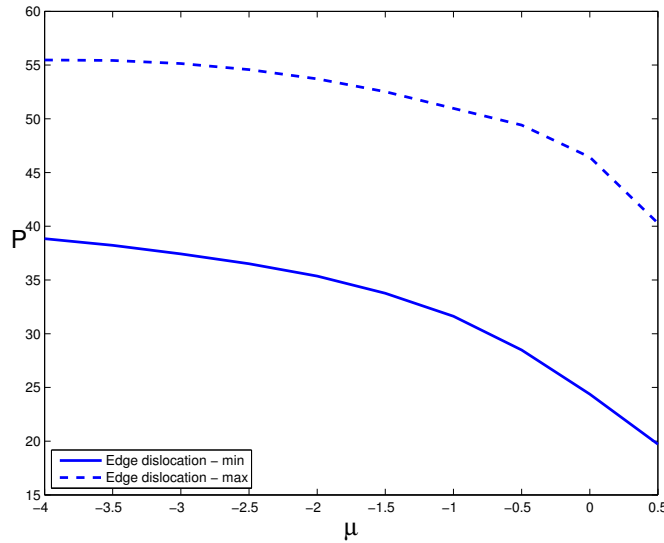


Figure 5.16 : The power versus μ (eigenvalue) of three-hump vortex for the lattice with an edge dislocation.

The nonlinear stability properties of the three-hump vortex on the minima of the lattice with an edge dislocation are demonstrated in Fig. 5.17. It can be seen from this figure that, the maximum amplitude of vortex solitons oscillates mildly and the vortex humps stay nearly at the same locations during the direct simulation (no drift instability). On the other hand, the breakup in the phase structure is observed. The breakup in the phase structure indicates the nonlinear instability of three-hump vortex located at the lattice minima.

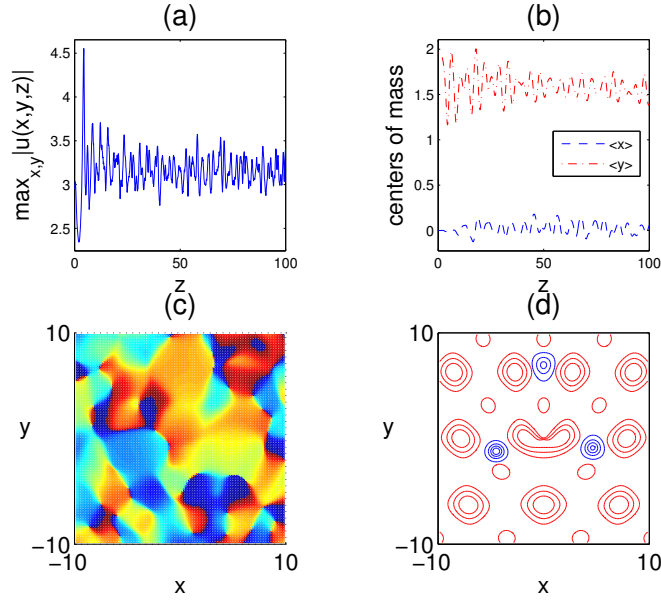


Figure 5.17 : Nonlinear instability of three vortex solitons on the minima of the lattice with an edge dislocation. (a) Maximum amplitude as a function of propagation distance; (b) Center of mass; (c) Contour plot of the complex-phase at $z = 100$; (d) Contour plot of the amplitude at $z = 100$.

Next, the nonlinear stability of three-hump vortex on the maxima of the lattice with an edge dislocation is examined (see Fig. 5.18) and it is observed that the maximum amplitude of vortex solitons increases significantly just after approximately $z = 0.2$ although there is no drift instability. This reveals that three-hump vortex at lattice maxima eventually become unstable and collapse after a finite propagation distance z .

5.4.2 Four-hump vortex on a lattice with a vacancy defect

Four-hump vortex structures on the lattice with a vacancy defect are obtained numerically. In order to generate this vortex, we take $k_x = k_y = 1$, $A = \pi$ and $M = 4$.

A four-hump vortex profile, its phase structure and contour plots superimposed on the minimum of the lattice with a vacancy defect close to defect, is shown in Fig.5.19; in this case we set $\theta_n = n\pi/2$ and $r = \pi$.

A four-hump vortex profile, its phase structure and contour plots superimposed on the minimum of the lattice with a vacancy defect but farther away from the lattice center (away from the vacancy defect), is shown in Fig. 5.20. The locations of the vortex humps for this case are defined as $x_0 = -x_2 = 2\pi$, $-x_1 = x_3 = \pi$; $y_0 = -y_2 = \pi$, $y_1 = -y_3 = 2\pi$.

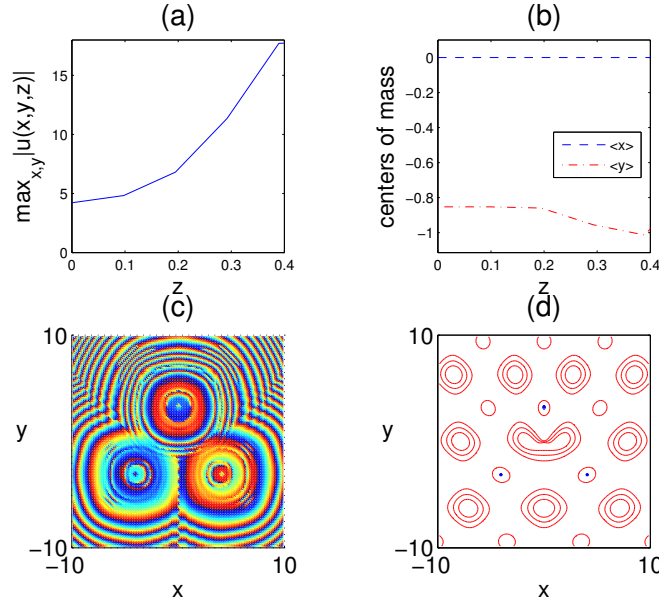


Figure 5.18 : Collapse of three vortex solitons on the maxima of the lattice with an edge dislocation. (a) Maximum amplitude as a function of propagation distance; (b) Center of mass; (c) Contour plot of the complex-phase at $z = 0.4$; (d) Contour plot of the amplitude at $z = 0.4$.

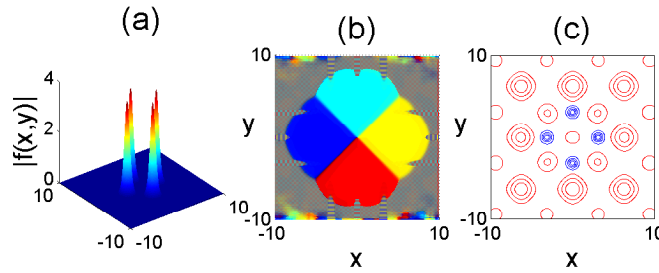


Figure 5.19 : (a) A four-hump vortex profile centered at the minima of the lattice with a vacancy defect (close to defect); (b) The phase structure of the vortex; (c) The contour plot of the vortex humps superimposed on the underlying lattice.

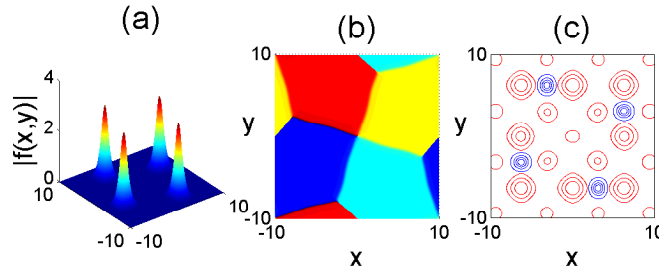


Figure 5.20 : (a) A four-hump vortex profile centered at the minima of the lattice with a vacancy defect; (b) The phase structure of the vortex; (c) The contour plot of the vortex humps superimposed on the underlying lattice.

We next show the existence of a four-hump vortex located at the maxima of the lattice with a vacancy defect in Fig. 5.21. In this case, we set $\theta_n = n\pi/2 + \pi/4$ and $r = 0.96\pi$.

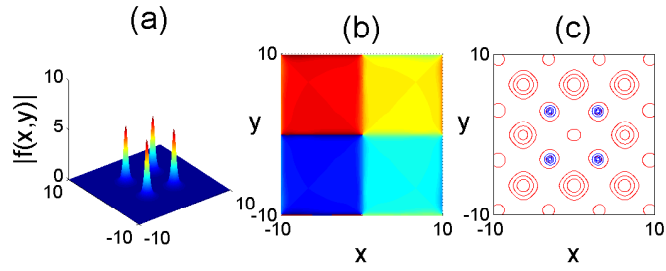


Figure 5.21 : (a) A four-hump vortex profile centered at the maxima of the lattice with a vacancy defect; (b) The phase structure of the vortex; (c) The contour plot of the vortex humps superimposed on the underlying lattice.

In Fig. 5.22, the soliton power versus the propagation constant μ for four-hump vortices on a lattice with a vacancy defect is depicted. It is observed from the figure that, the slope condition is satisfied for four-hump vortex on the lattice minima but is violated for vortices on the lattice maxima.

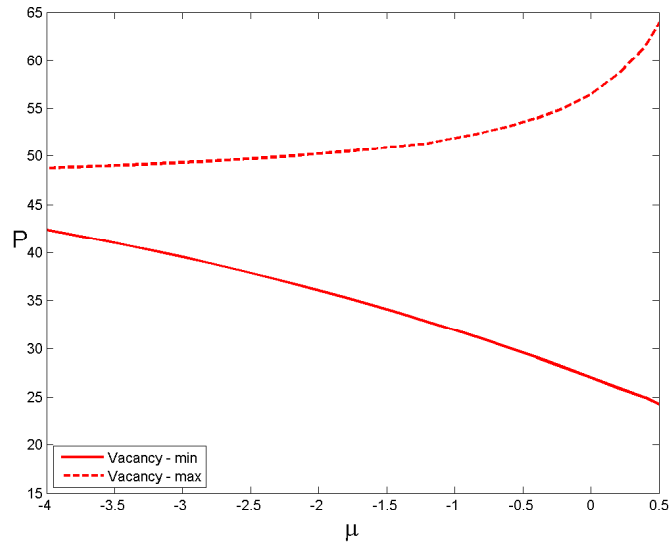


Figure 5.22 : The power versus μ (eigenvalue) of four-hump vortex for the lattice with a vacancy defect.

We also examined the nonlinear stability of four-hump vortex solitons on the lattice with a vacancy defect. We first investigate the nonlinear stability of the vortex solitons (see Fig. 5.19) that located on minimum of the lattice (see Fig. 5.23). It is seen from this figure that the maximum amplitude of vortex solitons decreases significantly until approximately $z = 0.8$, and after this value, it starts to increase again. Besides, the phase structure breaks up during the propagation and vortex humps spread to the neighboring lattice sites. These facts indicate the nonlinear instability of four-vortex solitons located on the minima of the lattice with a vacancy defect (close to the defect) in this parameter regime.

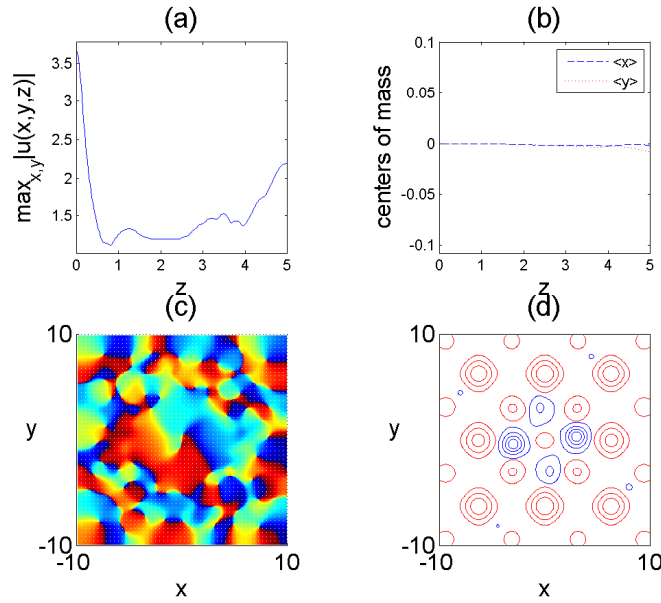


Figure 5.23 : Nonlinear instability of four vortex solitons on the minima of the lattice with a vacancy defect (close to defect). (a) Maximum amplitude as a function of propagation distance; (b) Center of mass; (c) Contour plot of the complex phase at $z = 5$; (d) Contour plot of the amplitude at $z = 5$.

In order to investigate the effect of the locations of the vortex humps (being away from or close to the vacancy defect), we examined the nonlinear stability of four-hump vortex solitons on the lattice with a vacancy defect but farther away from the lattice center (Fig. 5.20). It is observed that, the maximum amplitude of the vortex solitons oscillates with small amplitude and during the evolution, the vortex solitons do not move from their locations; meaning that there is no drift instability either but the phase structure becomes entangled (see Fig. 5.24). Therefore, moving the vortex humps away from the lattice center where the vacancy defect is located, improves the nonlinear stability of the four vortex solitons.

The nonlinear instability of four vortex solitons on the maxima of the lattice with a vacancy defect is demonstrated in Fig. 5.25. The vortex solitons are found to be nonlinearly unstable since the maximum amplitude increases significantly just after $z = 0.7$ and, the phase structure is not preserved either, although the vortex humps stay nearly at their initial locations (no drift instability is observed).

In order to compare the collapse dynamics of the four-hump vortex solitons located on a perfectly periodic lattice (which can be obtained by substituting $N = 4$ in Eq. (5.2)), to the four-vortex solitons located on a lattice with a vacancy defect, we demonstrated the stability properties of four-hump vortex structure located on periodic lattice.

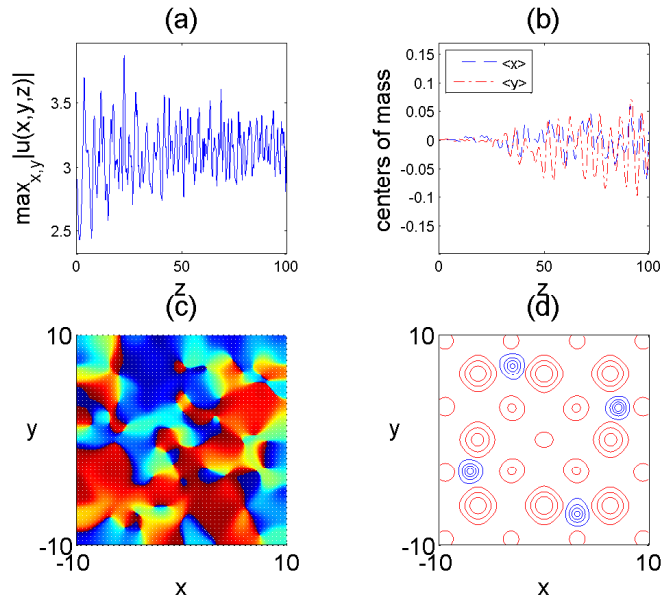


Figure 5.24 : Nonlinear instability of four vortex solitons on the minima of the lattice with a vacancy defect (away from defect). (a) Maximum amplitude as a function of propagation distance; (b) Center of mass; (c) Contour plot of the complex phase at $z = 100$; (d) Contour plot of the amplitude at $z = 100$.

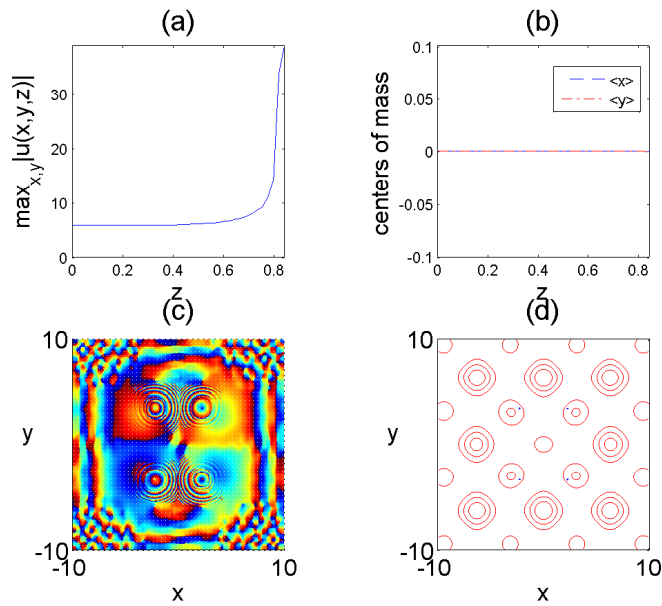


Figure 5.25 : Collapse of four vortex solitons on the maxima of the lattice with a vacancy defect. (a) Maximum amplitude as a function of propagation distance; (b) Center of mass; (c) Contour plot of the complex phase at $z = 0.84$; (d) Contour plot of the amplitude at $z = 0.84$.

In Fig. 5.26, we plot: the maximum amplitude, the location of the centers of mass of the vortex humps versus the propagation distance $z = 100$, the phase structure and contour plots of the vortex hump amplitudes on the periodic lattice at the final distance $z = 100$. It is seen that the maximum amplitude of the vortex solitons oscillates

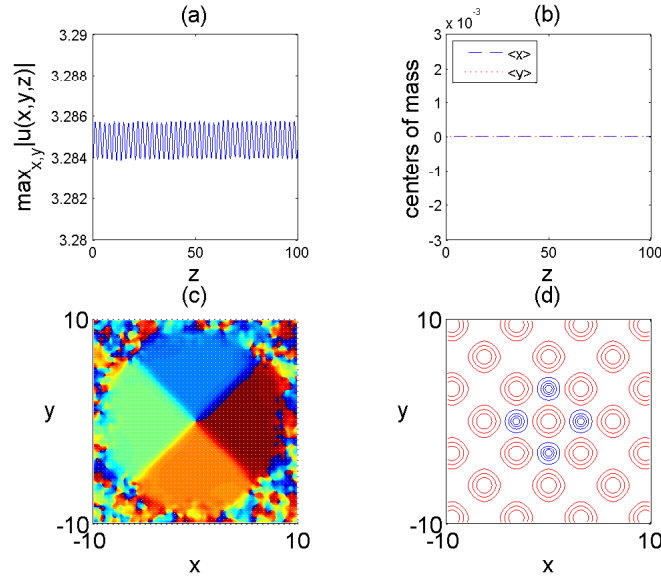


Figure 5.26 : Nonlinear stability of four vortex solitons on the minima of the periodic lattice. (a) Maximum amplitude as a function of propagation distance; (b) Center of mass; (c) Contour plot of the complex phase at $z = 100$; (d) Contour plot of the amplitude at $z = 100$.

with small amplitude. Furthermore, during the evolution, the vortex solitons do not move from their locations; meaning that there is no drift instability either. The same figure also reveals that, during the evolution, the phase structure is perfectly preserved. Resulting these facts, four hump vortex solitons at periodic lattice minima are found to be nonlinearly stable as opposed to the fact that, four vortex solitons on the minima of the lattice with a vacancy defect is found to be nonlinearly unstable.

Following the same order with that of lattice with a vacancy defect case, we continue with the four hump vortex solitons on periodic lattice maxima. Taking the four hump vortex on periodic lattice maxima as the initial condition, the nonlinear stability properties are examined.

As can be seen from Fig. 5.27, the maximum amplitude of the four hump vortex solitons centered at the periodic lattice maxima increases very sharply, after a short propagation distance (around $z = 0.4$) indicating that these vortex solitons are nonlinearly unstable. The break up in the phase is also quite clear in the same figure. This figure also indicates the similar collapse behavior of four vortex solitons on lattice maxima, for both of the lattices (periodic and vacancy defect).

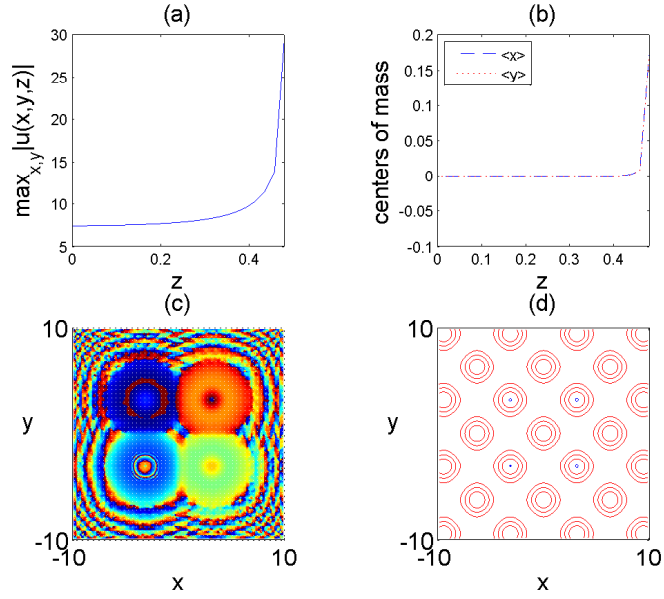


Figure 5.27 : Collapse of four vortex solitons on the maxima of the periodic lattice. (a) Maximum amplitude as a function of propagation distance; (b) Center of mass; (c) Contour plot of the complex-phase at $z = 0.48$; (d) Contour plot of the amplitude at $z = 0.48$.

5.5 Conclusion

We have numerically investigated dipole and multiple vortex structures associated with irregular lattices, possessing edge dislocations and vacancy defects. The results of this study indicate that, despite the irregularities, dipole and vortex solitons do exist both on the lattice with an edge dislocation and on the lattice with a vacancy defect. We investigated the nonlinear stability properties of these solitons by direct simulations of the NLSE.

The simulations of the NLSE showed that, on the lattices with defects,

(i) except the dipole and the four vortex solitons (located away from the defect) on the lattice with a vacancy defect, all of the dipoles and multiple vortex structures are found to be nonlinearly unstable on *lattice minima*.

The nonlinear instabilities of these dipoles and multiple vortex solitons are due to the degenerations in the phase structures and for the four hump vortex, instability is also accompanied by an irregularity in the amplitude. Although phase entanglement is observed during the direct evolution, locating the vortex humps on minima of a

defected lattice can be considered as a collapse arrest mechanism in the sense of stabilization of the maximum amplitude.

(ii) all of the dipoles and multiple vortex structures are found to be nonlinearly unstable on *lattice maxima*. The nonlinear instabilities of these dipoles and multiple vortex solitons occur as a result of collapse (sharp increment in the amplitude), whereas the phase structure remains fairly stable up until the collapse points.

(iii) for the perfectly periodic lattice and for the lattice with a vacancy defect, the collapse distances are more or less the same ($z \approx 0.5$) for four hump vortices and for dipoles at lattice maxima, furthermore, the blow-up dynamics are quite similar for all the above mentioned dipole and vortex solitons.

It is known that, suppressing collapse in periodic and quasiperiodic lattice solitons (for fundamental, dipole and vortex) can be achieved by increasing the lattice depth. Adding saturation to the system may also act like a collapse arrest mechanism for such structures. Thus, it would be interesting to study dipoles/vortices in deeper defected lattices in Kerr and in saturable media. Investigating collapse arrest mechanisms for dipole and vortex solitons in lattices with defects will be left for future studies.

Although computational results do not prove rigorously the existence of multiple solitons on lattices with defects, the results of this work may be encouraging for further investigations of dipole and vortex structures on complex lattices in nonlinear optics.

6. NLSM SOLITONS IN A LATTICE WITH A VACANCY DEFECT

In this part of the study, we numerically investigate fundamental, dipole and vortex solitons in the (2+1)-dimensional NLSM (or DS type) system with an external potential (lattice) that possesses a vacancy defect. Linear and nonlinear stability properties of these solitons are also examined.

Here, we use the NLSM system with an external potential as model;

$$iu_z + \frac{1}{2}\Delta u + |u|^2 u - \rho\phi u - V(x,y)u = 0, \quad \phi_{xx} + v\phi_{yy} = (|u|^2)_{xx}. \quad (6.1)$$

We consider an irregular 2D square lattice with a vacancy defect

$$V(x,y) = \frac{V_0}{25} \left| 2\cos(k_x x) + 2\cos(k_y y) + e^{i\theta(x,y)} \right|^2 \quad (6.2)$$

where $V_0 > 0$ is constant and corresponds to the peak depth of the potential, i.e., $V_0 = \max_{x,y} V(x,y)$ and the phase function θ is given by

$$\theta(x,y) = \tan^{-1}\left(\frac{y-y_0}{x}\right) - \tan^{-1}\left(\frac{y+y_0}{x}\right) \quad (6.3)$$

Physically, $\theta(x,y)$ corresponds to two first order phase dislocations displaced in the y direction by a distance of $2y_0$ in the y direction. A vacancy defect can thus be obtained using $y_0 = \pi/K$ where $K = k_x = k_y$ [25].

By setting $\theta = 0$ in Eq. (6.2), the irregularity in the lattice with a vacancy defect is removed and this lattice becomes a perfectly periodic one.

Contour images and diagonal cross-sections of a periodic lattice and the lattices with a vacancy defect are displayed in Fig. 6.1.

As can be seen from this figure, there is an empty cell at the center of the lattice with a vacancy defect.

We use the spectral renormalization method (which explained in Chapter 3 in detail) to calculate soliton solutions of the NLSM system. To do this, we seek solution of the system (6.1) in the form $u(x,y,z) = f(x,y)e^{-i\mu z}$ where $f(x,y)$ is a complex-valued function and μ is the propagation constant (or eigenvalue).

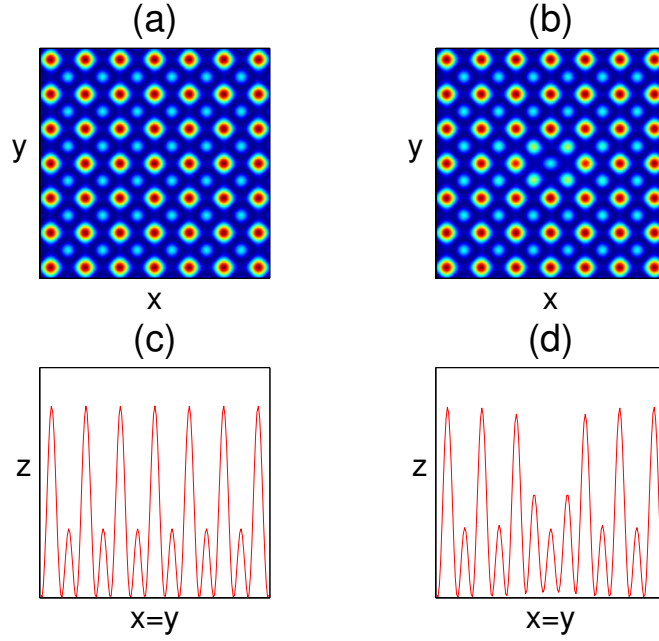


Figure 6.1 : Contour image of (a) The lattice without defect (periodic); (b) Lattice with a vacancy defect; and diagonal cross-section of (c) The lattice without defect; (d) The lattice with a vacancy defect.

For all calculations in this part, we fix the lattice depth $V_0 = 12.5$, $\mu = 0.5$, $\rho = 1$. $\nu = 1$ and $K = k_x = k_y = 2\pi$.

6.1 Numerical Existence of Fundamental Solitons and Stability Analysis

Here, we show the existence of fundamental solitons in the lattice with a vacancy defect and investigate their stability properties.

6.1.1 Numerical existence of fundamental solitons

Fundamental solitons in the lattice are found numerically (by SR method) with the initial condition

$$w_0(x, y) = e^{-A[(x+x_0)^2 + (y+y_0)^2]} \quad (6.4)$$

where x_0 and y_0 represent the location of fundamental soliton on the lattice. In order to see the effect of the vacancy defect, we locate our initial condition at center ($x_0 = 0$, $y_0 = 0$) of the lattice with a vacancy defect.

The fundamental soliton at center of the lattice with a vacancy defect is shown in Fig. 6.2 for potential depth $V_0 = 12.5$ and eigenvalue $\mu = 0.5$.

The first nonlinear band-gap structure of the periodic lattice ($\theta = 0$ in Eq. (6.2)) and the lattice with a vacancy defect are plotted in Fig. 6.3 for $K = k_x = k_y = 2\pi$.

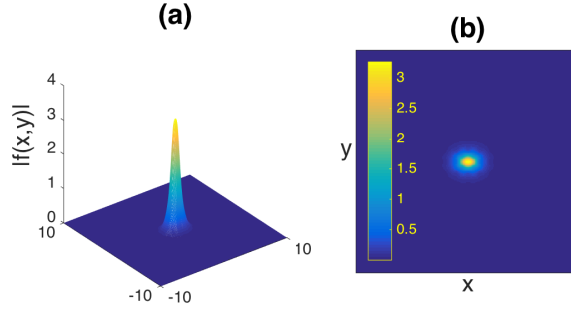


Figure 6.2 : Fundamental soliton situated at center of the lattice with a vacancy defect. (a) 3D view of the soliton; (b) Contour image of the soliton.

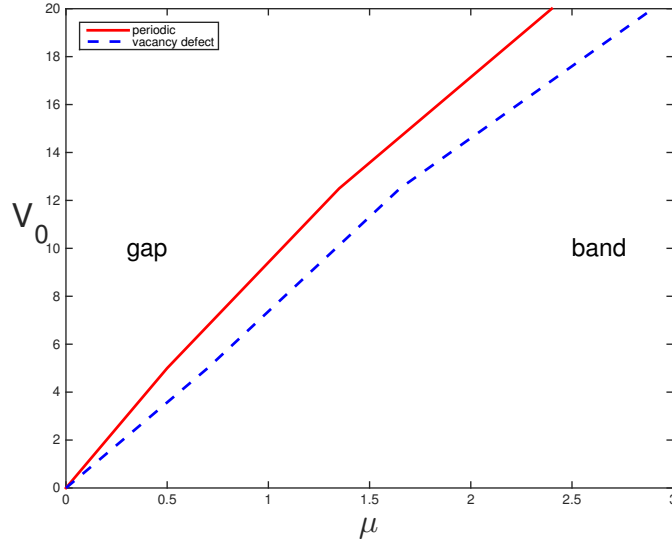


Figure 6.3 : Band-gap formation of NLSM system with periodic potential and the lattice with a vacancy defect.

As can be seen from Fig. 6.3, the gap region for the lattice with a vacancy defect is narrower than that of the periodic (original) lattice.

6.1.2 Stability analysis of fundamental solitons

Evolution of solitons under perturbations is very important for applications and, the soliton power ($P \equiv P[u] := \iint_{-\infty}^{\infty} |u|^2 dx dy$) plays an important role to determine the nonlinear stability of fundamental solitons. The soliton is stable only if its power decreases with increasing propagation constant μ . This condition is called the slope condition ($dP/d\mu < 0$) [52–54].

We investigate soliton power of the lattice with a vacancy defect in Fig. 6.4 for $\rho = 1$, $v = 1$ and $V_0 = 12.5$.

As can be seen from Fig. 6.4, fundamental soliton located at center of the lattice with a vacancy defect meet the slope condition for $\mu = 0.5$ and $V_0 = 12.5$.

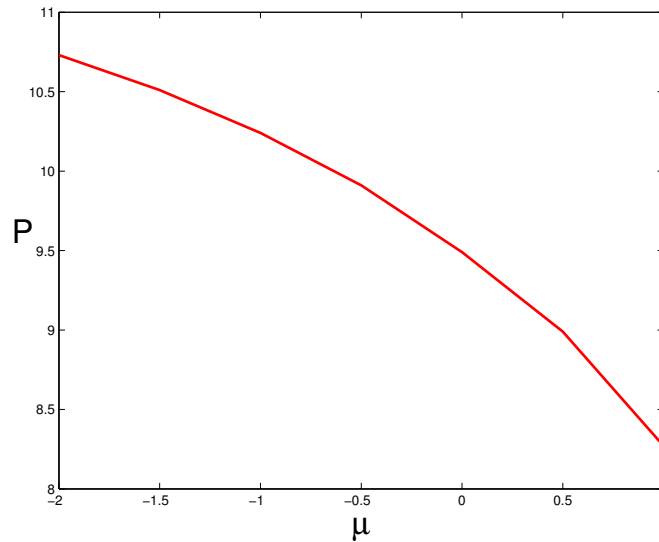


Figure 6.4 : Soliton power as a function of the eigenvalue μ within the semi-infinite band gap for the lattice with a vacancy defect.

Linear stability of the fundamental soliton (that obtained in Fig. 6.2) is examined by plotting linear evolution of the peak amplitude from $z = 0$ to $z = z_{max}$ (see Fig. 6.5).

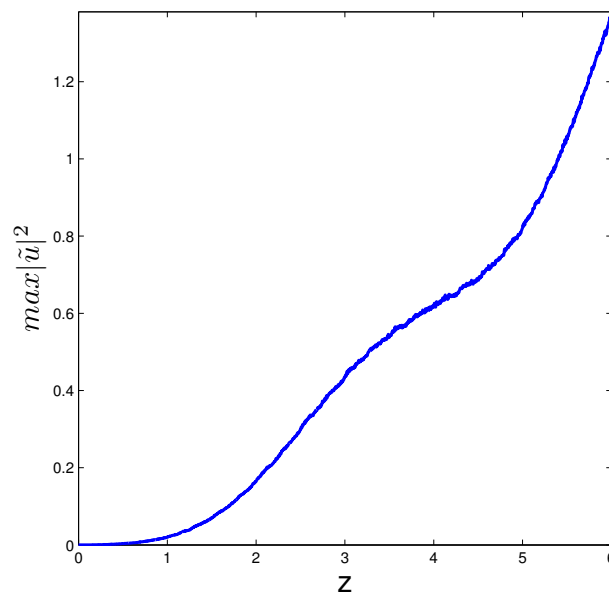


Figure 6.5 : Linear evolution of the fundamental soliton located in the lattice with a vacancy defect.

The peak amplitude of the perturbed soliton grows significantly in a finite distance. This indicates the linear instability of the fundamental soliton in the lattice with a vacancy defect.

Furthermore, the nonlinear stability of the fundamental soliton is examined in Fig. 6.6 by plotting the contour image and maximum amplitude of the soliton during the evolution.

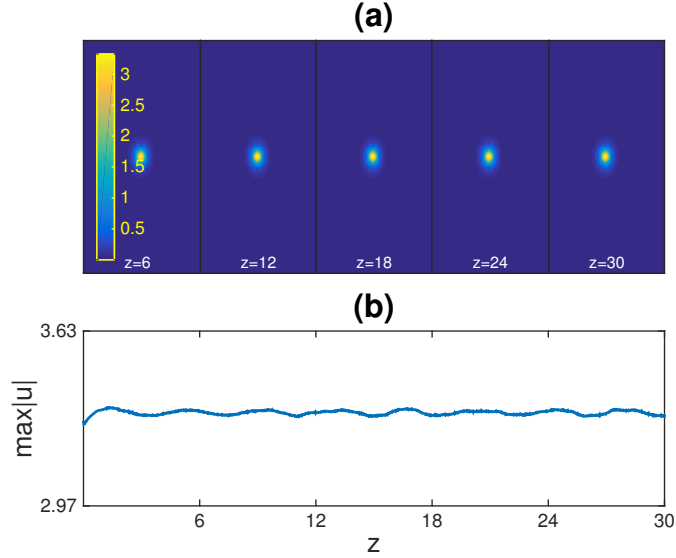


Figure 6.6 : Evolution of the fundamental soliton located at center of the lattice with a vacancy defect; (a) Contour image of the soliton; (b) Peak amplitude as a function of the propagation distance.

Contour image of the fundamental soliton keeps its shape (not shrinks or extends) and, peak amplitude of the fundamental soliton oscillates with relatively small amplitude during the evolution (see Fig. 6.6). This shows that the fundamental soliton located at center of the lattice with a vacancy defect is nonlinearly stable for these parameters.

6.2 Numerical Existence of Dipole Solitons and Stability Analysis

Similar to the fundamental solitons, we numerically demonstrate the existence of dipole solitons in the lattice with a vacancy defect and investigate their stability properties. For the spectral renormalization, we used the following initial conditions:

$$w_0(x, y) = e^{-A[(x+x_0)^2+(y+y_0)^2]+i\theta_0} + e^{-A[(x+x_1)^2+(y+y_1)^2]+i\theta_1} \quad (6.5)$$

where x_0, x_1, y_0, y_1 represent the locations of dipole solitons, θ_0, θ_1 show the phase differences and, A is a positive integer.

A dipole or two-phased localized vortex on the periodic lattice found numerically with

$$A = \pi, \quad x_n = r \cos \theta_n, \quad y_n = r \sin \theta_n \quad (6.6)$$

r is adjusted to locate dipole soliton and, numerical convergence of the mode can be quite sensitive to the value of r . A dipole soliton profile, the contour image and phase structure of dipole humps located near the vacancy defect is plotted in Fig. 6.7; we set $\theta_n = n\pi + \pi/2$ and $r = 2\pi$.

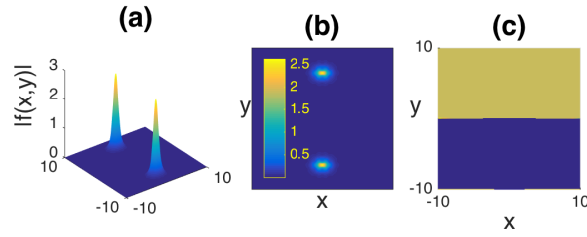


Figure 6.7 : (a) A dipole profile located near empty (vacancy) cell of the lattice with a vacancy defect; (b) Contour image of the dipole; (c) Phase structure of the dipole.

Furthermore, the linear and nonlinear stability properties of the dipole solitons (that obtained above) are studied.

Linear evolution of the dipole solitons in the lattice with a vacancy defect is investigated in Fig. 6.8.

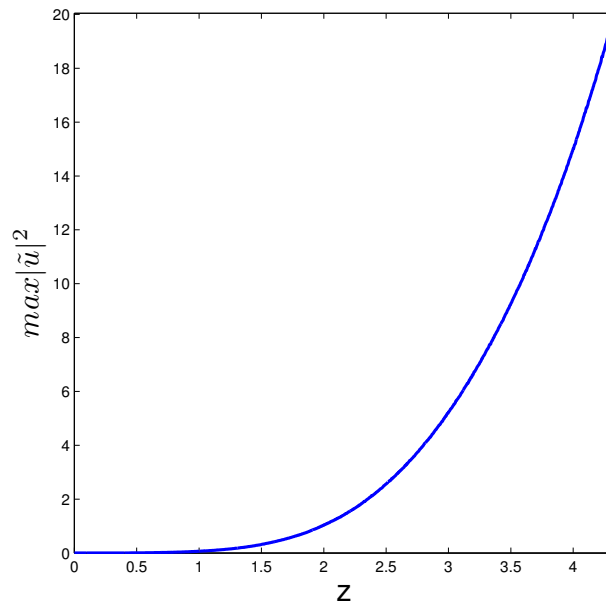


Figure 6.8 : Linear evolution of the dipole solitons in the lattice with a vacancy defect.

It can be seen from Fig. 6.8 that the peak amplitude of the dipole solitons blows up rapidly in a finite distance. Thus, the dipole in the lattice with a vacancy defect is linearly unstable.

The nonlinear stability properties of dipole solitons (see Fig. 6.7) near the empty cell of the lattice with a vacancy defect is investigated in Fig. 6.9.

As can be seen from the Fig. 6.9, contour image of the dipole solitons save their location and shape and, the maximum amplitude of the dipole oscillates mildly during

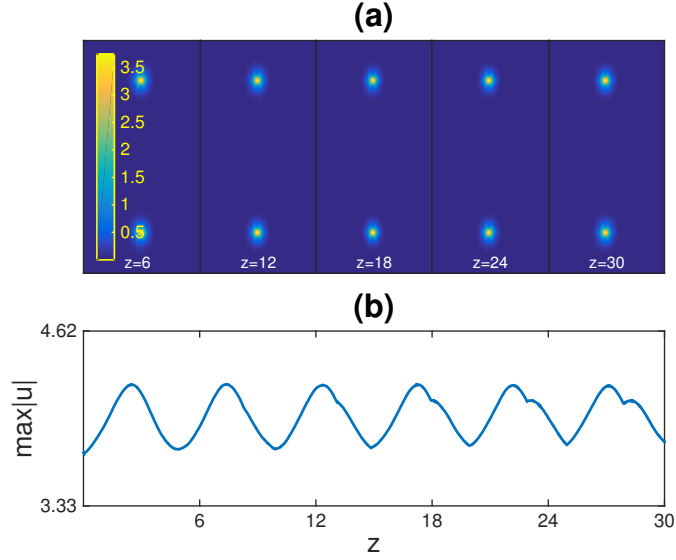


Figure 6.9 : Evolution of the dipole solitons located near vacancy defect of the lattice; (a) Contour image of the dipole; (b) Peak amplitude as a function of the propagation distance.

the evolution. Hence, the dipole that located near vacancy cell of the lattice is found to be nonlinearly stable.

6.3 Numerical Existence of Vortex Solitons and Stability Analysis

Four humps vortex solitons are obtained in the lattice with a vacancy defect and the stability of these vortex structures are examined. These solitons are found numerically with the initial condition;

$$w_0(x, y) = \sum_{n=0}^{M-1} e^{-A[(x+x_n)^2+(y+y_n)^2]+i\theta_n} \quad (6.7)$$

where x_n, y_n represent the location of the vortex humps, θ_n is the phase difference, M corresponds to the number of humps and A is a positive integer. To generate four-hump vortex on the periodic lattice, we set

$$M = 4, \quad A = \pi, \quad x_n = r \cos \theta_n, \quad y_n = r \sin \theta_n. \quad (6.8)$$

A four-hump vortex profile, its contour image and phase structure on the lattice with a vacancy defect is shown in Fig. 6.10; the locations of the vortex humps for this case are defined as $x_0 = -x_2 = 2\pi, -x_1 = x_3 = \pi; y_0 = -y_2 = \pi, y_1 = -y_3 = 2\pi$.

Vortex solitons' linear evolution in the lattice with a vacancy defect is investigated in Fig. 6.11.

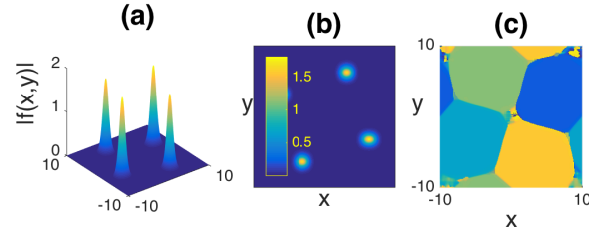


Figure 6.10 : (a) A vortex profile located near empty (vacancy) cell of the lattice; (b) Contour image of the vortex; (c) Phase structure of the vortex.

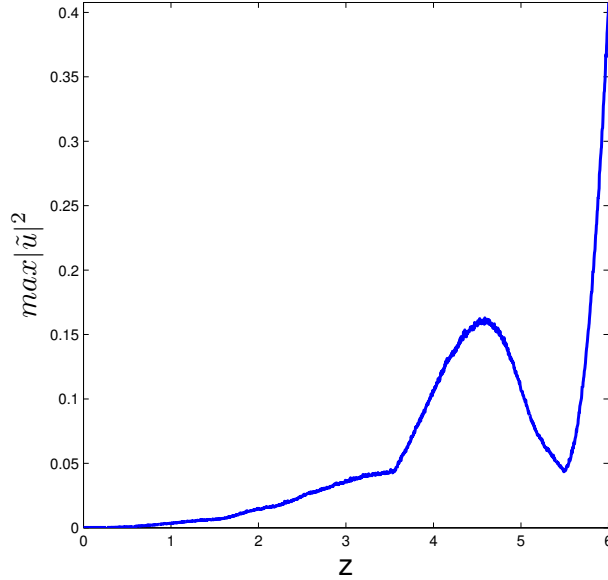


Figure 6.11 : Linear evolution of the vortex solitons in the lattice with a vacancy defect.

The peak amplitude of the vortex blows up in a finite distance (see Fig. 6.11). This indicates the linear instability of the vortex solitons in the lattice with a vacancy defect.

The nonlinear stability of four-hump vortex in the lattice with a vacancy defect is examined in Fig. 6.12.

As can be seen from the Fig. 6.12, the contour image of the vortex preserved and four humps stay nearly at the same place (no drift instability) during direct simulation. Also, the maximum amplitude of the vortex oscillates gently. This reveals that the vortex that located on the lattice with a vacancy defect is nonlinearly stable.

6.4 Comparison of the NLS and NLSM Models

In previous chapter, the existence and nonlinear stability properties of dipole and vortex soliton structures in the lattice with a vacancy defect were investigated for the NLSE. In this chapter, we have investigated properties of the fundamental, dipole and vortex

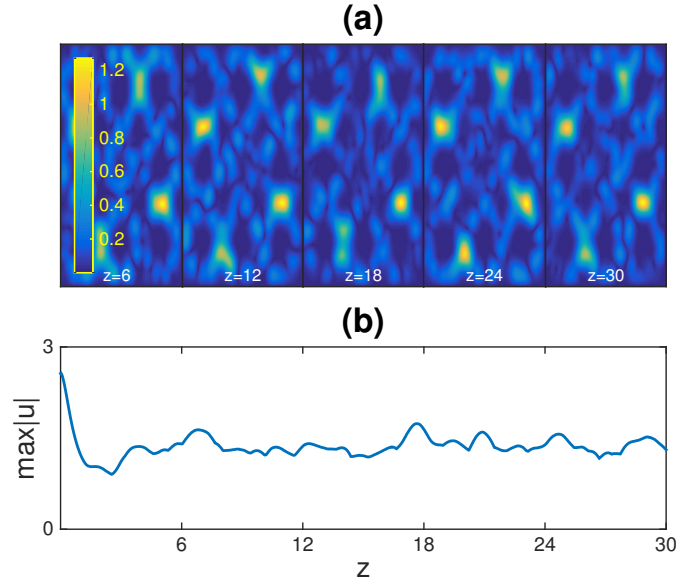


Figure 6.12 : Evolution of the vortex solitons on the lattice with a vacancy defect; (a) Contour image of the vortex; (b) Peak amplitude as a function of the propagation distance.

solitons in the NLSM system. Here, we compare the first nonlinear band-gap structures and the soliton powers of the NLSE and NLSM system with an external lattice that include a vacancy defect. We set $K = 2\pi$ and $\nu = 1$.

In Fig. 6.13, the first nonlinear band-gap boundaries of the lattice with a vacancy defect are determined for the NLSE and NLSM system.

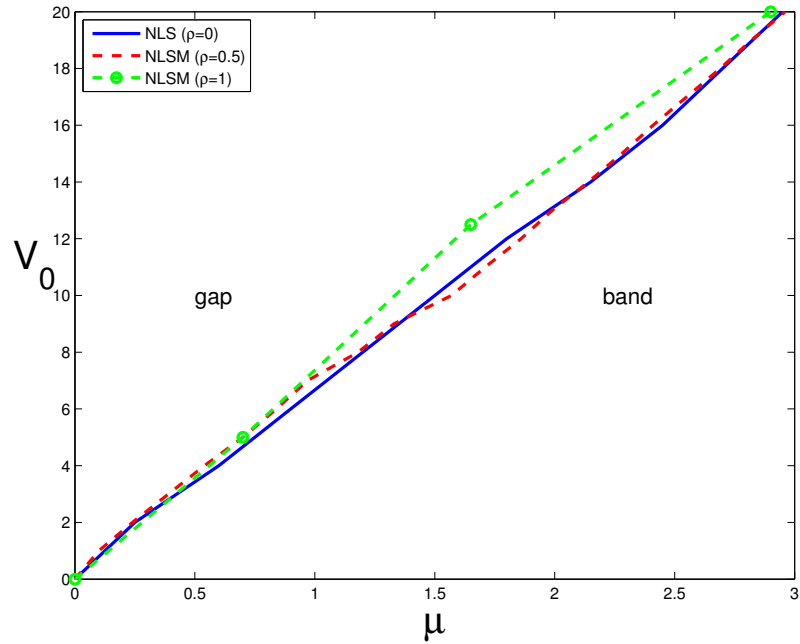


Figure 6.13 : The first nonlinear band-gap formation for the NLSE and NLSM system with the lattice that possesses a vacancy defect.

It can be seen from the band-gap analysis that the NLSE and NLSM systems have almost the same bound for the lattice with a vacancy defect. This reveals that the soliton solutions of the NLSE and NLSM system are generated nearly in the same propagation constant (μ) domain for the lattice with a vacancy defect.

Furthermore, soliton powers of the NLSE and NLSM system are compared in Fig. 6.14 for the lattice with a vacancy defect.

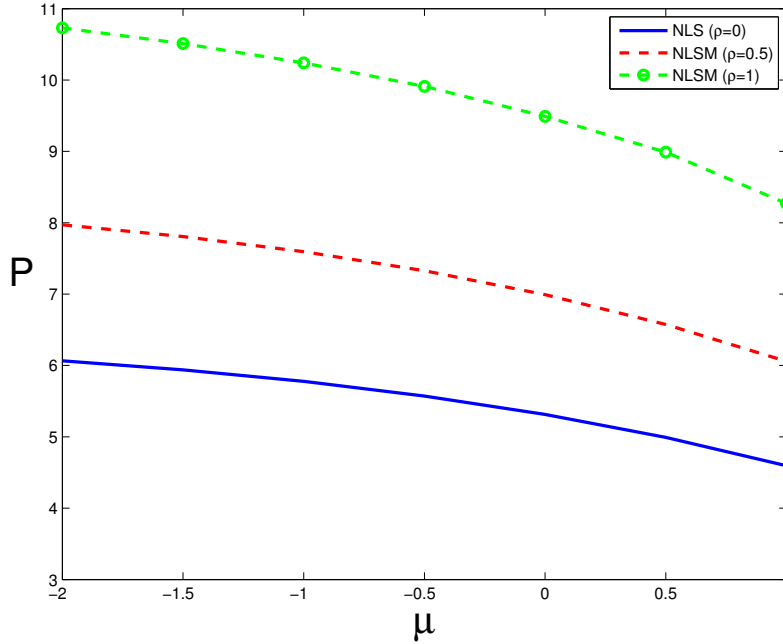


Figure 6.14 : Soliton power as a function of the eigenvalue μ within the semi-infinite band gap for the NLSE and NLSM systems with the lattice that possesses a vacancy defect. In all cases, we set peak depth $V_0 = 12.5$.

Although the band-gap boundaries are almost overlapping for the NLSE and NLSM system, there is a marked difference between the soliton powers of these models (see Fig. 6.14). The soliton power of NLSM system is greater than the NLSE for the lattice with a vacancy defect.

Increased power value has a negative effect on nonlinear stability properties of lattice solitons and, after a critical value of the power none of the solitons found stable [23].

Comparing NLSE and NLSM cases, one can see that dipole and vortex solitons of the NLSE are found stable when $\mu = -1$ and $V_0 = 12.5$ in the lattice with a vacancy defect (see Chapter 5), but here, we have to choose greater values of μ (as 0.5) to find nonlinearly stable solitons in the NLSM system. When we set $\mu = -1$ in the NLSM

system (with $\rho = 1$ and $\nu = 1$), the soliton power increases and the soliton structures become unstable in the lattice with a vacancy defect.

6.5 Conclusion

Numerical existence of the fundamental, dipole and vortex solitons have been demonstrated for NLSM system with an external lattice that include a vacancy defect. The band-gap structure has shown that the gap region of the lattice with a vacancy defect is narrower than that of the periodic lattice.

Furthermore, the linear and nonlinear stability properties of these solitons have been examined by direct simulations of NLSM system. It has seen that none of the solitons in the lattice with a vacancy defect is linearly stable due to blow-up. The results of nonlinear stability investigations showed that the fundamental, dipole and vortex solitons can be stable near vacancy defect under suitable conditions.

In final part, the NLSE and NLSM system are compared as model with the lattice that include a vacancy defect. The comparison has shown that although the first nonlinear band-gap structures are almost same for the NLSE and NLSM system, there is a marked difference between the soliton powers of these models.

7. FUNDAMENTAL SOLITONS OF THE NLSE IN PARITY-TIME SYMMETRIC LATTICE WITH A VACANCY DEFECT

In this chapter, we put forward a mechanism for delaying the collapse of the fundamental solitons in nonlinear media whose dynamics is governed by the two-dimensional NLSE with parity-time symmetric (\mathcal{PT} -symmetric) periodic potentials with/without a vacancy defect. This part of the study has been published in journal of "Optics Communications" under the title of "Fundamental Solitons in Parity-Time Symmetric Lattice with a Vacancy Defect" [41].

Solitons are special nonlinear waves and studies on soliton properties have provided a significant contribution to understanding of complex nonlinear systems.

The external potential of complex systems can be much more general and physically richer than a periodic lattice. For example, atomic crystals can have various irregularities, such as defects and edge dislocations or the optical potential may be complex. Recently, in [40], the numerical existence of dipole and vortex solitons for the two-dimensional NLSE with external potentials that possess strong irregularities, i.e., edge dislocations and vacancy defects are investigated and multi-humped solitons are computed by employing a spectral fixed-point computational scheme.

If the complex potential satisfies parity-time (\mathcal{PT}) symmetry, then the linear spectrum can still be all-real. Here, \mathcal{PT} -symmetry means that the potential is invariant under complex conjugation and simultaneous reflection in all spatial directions ($V^*(x, y) = V(-x, -y)$) [86, 87].

It is known that, in quantum mechanics, the eigenvalues of all operators (e.g., Hamiltonian) required to be real quantities and, it was accepted that operators should be Hermitian (self adjoint) to produce a real spectrum.

In 1998, exploration of Bender and Boettcher showed that non-Hermitian Hamiltonians can produce entirely real spectra, when they possess something known as \mathcal{PT} (parity-time) symmetry [88]. Also, it is demonstrated that in many cases a threshold exists in the Hamiltonians, above which the spectrum is no longer completely

real and instead becomes complex. This threshold shows the boundary between the \mathcal{PT} -symmetric and broken-symmetry phases [89–93].

In recent years, it is shown that complex \mathcal{PT} -symmetric structures could be realized within an optical framework in which the dynamics are governed by Schrödinger-like equations [94–96]. Furthermore, a \mathcal{PT} -symmetric optical system with a complex potential is observed experimentally in [97].

Fundamental solitons in the presence of a (optically or magnetically) induced lattice have been investigated analytically and experimentally in Bose-Einstein condensates (BECs) and in optical Kerr media (cf. [1, 76–80]). Such structures appear as special solutions of the focusing two-dimensional cubic NLSE with an external potential.

The purpose of this study is to compute fundamental solitons of the focusing cubic (2+1)-dimensional NLSE with a \mathcal{PT} -symmetric external potential (which includes a vacancy defect or not). Linear and nonlinear stability properties of these solitons are also investigated.

The model for nonlinear propagation light beams in optical external potential is

$$iu_z + \Delta u + |u|^2 u - V(x, y)u = 0. \quad (7.1)$$

In optics, $u(x, y, z)$ corresponds to the complex-valued, slowly varying amplitude of the electric field in the xy plane propagating in the z direction, $\Delta u \equiv u_{xx} + u_{yy}$ corresponds to diffraction, the cubic term in u originates from the nonlinear (Kerr) change of the refractive index and $V(x, y)$ is an external optical potential that can be written as the intensity of a sum of N phase-modulated plane waves, see ([25]), i.e.,

$$V(x, y) = \frac{V_0}{N^2} \left| \sum_{n=0}^{N-1} e^{i\vec{k}_n \cdot \vec{x} + i\theta_n(x, y)} \right|^2 + iW(x, y) \quad (7.2)$$

where $V_0 > 0$ is constant and corresponds to the peak depth of the potential, i.e., $V_0 = \max_{x, y} V(x, y)$, $\vec{x} = (x, y)$, \vec{k}_n is a wave vector, $\theta_n(x, y)$ is a phase function that characterizes edge irregularities or vacancy defects and $W(x, y)$ is imaginary part (gain-loss component) of the potential.

To calculate the fundamental solitons of Eq. (7.1) on a \mathcal{PT} -symmetric lattice with a vacancy defect, we use a fixed-point spectral computational method, namely spectral renormalization (SR) method (which explained in Chapter 3) [39].

The linear and nonlinear (in)stabilities are also examined for these localized structures by direct computations of Eq. (7.1).

7.1 \mathcal{PT} -symmetric Vacancy Defect

The actions of the parity, \hat{P} , and time, \hat{T} , operators are defined as follows:

$$\begin{aligned}\hat{P} : \hat{p} &\rightarrow -\hat{p}, & \hat{x} &\rightarrow -\hat{x}, \\ \hat{T} : \hat{p} &\rightarrow -\hat{p}, & \hat{x} &\rightarrow \hat{x}, & i &\rightarrow -i\end{aligned}\tag{7.3}$$

where \hat{p} and \hat{x} are the momentum and position operators, respectively [98].

In general, the Hamiltonian is defined as $\hat{H} = \hat{p}^2/2m + V(\hat{x})$, where m is the mass and V is the potential. If a Hamiltonian shares the same eigenfunctions with $\hat{P}\hat{T}$ operator and satisfies,

$$\hat{P}\hat{T}\hat{H} = \hat{H}\hat{P}\hat{T}\tag{7.4}$$

then it is defined as \mathcal{PT} -symmetric [89].

Therefore, in order to be \mathcal{PT} -symmetric, the \hat{H} operator should commute with the $\hat{P}\hat{T}$ operator (this is necessary but not sufficient),

$$\begin{aligned}\hat{P}\hat{T}\hat{H} &= \hat{p}^2/2m + V(x), \\ \hat{H}\hat{P}\hat{T} &= \hat{p}^2/2m + V^*(-x)\end{aligned}\tag{7.5}$$

which implies

$$V(x) = V^*(-x).\tag{7.6}$$

This indicates that the real part of the potential must be an even function and the imaginary part an odd function of x .

Although the commutativity condition (7.4) is met, if the Hamiltonian does not share its eigenfunctions with the $\hat{P}\hat{T}$ operator then the Hamiltonian is considered to possess broken \mathcal{PT} -symmetry.

7.1.1 The \mathcal{PT} -Symmetric lattice with a vacancy defect

In 2D, a \mathcal{PT} -symmetric lattice $V(x,y)$ must satisfy $V(x,y) = V^*(-x,-y)$ which indicates that the real part of the lattice must be an even function and the imaginary part of the lattice must be an odd function of x and y .

In this study, we consider a \mathcal{PT} -symmetric lattice with a vacancy defect as external potential. For simplicity we take this \mathcal{PT} -symmetric lattice potential to be

$$V(x, y) = \frac{V_0}{25} \left| 2\cos(k_x x) + 2\cos(k_y y) + \varepsilon e^{i\theta(x, y)} \right|^2 + iV_0 W_0 [\sin(2x) + \sin(2y)] \quad (7.7)$$

where the phase dislocation function θ is given by

$$\theta(x, y) = \tan^{-1}\left(\frac{y - y_0}{x}\right) - \tan^{-1}\left(\frac{y + y_0}{x}\right). \quad (7.8)$$

Physically, $\theta(x, y)$ corresponds to two first order phase dislocations displaced in the y direction by a distance of $2y_0$ and, ε is a constant that determines the strength (or depth) of the defect. A vacancy defect can thus be obtained using $y_0 = \pi/K$ where $K = k_x = k_y$ [25]. By setting $\varepsilon = 0$, the vacancy defect in the \mathcal{PT} -symmetric lattice is removed and the periodic lattice counterpart of this lattice obtained.

Here, W_0 is the relative magnitude of the imaginary component. We will investigate effect of the gain-loss component (the imaginary part of $V(x, y)$) on vacancy defect lattice solitons by taking various values of W_0 (as 0.1 and 0.3). 0.1 is taken to study solitons that localized in the \mathcal{PT} -symmetric region and 0.3 is taken to study near the edge of \mathcal{PT} -symmetric and broken-symmetry phases (above which the lattice is not \mathcal{PT} -symmetric).

Hereafter, if different values are not specifically defined, the potential depth is set to be $V_0 = 12.5$ and the propagation constant is set to be $\mu = -1$.

In Fig.7.1, real part of the \mathcal{PT} -symmetric lattices without defect ($\varepsilon = 0$) and with a vacancy defect ($\varepsilon = 1$) are plotted for a bounded region with $K = k_x = k_y = 2\pi$, $V_0 = 12.5$ and $W_0 = 0.1$. Also, imaginary parts of these lattices can be seen in Fig. 7.2.

As can be seen from Fig. 7.1(b), there is an empty cell at the center of the lattice with a vacancy defect in real part.

In Fig. 7.3, it is shown that the \mathcal{PT} -symmetric lattice with a vacancy defect meets the condition $V(x, y) = V^*(-x, -y)$. The real part of this potential is even and, the imaginary part is odd (see Fig. 7.3).

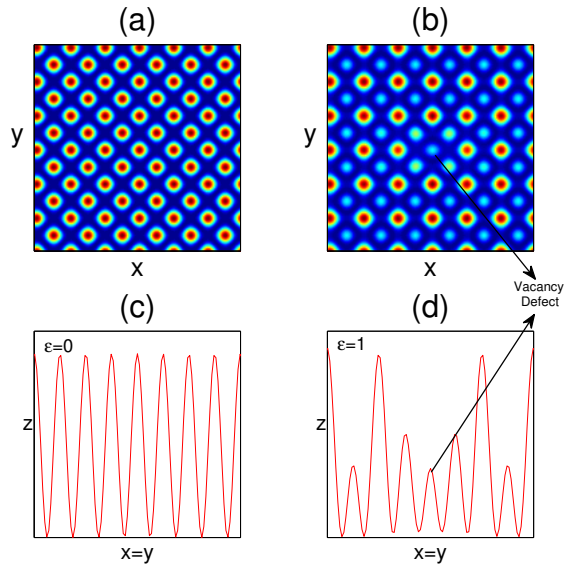


Figure 7.1 : Contour image of real part for the \mathcal{PT} -symmetric (a) lattice without defect; (b) lattice with a vacancy defect. Diagonal cross-section of (c) lattice without defect; (d) lattice with a vacancy defect.

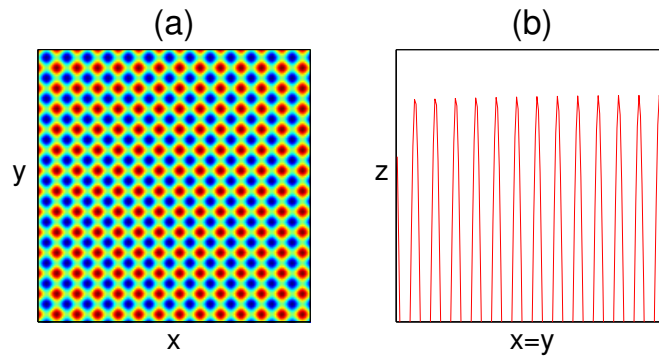


Figure 7.2 : (a) Contour image of imaginary part for the \mathcal{PT} -symmetric lattices; (b) Diagonal cross-section of imaginary part for the \mathcal{PT} -symmetric lattices.

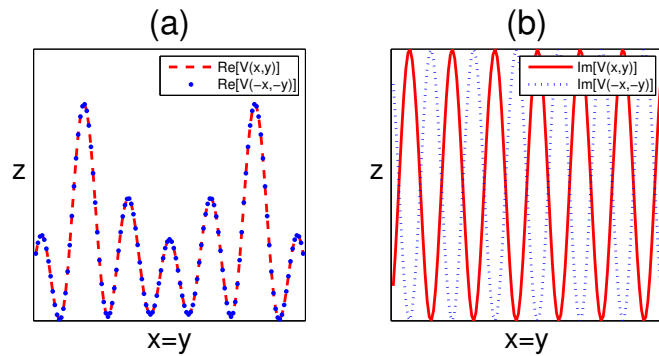


Figure 7.3 : Diagonal cross-section of (a) real parts; (b) imaginary parts in $V(x,y)$ and $V(-x,-y)$ for $V_0 = 12.5$, $W_0 = 0.1$ and $\varepsilon = 1$.

7.2 Linear Stability Analysis

The question of fundamental solitons' evolutions under perturbations is very important for applications. In this study, we consider the (linear and nonlinear) stability of soliton solutions of the (2+1)D NLSE with an external potential which given in Eq. (7.1).

In order to obtain linear spectrum of these solutions, we linearize the Eq. (7.1) around the fundamental soliton structures (which computed by SR method) and a linear eigenvalue problem results:

$$L\boldsymbol{\psi} = \sigma\boldsymbol{\psi} \quad (7.9)$$

Here L is the linearization operator (which is usually non-Hermitian), σ is the eigenvalue, $\boldsymbol{\psi}(\mathbf{x})$ is the corresponding eigenfunction, $\mathbf{x} = (x_1, x_2, \dots, x_N)$ is the spatial coordinates. We focus on the computation of discrete eigenvalues of L . Eigenvalues with positive real parts are unstable eigenvalues. The other eigenvalues are stable. Purely imaginary eigenvalues are called internal modes [99].

The perturbed soliton structure is defined as

$$u(x, y, z) = e^{-i\mu z} [u_0(x, y) + [v(x, y) - w(x, y)]e^{\sigma z} + [v(x, y) + w(x, y)]^* e^{\sigma^* z}], \quad (7.10)$$

where $u_0(x, y)$ is the fundamental soliton, the superscript $(*)$ represents complex conjugation, and $v, w \ll 1$. Substituting this perturbation into Eq. (7.1) and linearizing, we obtain eigenvalue problem which is given in Eq. (7.9) as

$$i \begin{pmatrix} L_1 & L_2 \\ -L_2^* & -L_1^* \end{pmatrix} \begin{pmatrix} v \\ w \end{pmatrix} = \sigma \begin{pmatrix} v \\ w \end{pmatrix}, \quad (7.11)$$

where $L_1 = \Delta + \mu + 2|u_0|^2 - V$ and $L_2 = u_0^2$.

We use the Fourier collocation method (which is developed by Yang in [99]), to compute the eigenvalues (σ) in Eq. (7.11).

7.3 Nonlinear Stability Analysis

In order to investigate the nonlinear stability of solitons, we plot the contour image and the maximum amplitude of the fundamental soliton versus the propagation distance z . A stable soliton should nearly preserve:

1. its peak amplitude, as opposed undergoing self-focusing and / or finite-distance collapse.

2. its position on the lattice, i.e., be drift-stable (drift-unstable solitons are typically characterized by “humps” that drift from lattice maxima toward nearby minima).

If these conditions are met then the soliton will be considered nonlinearly stable.

7.4 Numerical Existence of Fundamental Solitons and Stability Analysis

In this section, the numerical existence of fundamental solitons are shown in the \mathcal{PT} -symmetric lattices with or without a vacancy defect by setting defect's strength $\varepsilon = 0$ and $\varepsilon = 1$, respectively. The linear stability spectrum and nonlinear evolution of these solitons are also investigated.

7.4.1 Numerical existence of fundamental solitons

Fundamental solitons are obtained numerically in \mathcal{PT} -symmetric lattices with $K = k_x = k_y = 2\pi$ by the use of the spectral renormalization (SR) method. The initial condition for SR method is defined in Eq. (3.12) (in Chapter 3) and the parameters in this initial condition are taken as follows

$$M = 1, \quad A = 1, \quad x_n = 0, \quad y_n = 0, \quad \theta_n = 0. \quad (7.12)$$

We locate the initial condition on the center of the lattice in both cases (for $\varepsilon = 0$ and $\varepsilon = 1$). It should be mentioned that, for the periodic lattice case ($\varepsilon = 0$), the lattice center is a local maximum, and on the other hand, for the lattice with a vacancy defect ($\varepsilon = 1$), the lattice center (the location of the vacant cell) is a local minimum of the corresponding lattice.

In order to see the effect of vacancy defect in \mathcal{PT} -symmetric periodic lattice, we will investigate the fundamental soliton which is located on the vacant cell (center of the lattice, see Fig. 7.1).

Fundamental solitons in \mathcal{PT} -symmetric lattice without defect ($\varepsilon = 0$ in Eq.(7.7)) are plotted for $W_0 = 0.1$ and $W_0 = 0.3$ in Fig. 7.4 and Fig. 7.5, respectively.

Similarly, fundamental solitons at the center of the \mathcal{PT} -symmetric lattice with a vacancy defect ($\varepsilon = 1$ in Eq.(7.7)) are plotted for $W_0 = 0.1$ and $W_0 = 0.3$ in Fig. 7.6 and Fig. 7.7, respectively.

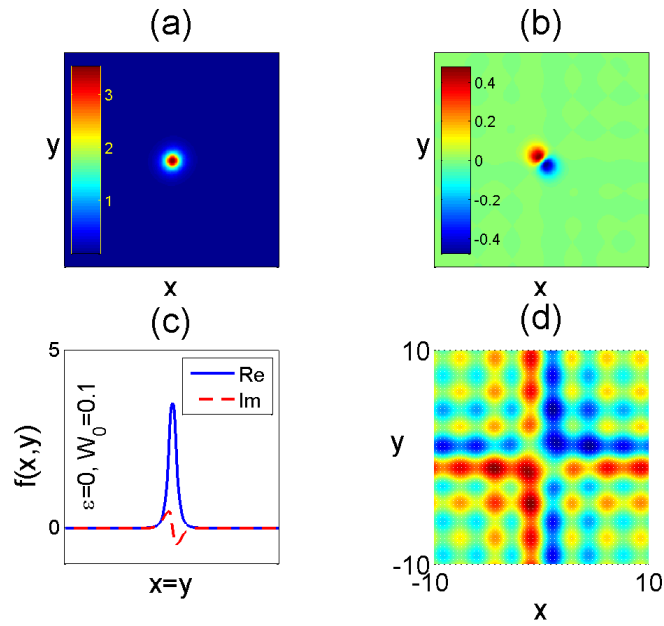


Figure 7.4 : Fundamental soliton located at the center of the \mathcal{PT} -symmetric periodic lattice for $\varepsilon = 0$ and $W_0 = 0.1$. Contour image of (a) Real part; (b) Imaginary part; (c) Diagonal cross-section of the soliton; (d) Phase portrait of the soliton.

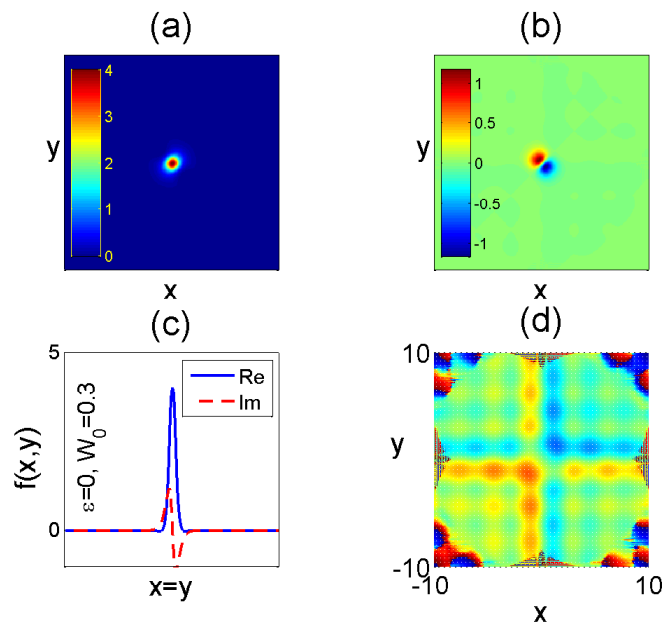


Figure 7.5 : Fundamental soliton located at the center of the \mathcal{PT} -symmetric periodic lattice for $\varepsilon = 0$ and $W_0 = 0.3$. Contour image of (a) Real part; (b) Imaginary part; (c) Diagonal cross-section of the soliton; (d) Phase portrait of the soliton.

Furthermore, the fundamental solitons are shown to exist in the \mathcal{PT} -symmetric lattice with a vacancy defect in a semi-infinite gap $\mu \leq 1.8$ for $V_0 = 12.5$, $\varepsilon = 1$ and $0 \leq W_0 \leq 0.3$.

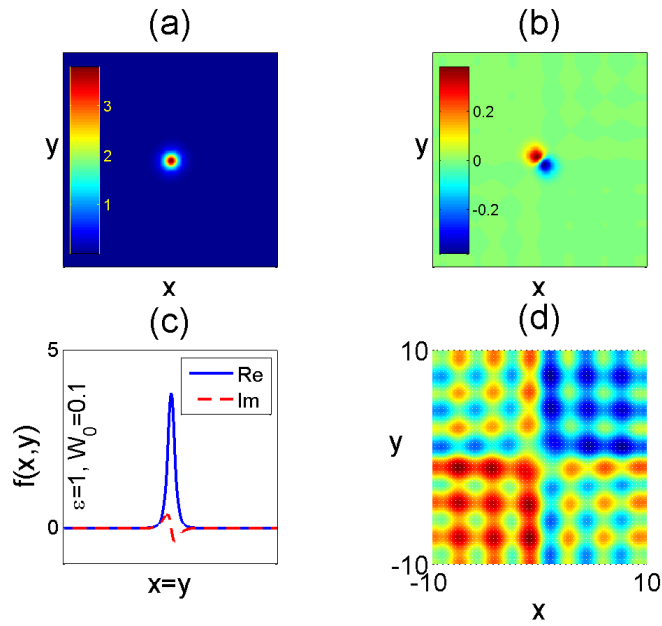


Figure 7.6 : Fundamental soliton located at the center of the \mathcal{PT} -symmetric lattice with a vacancy defect for $\varepsilon = 1$ and $W_0 = 0.1$. Contour image of (a) Real part; (b) Imaginary part; (c) Diagonal cross-section of the soliton; (d) Phase portrait of the soliton.

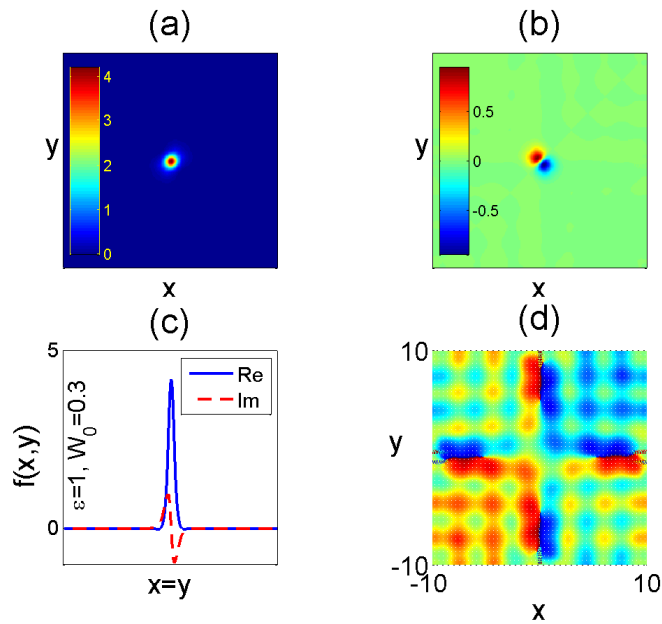


Figure 7.7 : Fundamental soliton located at the center of the \mathcal{PT} -symmetric lattice with a vacancy defect for $\varepsilon = 1$ and $W_0 = 0.3$. Contour image of (a) Real part; (b) Imaginary part; (c) Diagonal cross-section of the soliton; (d) Phase portrait of the soliton.

7.4.2 Stability analysis of fundamental solitons

Herein, we investigate the linear stability spectrum and the nonlinear stability properties of fundamental solitons that were previously obtained by spectral renormalization method.

The soliton power P ($P = \iint_{-\infty}^{\infty} |u|^2 dx dy$) versus the eigenvalue μ graph of the fundamental gap solitons on periodic and defect lattices are shown in Fig. 7.8 for $W_0 = 0$ (in case the potential is real), $W_0 = 0.1$ and $W_0 = 0.3$. It is observed from the Fig. 7.8 that, the soliton powers in periodic ($\varepsilon = 0$) case exceed the critical power for collapse of the NLSE soliton ($P_c \approx 11.72$) ([23]) whereas in lattice with a vacancy defect ($\varepsilon = 1$) case, the soliton powers are below the critical power for collapse.

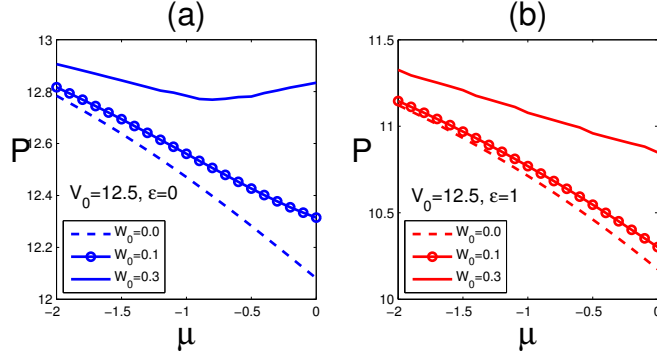


Figure 7.8 : Soliton power as a function of the eigenvalue μ within the semi-infinite band gap for lattices (a) without defect ($\varepsilon = 0$); (b) with a vacancy defect ($\varepsilon = 1$). All lattices share a common peak depth $V_0 = 12.5$.

In Fig. 7.9, the linear stability spectrum of the fundamental solitons (see Fig. 7.4 and Fig. 7.5) in \mathcal{PT} -symmetric lattice without defect is shown for $W_0 = 0.1$ and $W_0 = 0.3$. It can be seen that there are unstable ($Re(\sigma) > 0$) eigenvalues (see Fig. 7.9) in both cases. Thus, these solitons that are located at the center of the \mathcal{PT} -symmetric lattice, without defect are linearly unstable.

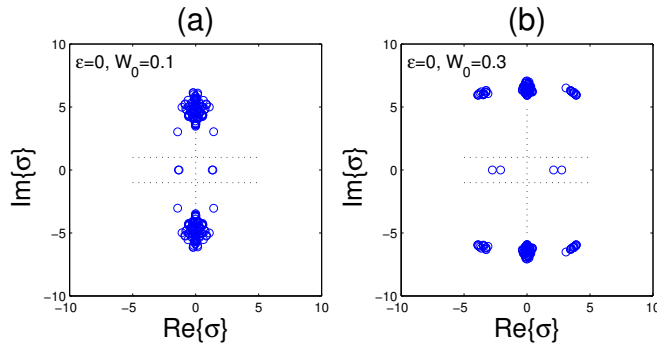


Figure 7.9 : Eigenvalues in the stability spectrum of the fundamental soliton located at the center of the \mathcal{PT} -symmetric lattice without defect (a) for $W_0 = 0.1$; (b) for $W_0 = 0.3$.

The linear stability spectrum is also computed for the fundamental solitons (see Fig. 7.6 and Fig. 7.7) in \mathcal{PT} -symmetric lattice with a vacancy defect for $W_0 = 0.1$ and $W_0 = 0.3$ (see Fig. 7.10).

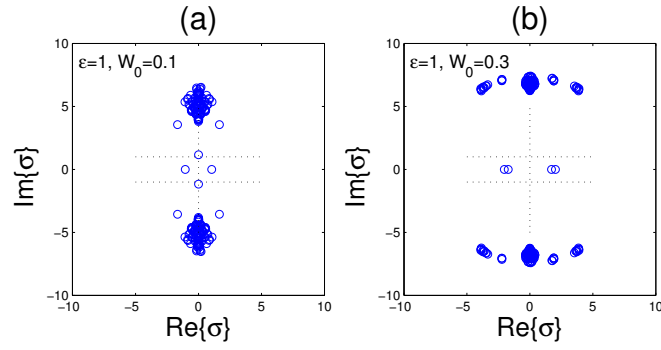


Figure 7.10 : Eigenvalues in the stability spectrum of the fundamental soliton located at the center of the \mathcal{PT} -symmetric lattice with a vacancy defect (a) for $W_0 = 0.1$; (b) for $W_0 = 0.3$.

As can be seen from Fig. 7.10, similar to the periodic (without defect) lattice case, fundamental solitons in the \mathcal{PT} -symmetric lattice with a vacancy defect have eigenvalues with positive real parts which indicates the linear instability of these solitons.

Furthermore, we investigate the nonlinear stability properties of these numerically computed fundamental solitons. To examine the nonlinear stability of the solitons, we plot contour image and peak amplitude of the real part during the evolution (from $z = 0$ to $z = z_{\max}$).

We plot evolution of the fundamental soliton (see Fig. 7.4) located at the center of the \mathcal{PT} -symmetric lattice without defect for $\varepsilon = 0$ and $W_0 = 0.1$ in Fig. 7.11.

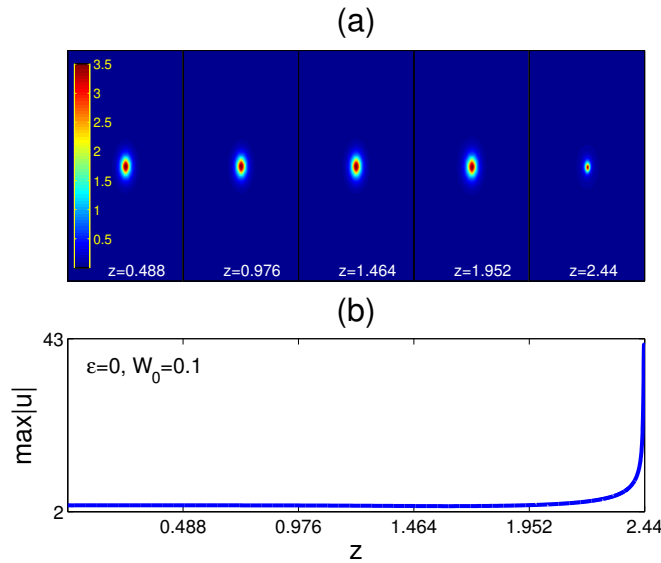


Figure 7.11 : Evolution of fundamental soliton located at the center of the \mathcal{PT} -symmetric lattice without defect for $\varepsilon = 0$ and $W_0 = 0.1$; (a) Contour image of the soliton; (b) Peak amplitude as a function of the propagation distance.

It can be seen from Fig. 7.11, during the evolution, the contour image of the fundamental soliton shrinks which indicates the self focusing of the mode, and peak amplitude increases sharply just after $z = 2.4$ approximately. Therefore, the fundamental soliton located at the center of the \mathcal{PT} -symmetric lattice without defect is found to be nonlinearly unstable in this parameter regime.

Similarly, evolution of the fundamental soliton (see Fig. 7.5) in the \mathcal{PT} -symmetric lattice without defect for $\varepsilon = 0$ and $W_0 = 0.3$ (strengthened imaginary part) is plotted in Fig. 7.12.

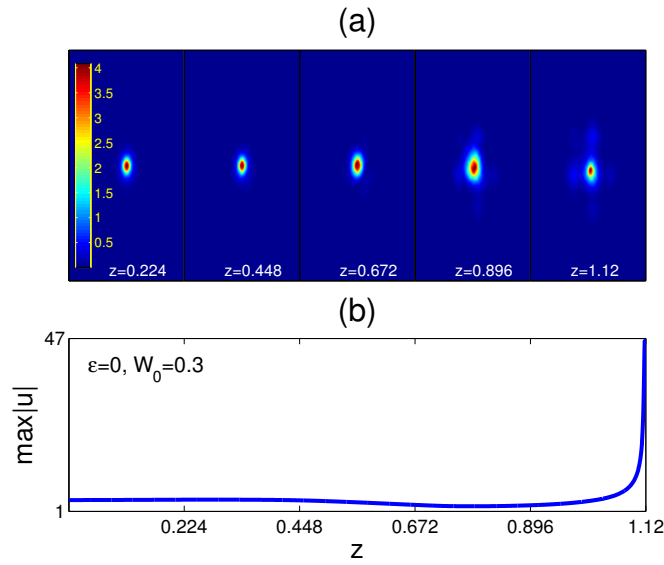


Figure 7.12 : Evolution of fundamental soliton located at the center of the \mathcal{PT} -symmetric lattice without defect for $\varepsilon = 0$ and $W_0 = 0.3$; (a) Contour image of the soliton; (b) Peak amplitude as a function of the propagation distance.

As can be seen from Fig. 7.12, the contour image of the soliton shrinks and peak amplitude increases significantly just after few diffraction lengths (approximately $z = 1.12$). This indicates that the fundamental soliton located at the center of the \mathcal{PT} -symmetric lattice without defect is nonlinearly unstable.

In order to see the effect of vacancy defect on the nonlinear stability properties of fundamental solitons, nonlinear stability of fundamental solitons (see Fig. 7.6 and Fig. 7.7) in \mathcal{PT} -symmetric lattice with a vacancy defect ($\varepsilon = 1$) are examined for $W_0 = 0.1$ and $W_0 = 0.3$ in Fig. 7.13 and Fig. 7.14, respectively.

It can be seen from Fig. 7.13 that the contour image of the fundamental soliton shrinks and peak amplitude of the soliton increases sharply after approximately $z = 5.7$. This

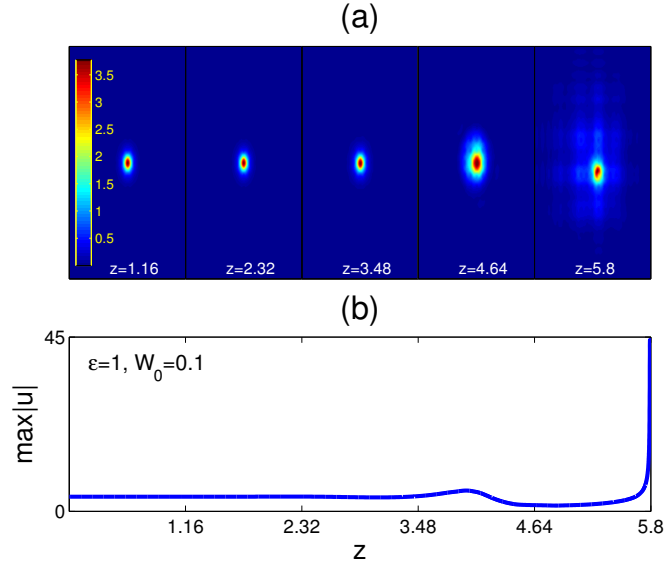


Figure 7.13 : Evolution of fundamental soliton located at the center of the \mathcal{PT} -symmetric lattice with a vacancy defect for $\varepsilon = 1$ and $W_0 = 0.1$; (a) Contour image of the soliton; (b) Peak amplitude as a function of the propagation distance.

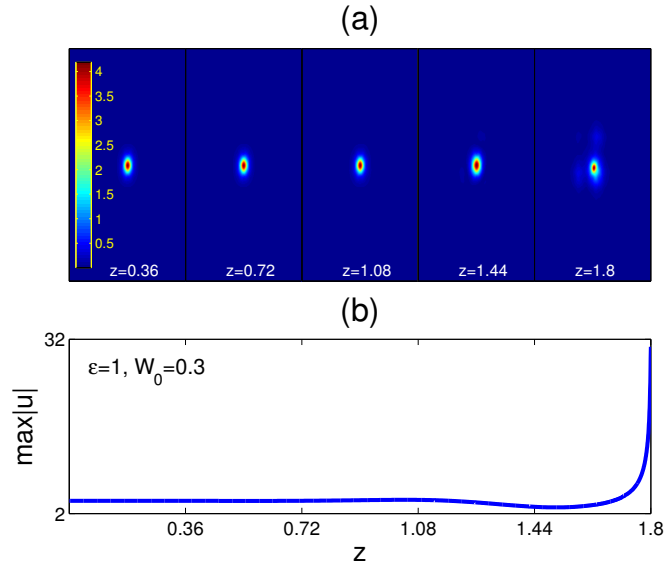


Figure 7.14 : Evolution of fundamental soliton located at the center of the \mathcal{PT} -symmetric lattice with a vacancy defect for $\varepsilon = 1$ and $W_0 = 0.3$; (a) Contour image of the soliton; (b) Peak amplitude as a function of the propagation distance.

shows that the fundamental soliton located at the center of the \mathcal{PT} -symmetric lattice with a vacancy defect for $W_0 = 0.1$ is nonlinearly unstable for these parameters. Also, the fundamental soliton with strengthened imaginary part ($W_0 = 0.3$) is nonlinearly unstable (see Fig. 7.14) and it has a shorter blow-up distance ($z_{\max} = 1.8$) than $W_0 = 0.1$ case ($z_{\max} = 5.8$).

By comparing Fig. 7.12 and Fig. 7.14, one can conclude that the blow-up distance of fundamental soliton increases when the \mathcal{PT} -symmetric lattice possesses a vacancy defect.

In addition to nonlinear evolution of the fundamental lattice solitons, it is also observed that, during the evolution, the soliton power is increasing with the propagation distance z for all solitons in \mathcal{PT} -symmetric lattices. For instance, for the soliton in Fig. 7.6, it is seen that, the power grows without bound approximately at the blow-up distance $z = 5.8$ (see Fig. 7.15).

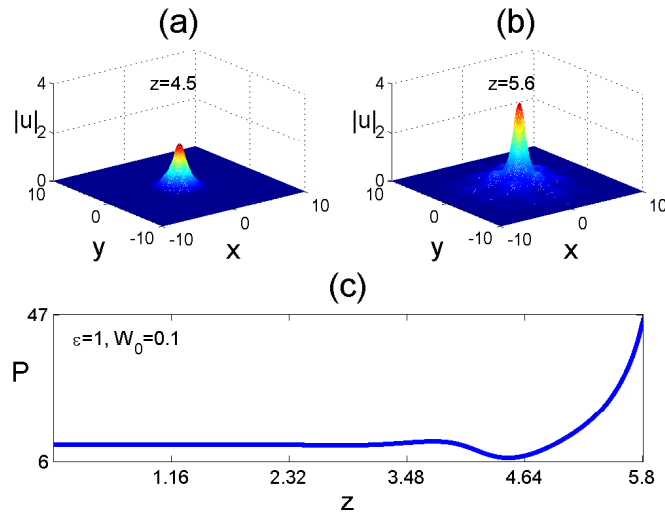


Figure 7.15 : Nonlinear evolution of an unstable fundamental soliton in the \mathcal{PT} -symmetric lattice with a vacancy defect for $\epsilon = 1$ and $W_0 = 0.1$; (a) Solution profile at $z = 4.5$; (b) Solution profile at $z = 5.6$; (c) Power evolution versus distance z .

Furthermore, we examine nonlinear evolution of the fundamental solitons for various defect's strength that determined by ϵ in Eq. (7.7). In Fig. 7.16, diagonal cross-section of the \mathcal{PT} -symmetric lattice with a vacancy defect is plotted for several values of ϵ .

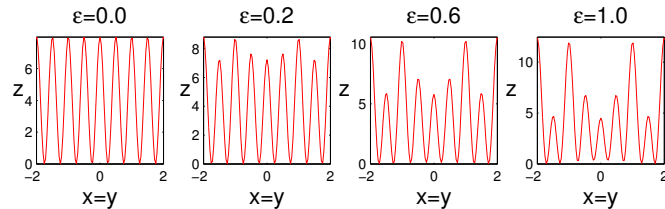


Figure 7.16 : Diagonal cross-section of the lattice with a vacancy defect while $\epsilon = 0.0$, $\epsilon = 0.2$, $\epsilon = 0.6$ and $\epsilon = 1.0$ in Eq. (7.7).

The power of fundamental solitons versus defect's strength is investigated in Fig. 7.17 for $W_0 = 0.1$ and $W_0 = 0.3$.

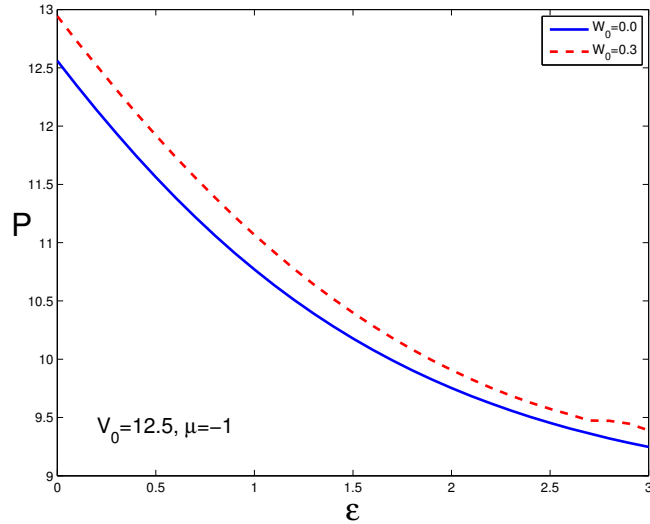


Figure 7.17 : Soliton power versus defect's strength (ϵ) for the \mathcal{PT} -symmetric lattice with a vacancy defect for $V_0 = 12.5$ and $\mu = -1$.

The power analysis in Fig. 7.17 shows that, the power of fundamental solitons decrease as the defect's strength (ϵ) grows whereas the power of fundamental solitons increase by the strengthened imaginary part ($W_0 = 0.3$) in the \mathcal{PT} -symmetric lattices.

Fundamental solitons' nonlinear evolution for different defect's strengths are shown in Fig. 7.18 for $W_0 = 0.1$ and $W_0 = 0.3$, respectively. As can be seen from Fig. 7.18, the

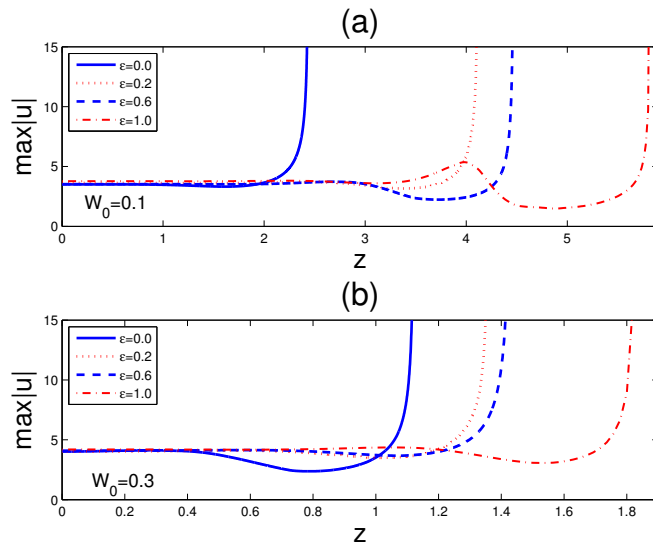


Figure 7.18 : Nonlinear evolution of the fundamental solitons in the \mathcal{PT} -symmetric lattice with a vacancy defect for four values of ϵ . Peak amplitude as a function of the propagation distance (a) when $W_0 = 0.1$; (b) when $W_0 = 0.3$.

propagation distance is lengthened by increased values of ϵ in both cases. In the other words, the blow-up of the fundamental solitons are delayed by strengthened vacancy defect in \mathcal{PT} -symmetric lattices.

Also, we notice that, at large values of ε , structure of the vacancy defect changes and the cell at center of the lattice turns into an irregular local minimum (see Fig. 7.19).

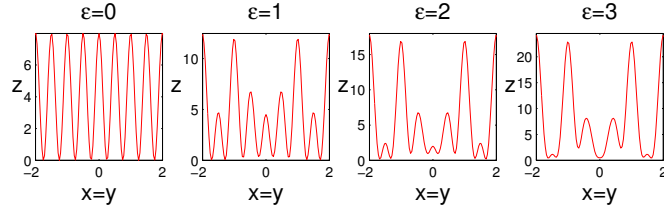


Figure 7.19 : Diagonal cross-section of the lattice with a vacancy defect while $\varepsilon = 0$, $\varepsilon = 1$, $\varepsilon = 2$ and $\varepsilon = 3$ in Eq. (7.7).

7.5 Conclusion

Fundamental solitons are investigated in self-focusing media with \mathcal{PT} -symmetric lattices with or without a vacancy defect. It is shown that there is a marked difference between the soliton powers of the lattice with a vacancy defect and its periodic lattice counterpart. The powers of \mathcal{PT} -symmetric lattice solitons decrease by adding a vacancy defect.

In literature (see [14, 25, 40]), it can be seen that fundamental and dipole solitons in the periodic lattices (with or without defects) can be stable under suitable conditions, in the absence of \mathcal{PT} -Symmetries. The results of stability analysis in this study show that, \mathcal{PT} -symmetric periodic lattice solitons have shorter blow-up distances than solitons in the lattice with a vacancy defect and, none of fundamental solitons in \mathcal{PT} -symmetric lattices (with or without a vacancy defect) are stable due to instant formation of collapse. Therefore, one can conclude that obtaining a stable soliton in a \mathcal{PT} -symmetric lattice is more demanding than obtaining a stable soliton in a lattice with a defect and certainly in a periodic lattice.

In view of the conducted numerical observations that are presented in this work, for \mathcal{PT} -symmetric lattices, one can certainly state that strengthened gain-loss component (imaginary part of the potential) in the periodic lattices impoverish the stability properties of the fundamental solitons. On the other hand, adding a vacancy defect to the periodic \mathcal{PT} -symmetric lattice, acts as a delaying mechanism for collapsing solitons. Solitary waves on \mathcal{PT} -symmetric lattices with defects are fairly new and warrant further investigation including their existences and their stability analysis.

8. CONCLUSIONS AND RECOMMENDATIONS

In this dissertation, we have investigated the existence and stability properties of solitons in the (2+1)-dimensional NLSE and NLSM system with various type external lattices.

At the beginning, physical derivation of governing equations (models) have been described and a numerical algorithm to compute the solutions of these models have been explained as a modification of spectral renormalization (SR) method.

By using SR method, we have first demonstrated numerical existence of the fundamental and dipole solitons in NLSM systems with/without a periodic external lattice. The linear and nonlinear evolution of these solitons have been examined by direct simulations of the model. It has been observed that wave collapse can be arrested in NLSM systems by adding an external potential (lattice) to the governing equation and there is a relation between mode profiles and stability properties of the fundamental solitons.

Furthermore, in Chapter 5, we have shown the numerical existence of dipole and vortex solitons for the two-dimensional NLSE with external potentials that possess strong irregularities, i.e., edge dislocations and vacancy defects. Multi-humped solitons are computed by SR method. The nonlinear stability of these solitons have been investigated using direct simulations of the NLSE and it has observed that these multi-humped modes in the defect lattices can be stable or unstable.

In Chapter 6, we have numerically obtained the fundamental, dipole and vortex solitons in the NLSM system with a lattice that possesses a vacancy defect. The linear and nonlinear stability properties of these solitons have been examined by direct simulations of the NLSM system. Results of stability investigations have shown that, although none of the solitons in the lattice with a vacancy defect is linearly stable, the fundamental, dipole and vortex solitons can be nonlinearly stable near vacancy defect under suitable conditions.

Moreover, the NLSE and NLSM system have been compared for a lattice that includes a vacancy defect. The comparisons have showed that although the first nonlinear band-gap structures are almost same for the NLS equation and NLSM system, there is a marked difference between the soliton powers of these models.

In the final part of the dissertation, we put forward a mechanism for delaying the collapse of the fundamental solitons in nonlinear media whose dynamics is governed by the two-dimensional NLSE with parity-time symmetric (\mathcal{PT} -symmetric) periodic potentials with/without a vacancy defect. We have observed that strengthened gain-loss component (imaginary part of the potential) in the periodic lattice impoverish the stability properties of the solitons, on the other hand adding a vacancy defect to the periodic \mathcal{PT} -symmetric lattice, acts as a delaying mechanism for collapsing solitons.

It is known that, suppressing collapse in periodic and quasiperiodic lattice solitons (for fundamental, dipole and vortex) can be achieved by increasing the lattice depth. Adding saturation to the system may also act like a collapse arrest mechanism for such structures. Thus, it would be interesting to study dipoles/vortices in deeper defected lattices in Kerr and in saturable media. Investigating collapse arrest mechanisms for dipole and vortex solitons in lattices with defects will be left for future studies.

Although computational results do not rigorously prove the existence of multiple solitons on lattices with defects, the results of this work may be encouraging for further investigations of dipole and vortex structures on complex lattices in nonlinear optics.

REFERENCES

- [1] **Kartashov, Y.V., Malomed, B.A. and Torner, L.** (2011). Solitons in nonlinear lattices, *Reviews of Modern Physics*, *83*, 247–306.
- [2] **Bosshard, C., Spreiter, R., Zgonik, M. and Günther, P.** (1995). Kerr nonlinearity via cascaded optical rectification and the linear electro-optic effect, *Physical Review Letters*, *74*, 2816–2819.
- [3] **Zozulya, A.A. and Anderson, D.Z.** (1995). Propagation of an optical beam in a photorefractive medium in the presence of a photogalvanic nonlinearity or an externally applied electric field, *Physical Review A*, *51*, 1520–1531.
- [4] **Kalocsai, A.G. and Haus, J.W.** (1993). Self-modulation effects in quadratically nonlinear materials, *Optics Communications*, *97*, 239–244.
- [5] **Kalocsai, A.G. and Haus, J.W.** (1994). Nonlinear Schrödinger equation for optical media with quadratic nonlinearity, *Physical Review A*, *49*, 574–585.
- [6] **Ablowitz, M.J. and Segur, H.** (1981). *Solitons and the Inverse Scattering Transform*, SIAM, Philadelphia.
- [7] **Cipolatti, R.** (1992). On the existence of standing waves for the Davey-Stewartson system, *Communications in Partial Differential Equations*, *17*, 967–988.
- [8] **Fibich, G. and Ilan, B.** (2000). Self-focusing of elliptic beams: an example for the failure of the aberrationless approximation, *Journal of the Optical Society of America*, *17*, 1749–1758.
- [9] **Whitham, G.B.** (1974). *Linear and Nonlinear Waves*, Wiley, New York.
- [10] **Fokas, A.S. and Ablowitz, M.J.** (1983). On a method of solution for a class of multidimensional nonlinear evolution equations, *Journal of the Optical Society of America*, *51*, 7–10.
- [11] **Merle, F. and Tsutsumi, Y.** (1990). L² concentration of blow-up solutions for the nonlinear Schrödinger equation with critical power nonlinearity, *Journal of Differential Equations*, *84*, 205–214.
- [12] **Zabusky, N.J. and Kruskal, M.D.** (1965). Interaction of Solitons in a Collisionless Plasma and the Recurrence of Initial States, *Physical Review Letters*, *15*, 240–243.
- [13] **Petviashvili, V.I.** (1976). Equation of an extraordinary soliton, *Soviet Journal of Plasma Physics*, *2*, 257–258.

- [14] **Ablowitz, M.J., Antar, N., Bakırtaş, İ. and Ilan, B.** (2010). Band-gap boundaries and fundamental solitons in complex two-dimensional nonlinear lattices, *Physical Review A*, *81*, 033834.
- [15] **Ablowitz, M.J., Antar, N., Bakırtaş, İ. and Ilan, B.** (2012). Vortex and dipole solitons in complex two-dimensional nonlinear lattices, *Physical Review A*, *86*, 033804.
- [16] **Fibich, G. and Wang, X.P.** (2003). Stability of solitary waves for nonlinear Schrödinger equations with inhomogeneous nonlinearities, *Physica D*, *175*, 96–108.
- [17] **Zakharov, V.E. and Shabat, A.B.** (1972). Exact theory of two-dimensional self-focusing and one dimensional self-modulation of waves in nonlinear media, *Soviet Physics JETP*, *34*, 62–69.
- [18] **Chao hao, G.** (1995). *Soliton theory and its applications*, Springer-Verlag, Berlin.
- [19] **Malomed, B.A.** (2006). *Soliton Management in Periodic Systems*, Springer, New York.
- [20] **Iliev, I.D., Khristov, E.K. and Kirchev, K.P.** (1994). *Spectral Methods in Soliton Equations*, John Wiley and Sons Inc., New York.
- [21] **Kelley, P.L.** (1965). Self focusing of optical beams, *Physical Review Letters*, *15*, 1005–1008.
- [22] **Vlasov, S., Petrishchev, V. and Talanov, V.** (1971). Averaged description of wave beams in linear and nonlinear media, *Radiophysics and Quantum Electronics*, *14*, 1062–1070.
- [23] **Weinstein, M.I.** (1983). Nonlinear Schrödinger equation and sharp interpolation estimates, *Communications in Mathematical Physics*, *87*, 567–576.
- [24] **Abdullaev, F.K. and Konotop, V.V.** (2003). *Nonlinear Waves: Classical and Quantum Aspects*, Kluwer Academic Publishers, The Netherlands.
- [25] **Ablowitz, M.J., Ilan, B., Schonbrun, E. and Piestun, R.** (2006). Solitons in two-dimensional lattices possessing defects, dislocations, and quasicrystal structures, *Physical Review E*, *74*, 035601(R).
- [26] **Ablowitz, M.J., Biondini, G. and Blair, S.** (2001). Localized multi-dimensional optical pulses in non-resonant quadratic materials, *Mathematics and Computers in Simulation*, *56*, 511–519.
- [27] **Ablowitz, M.J., Biondini, G. and Blair, S.** (1997). Multi-dimensional pulse propagation in non-resonant $\chi^{(2)}$ materials, *Physics Letters A*, *236*, 520–524.
- [28] **Ablowitz, M.J., Biondini, G. and Blair, S.** (2001). Nonlinear Schrödinger equations with mean terms in non-resonant multi-dimensional quadratic materials, *Physical Review E*, *63*, 605–620.

- [29] **Ablowitz, M.J.** (2011). *Nonlinear Dispersive Waves Asymptotic Analysis and Solitons*, Cambridge University Press, New York.
- [30] **Benney, D.J. and Roskes, G.J.** (1969). Wave instabilities, *Studies in Applied Mathematics*, 48, 377–385.
- [31] **Davey, A. and Stewartson, K.** (1974). On three-dimensional packets of surface waves, *Proceedings of the Royal Society A*, 338, 101–110.
- [32] **Zakharov, V.E.** (1972). Collapse of Langmuir waves, *Soviet Physics JETP*, 35, 908–914.
- [33] **Ablowitz, M.J., Bakırtaş, İ. and İlan, B.** (2005). Wave collapse in a class of nonlocal nonlinear Schrödinger equations, *Physica D*, 207, 230–253.
- [34] **Crasovan, L.C., Torres, J.P., Mihalache, D. and Torner, L.** (2003). Arresting wave collapse by wave self-rectification, *Physical Review Letters*, 91, 063904.
- [35] **Ghidaglia, J.M. and Saut, J.C.** (1990). On the initial value problem for the Davey-Stewartson systems, *Nonlinearity*, 3, 475–506.
- [36] **Sulem, C. and Sulem, P.L.** (1999). *The Nonlinear Schrödinger Equation*, Springer-Verlag, New York.
- [37] **Talanov, V.I.** (1965). Self focusing of wave beams in nonlinear media, *Soviet Physics JETP Letters*, 2, 138–141.
- [38] **Fibich, G. and Papanicolaou, G.C.** (1999). Self-focusing in the perturbed and unperturbed nonlinear Schrödinger equation in critical dimension, *SIAM Journal on Applied Mathematics*, 60, 183–240.
- [39] **Ablowitz, M.J. and Musslimani, Z.H.** (2005). Spectral renormalization method for computing self-localized solutions to nonlinear systems, *Optics Letters*, 30, 2140–2142.
- [40] **Bağcı, M., Bakırtaş, İ. and Antar, N.** (2014). Vortex and dipole solitons in lattices possessing defects and dislocations, *Optics Communications*, 331, 204–218.
- [41] **Bağcı, M., Bakırtaş, İ. and Antar, N.** (2015). Fundamental solitons in parity-time symmetric lattice with a vacancy defect, *Optics Communications*, 356, 472–481.
- [42] **Ablowitz, M.J. and Haberman, R.** (1975). Nonlinear evolution equations – two and three dimensions, *Physical Review Letters*, 35, 1185–1188.
- [43] **Djordjevic, V.D. and Reddekopp, L.G.** (1977). On two-dimensional packets of capillary gravity waves, *Journal of Fluid Mechanics*, 79, 703–714.
- [44] **Papanicolaou, G.C., McLaughlin, D. and Weinstein, M.** (1982). Focusing singularity for the nonlinear Schrödinger equation, *Lecture Notes in Numerical and Applied Analysis*, 5, 253–257.

- [45] **Merle, F. and Raphael, P.** (2004). On the universality of blow-up profile for L2 critical nonlinear Schrödinger equation, *Inventiones Mathematicae*, 156, 565–672.
- [46] **Moll, K.D., Gaeta, A.L. and Fibich, G.** (2003). Self-similar optical wave collapse: observation of the Townes profile, *Physical Review Letters*, 90, 203902.
- [47] **Landau, L.D., Lifshitz, E.M. and Pitaevskii, L.P.** (1984). *Electrodynamics of Continuous Media*, Butterworth-Heinemann, London.
- [48] **Jackson, J.D.** (1998). *Classical Electrodynamics*, John Wiley, New York.
- [49] **Agrawal, G.P.** (2001). *Nonlinear Fiber Optics*, Academic Press, New York.
- [50] **Boyd, R.W.** (2003). *Nonlinear Optics*, Academic Press, New York.
- [51] **Agrawal, G.P.** (2002). *Fiber-Optic Communication Systems*, Wiley-Interscience, New York.
- [52] **Vakhitov, N.G. and Kolokolov, A.A.** (1973). Stationary solutions of the wave equation in a medium with nonlinearity saturation, *Radiophysics and Quantum Electronics*, 16, 783–789.
- [53] **Weinstein, M.I.** (1985). Modulational stability of ground states of nonlinear Schrödinger equations, *SIAM Journal on Mathematical Analysis*, 16, 472–491.
- [54] **Rose, H.A. and Weinstein, M.I.** (1988). On the bound states of the nonlinear Schrödinger equation with a linear potential, *Physica D*, 30, 207–218.
- [55] **Sivan, Y., Fibich, G., Ilan, B. and Weinstein, M.I.** (2008). Qualitative and quantitative analysis of stability and instability dynamics of positive lattice solitons, *Physical Review E*, 78, 046602.
- [56] **Christodoulides, D.N., Lederer, F. and Silberberg, Y.** (2003). Discretizing light behaviour in linear and nonlinear waveguide lattices, *Nature*, 424, 817–823.
- [57] **Sukhorukov, A.A., Kivshar, Y.S., Eisenberg, H.S. and Silberberg, Y.** (2003). Spatial optical solitons in waveguide arrays, *IEEE Journal of Quantum Electronics*, 39, 31–50.
- [58] **Efremidis, N.K., Hudock, J., Christodoulides, D.N., Fleischer, J.W., Cohen, O. and Segev, M.** (2003). Two-dimensional optical Lattice Solitons, *Physical Review Letters*, 91, 213906.
- [59] **Fleischer, J.W., Segev, M., Efremidis, N.K. and Christodoulides, D.N.** (2003). Observation of two-dimensional discrete solitons in optically induced nonlinear photonic lattices, *Nature*, 422, 147–150.
- [60] **Neshev, D., Kivshar, Y.S., Martin, H. and Chen, Z.** (2004). Soliton stripes in two-dimensional nonlinear photonic lattices, *Optics Letters*, 29, 486–488.

- [61] **Sakaguchi, H. and Malomed, B.A.** (2006). Gap solitons in quasiperiodic optical lattices, *Physical Review E*, 74, 026601.
- [62] **Kartashov, Y.V., Vysloukh, V.A. and Torner, L.** (2005). Topological Dragging of Solitons, *Physical Review Letters*, 95, 243902.
- [63] **Kartashov, Y.V., Vysloukh, V.A. and Torner, L.** (2009). Soliton shape and mobility control in optical lattices, *Progress in Optics*, 52, 63–148.
- [64] **Shechtman, D., Blech, I., Gratias, D. and Cahn, J.W.** (1984). Metallic Phase with Long-Range Orientational Order and No Translational Symmetry, *Physical Review Letters*, 53, 1951–1953.
- [65] **Senechal, M.** (1985). *Quasicrystals and Geometry*, Cambridge Univ. Press, Cambridge.
- [66] **Marder, M.P.** (2000). *Condensed Matter Physics*, Wiley, New York.
- [67] **Fedele, F., Yang, J. and Chen, Z.** (2005). Properties of defect modes in one-dimensional optically induced photonic lattices, *Studies in Applied Mathematics*, 115, 279–301.
- [68] **Buljan, H., Bartal, G., Cohen, O., Schwartz, T., Manela, O., Carmon, T., Segev, M., Fleischer, J.W. and Christodoulides, D.N.** (2005). Partially coherent waves in nonlinear periodic lattices, *Studies in Applied Mathematics*, 115, 173–208.
- [69] **Schonbrun, E. and Piestun, R.** (2006). Optical vortices for localized optical lattice site manipulation, *Optical Engineering*, 45, 028001.
- [70] **Pertsch, T., Peschel, U., Lederer, F., Burghoff, J., Will, M., Nolte, S. and Tünnermann, A.** (2004). Discrete diffraction in two-dimensional arrays of coupled waveguides in silica, *Optics Letters*, 29, 468–470.
- [71] **Qi, M., Lidorikis, E., Rakish, P.T., Johnson, S.G., Joannopoulos, J.D., Ippen, E.P. and Smith, H.I.** (2004). A three-dimensional optical photonic crystal with designed point defects, *Nature*, 429, 538–542.
- [72] **Cai, W. and Piestun, R.** (2006). Patterning of silica microsphere monolayers with focused femtosecond laser pulses, *Applied Physics Letters*, 88, 111112.
- [73] **Trombettoni, A. and Smerzi, A.** (2002). Discrete solitons and breathers with dilute Bose-Einstein Condensates, *Physical Review Letters*, 86, 2353–2356.
- [74] **Matthews, M.R., Anderson, B.P., Haljan, P.C., Hall, D.S., Wieman, C.E. and Cornell, E.A.** (1999). Vortices in a Bose-Einstein condensate, *Physical Review Letters*, 83, 2498–2501.
- [75] **Abo-Shaer, J.R., Raman, C., Vogels, J.M. and Ketterle, W.** (2001). Observation of vortex lattices in Bose-Einstein condensates, *Science*, 292, 476–479.

- [76] **Kivshar, Y.S. and Luther-Davies, B.** (1998). Dark optical solitons: physics and applications, *Physics Reports*, 298, 81–197.
- [77] **Manela, O., Cohen, O., Bartal, G., Fleischer, J.W. and Segev, M.** (2004). Two-dimensional higher-band vortex lattice solitons, *Optics Letters*, 29, 2049–2051.
- [78] **Fleischer, J.W., Bartal, G., Cohen, O., Manela, O., Segev, M., Hudock, J. and Christodoulides, D.N.** (2004). Observation of vortex-ring discrete solitons in 2D photonic lattices, *Physical Review Letters*, 92, 123904.
- [79] **Freedman, B., Bartal, G., Segev, M., Lifshitz, R., Christodoulides, D.N. and Fleischer, J.** (2006). Wave and defect dynamics in nonlinear photonic quasicrystals, *Nature*, 440, 1166–1169.
- [80] **Leblond, H., Malomed, B.A. and Mihalache, D.** (2011). Spatiotemporal vortex solitons in hexagonal arrays of waveguides, *Physical Review A*, 83, 063825.
- [81] **Yang, J.** (2010). *Nonlinear Waves in Integrable and Nonintegrable Systems*, SIAM Society for Industrial and Applied Mathematics.
- [82] **Lakoba, T.I. and Yang, J.** (2007). A generalized Petviashvili iteration method for scalar and vector Hamiltonian equations with arbitrary form of nonlinearity, *Journal of Computational Physics*, 226(2), 1668–1692.
- [83] **Lakoba, T.I. and Yang, J.** (2007). A mode elimination technique to improve convergence of iteration methods for finding solitary waves, *Journal of Computational Physics*, 226(2), 1693–1709.
- [84] **Lakoba, T.I.** (2009). Conjugate Gradient method for finding fundamental solitary waves, *Physica D*, 238(23-24), 2308–2330.
- [85] **Yang, J.** (2009). Newton-conjugate gradient methods for solitary wave computations, *Journal of Computational Physics*, 228(18), 7007–7024.
- [86] **Yang, J.** (2014). Partially \mathcal{PT} -symmetric optical potentials with all-real spectra and soliton families in multidimensions, *Optics Letters*, 39, 1133–1136.
- [87] **Nixon, S., Ge, L. and Yang, J.** (2012). Stability analysis for solitons in \mathcal{PT} -symmetric optical lattices, *Physical Review A*, 85, 023822.
- [88] **Bender, C.M. and Boettcher, S.** (1998). Real spectra in non-Hermitian Hamiltonians having \mathcal{PT} -Symmetry, *Physical Review Letters*, 80, 5243–5246.
- [89] **Bender, C.M., Brody, D.C. and Jones, H.F.** (2002). Complex extension of quantum mechanics, *Physical Review Letters*, 89, 270401.
- [90] **Bender, C.M.** (2003). Must a Hamiltonian be Hermitian?, *American Journal of Physics*, 71, 1095–1102.

- [91] **Ahmed, Z.** (2001). Real and complex discrete eigenvalues in an exactly solvable one-dimensional complex \mathcal{PT} -invariant potential, *Physics Letters A*, 282, 343–348.
- [92] **Bagchi, B. and Quesne, C.** (2000). $sl(2, \mathbb{C})$ as a complex Lie algebra and the associated non-Hermitian Hamiltonians with real eigenvalues, *Physics Letters A*, 273, 285–292.
- [93] **Markum, H., Pullirsch, R. and Wettig, T.** (1999). Non-Hermitian random matrix theory and lattice QCD with chemical potential, *Physical Review Letters*, 83, 484–487.
- [94] **El-Ganainy, R., Makris, K.G., Christodoulides, D.N. and Musslimani, Z.H.** (2007). Theory of coupled optical \mathcal{PT} -symmetric structures, *Optics Letters*, 32, 2362–2364.
- [95] **Zhong, W.P., Belic, M.R. and Huang, T.** (2012). Two-dimensional accessible solitons in \mathcal{PT} -symmetric potentials, *Nonlinear Dynamics*, 70(3), 2027–2034.
- [96] **Abdullaev, F.K., Kartashov, Y.V., Konotop, V.V. and Zezyulin, D.A.** (2011). Solitons in \mathcal{PT} symmetric nonlinear lattices, *Physical Review A*, 83, 041805(R).
- [97] **Ruter, C.E., Makris, K.G., El-Ganainy, R., Christodoulides, D.N., Segev, M. and Kip, D.** (2010). Observation of parity time symmetry in optics, *Nature Physics*, 6, 192–195.
- [98] **Hesketh, G.D.** (2010). *\mathcal{PT} -Symmetric Optical Lattices (M.Sc. Thesis)*, Imperial College London.
- [99] **Yang, J.** (2012). Iteration methods for stability spectra of solitary waves, *Journal of Computational Physics*, 227, 6862–6876.

CURRICULUM VITAE

Name Surname: Mahmut Bađcı

Place and Date of Birth: Adıyaman, 06.11.1983

Address: ŐiŐli, İstanbul

E-Mail: bagcimahmut@gmail.com

B.Sc.: ITU - Physics Engineering (February 2007)

M.Sc.: ITU - Mathematical Engineering (July 2010)

Professional Experience and Rewards: Lecturer at Istanbul Kavram Vocational College, Department of Computer Technology

PUBLICATIONS/PRESENTATIONS ON THE THESIS

- Bađcı, M., BakırtaŐ, İ., Antar, N. (2014). Vortex and Dipole Solitons in Lattices Possessing Defects and Dislocations, *Optics Communications*, 331, 204-218.
doi: 10.1016/j.optcom.2014.06.005
- Bađcı, M., BakırtaŐ, İ., Antar, N. (2015). Fundamental Solitons in Parity-Time Symmetric Lattice with a Vacancy Defect, *Optics Communications*, 356, 472-481.
doi: 10.1016/j.optcom.2015.08.008
- Bađcı, M., BakırtaŐ, İ., Antar, N., Nonlinear Lattice Solitons in NLSM Systems, *Physical Review E*.
(Under review)

Presentations in International Conferences

- Bađcı, M., BakırtaŐ, İ., Antar, N., Optical solitons of NLSM Systems in PT-Symmetric lattice with a vacancy defect, *Nonlinear Evolution Equations and Dynamical Systems*, May 24-31, 2015 (NEEDS 2015), Sardinia, Italy. (Poster with a short talk)
- Bađcı, M., BakırtaŐ, İ., Antar, N., Fundamental and dipole solitons in PT-Symmetric lattice with a vacancy defect, *ICAAMMP Conference*, Aug. 19-21, 2014, YTU, Istanbul, Turkey.
- Bađcı, M., BakırtaŐ, İ., Antar, N., Vortex and Dipole Solitons in Defect Lattices, *The Third International Conference: Nonlinear Waves–Theory and Applications*, June 12-15, 2013, Beijing, China.

Presentations in National Conferences

- Bađcı, M., Bakırtař, İ., Antar, N., 2013: Düzensiz Kafes (Latis) içinde temel, dipol ve vorteks solitonlar, 18. *Ulusal Mekanik Kongresi*, 26-30 Ağustos 2013, Manisa, Türkiye.
- Bađcı, M., Bakırtař, İ., Antar, N., 2015: Düzensiz Kafes (Latis) içinde Nİsm solitonları, 19. *Ulusal Mekanik Kongresi*, 24-28 Ağustos 2015, Trabzon, Türkiye.
- Bađcı, M., Bakırtař, İ., 2015: Kuadratik ortamda parite zaman (PT) simetrlili kafes solitonları, 19. *Ulusal Mekanik Kongresi*, 24-28 Ağustos 2015, Trabzon, Türkiye.